School of Biomedical Sciences

The Interaction of Insulin with the Insulin Receptor in a Membrane Environment

Thiruvarutchelvan Sabapathy

This thesis is presented for the Degree of
Doctor of Philosophy
of
Curtin University

August 2018

DECLARATION

To the best of my knowledge and belief this Thesis contains no material previously published by any other person except where due acknowledgment has been made. This Thesis contains no material which has been accepted for the award of any other degree or diploma in any university.

The research presented and reported in this Thesis was conducted in compliance with the National Health and Medical Research Council Australian code for the care and use of animals for scientific purposes 8th edition (2013). The proposed research study received animal ethics approval from the Curtin University Animal Ethics Committee, Approval Number # **AEC_2016_17**

Signature:

Date:

PREFACE

This Thesis examines the influence of plasma membrane lipid composition on insulin-insulin receptor interactions. Subject to time and resource constraints, every attempt was made to thoroughly investigate this topic, an area of research which is of direct relevance to diabetes research. The work was conducted in School of Pharmacy and Biomedical Sciences and Curtin Health Innovation Research Institute, Curtin University under the supervision of Associate Professor Cyril Mamotte and Adjunct Professor Erik Helmerhorst. All experimental work was solely conducted by me unless otherwise stated.

ACKNOWLEDGEMENTS

Firstly, I would like to express my sincere thanks and gratitude to my supervisors **Associate Professor Cyril Mamotte and Professor Erik Helmerhorst** for their invaluable guidance throughout my PhD candidacy. The support and motivation from both of my supervisors was critical to overcoming the problems and hurdles that are inevitable in the course of a PhD. Their extensive research experience, in-depth scientific knowledge and insight were also of enormous benefit, and something I truly appreciated.

I would like to also extend my sincere thanks and gratitude to **Dr. Steven Bottomley** who was also one of my supervisors, albeit for a shorter period of time. He too had helpful insights and suggestions that were helpful in context of numerous experimental aspects, even when no longer part of my official supervisory team.

Special thanks and gratitude to **Professor Arunasalam Dharmarajan** for introducing me to Curtin University and my supervisors through an India-initiative scholarship.

I also extend my thanks to **Mrs. Gaewyn Ellison**, who is my lab colleague and fellow PhD candidate. I am extremely thankful for the support, advice and care, both professionally and personally, I had from her throughout the course of my studies. Her energetic and vibrant personality was a big motivation for me. My sincere thanks and gratitude goes also to **Mr. Abhishek Kumar Singh, Dr. Abhijeet Deshmukh, Dr. Himel Nahreen Khaleeque, Mr. Behin Sundararajan and Dr. Imran Khan** for their invaluable time and support, both professionally and personally during this time.

I would like to express my sincere thanks to friends in Perth outside Curtin University for their help on numerous occasions. Special thanks to **Mr. Shadesh Ramachandran and Mr. Harish Prabhakaran** for their invaluable support during some of the tougher times in my personal life during my studies-I am truly indebted to them for the help and support they provided during that time.

I would also like to express my sincere thanks and gratitude to all CHIRI staff members for their invaluable support and a special thanks to **Mr. Sam Siem**, not just for his support as a Purchasing Officer but also for being a very good friend.

Last but not least, I would like to thank my wife, **Anithamani** for all her support and encouragement and being there for the many ups, but also the downs and the challenges over the 4 years of my candidacy. The biggest thanks also to my parents and to my sister for believing in me and supporting me during my PhD study as they have always done since the early days of my childhood.

This wonderful journey of four years as a PhD candidate also includes the birth of my son, **Kavin Thiru**. He has brought a lot of joy and happiness to my life, which is motivating me to go forge ahead and challenge myself in life and I dedicate this Thesis to him.

Conference presentations done during this thesis

Oral Presentations

Thiruvarutchelvan Sabapathy, Erik Helmerhorst and Cyril Mamotte. *"The interaction of insulin with the insulin receptor in a membrane environment"* at **Australian Society of Medical Research (ASMR) symposium** held in Curtin University, Perth, WA on 30th May 2015 and **Mark Liveris Research student seminar program** held in Curtin University, Perth WA on 3rd September 2015.

Thiruvarutchelvan Sabapathy, Erik Helmerhorst and Cyril Mamotte. *"Alterations in plasma membrane cholesterol content impairs insulin binding in HepG2 cells"* at **Australian Society of Medical Research (ASMR) symposium** held in Curtin University, Perth, WA on 2nd June 2016.

Poster Presentations

Thiruvarutchelvan Sabapathy, Erik Helmerhorst and Cyril Mamotte. *"The interaction of insulin with the insulin receptor in a membrane environment"* at **Combined Biological Sciences Meeting (CBSM)** held in University of Western Australia (UWA), WA, Perth on 28th August 2015.

Thiruvarutchelvan Sabapathy, Erik Helmerhorst and Cyril Mamotte. *"The influence of plasma membrane cholesterol on insulin binding and signalling in insulin-sensitive cells"* at **Mark Liveris Research student seminar program** held in Curtin University, Perth WA on 28th September 2017.

Thiruvarutchelvan Sabapathy, Erik Helmerhorst and Cyril Mamotte. *"The interaction of insulin with the insulin receptor in a membrane environment"* at **Science on the Swan** held in Perth from 5th to 7th June 2017.

Thiruvarutchelvan Sabapathy, Erik Helmerhorst and Cyril Mamotte. *"The interaction of insulin with the insulin receptor in a membrane environment"* at **ADS-ADEA Annual Scientific Meeting** held at Perth Convention Centre, WA from 28th September to 1st August 2017.

Publications arising from this thesis

Thiruvarutchelvan Sabapathy, Erik Helmerhorst, Steven Bottomley, Sharon Babaeff, Kylie Munyard, Philip Newsholme and Cyril Mamotte. "Use of virus-like particles (VLPs) as a native membrane model to study the interaction of insulin with the insulin receptor" Manuscript under review with *Biochimica Biophysica Acta-Biomembranes* (BBAMEM-18-380).

Thiruvarutchelvan Sabapathy, Erik Helmerhorst, Gaewyn Ellison and Cyril D Mamotte. "The influence of plasma membrane cholesterol composition on insulin sensitivity in target tissues" (manuscript under preparation).

TABLE OF CONTENTS

LIST OF FIGURES

LIST OF TABLES

ABSTRACT

The first event in insulin action is the interaction of insulin with its cognate receptor. While there is a detailed understanding of the insulin signalling mechanism at the intracellular level, knowledge on how insulin interacts with its cognate binding sites on the insulin receptor and the influence of plasma membrane lipid composition on this interaction is not known. This Thesis examines the influence of cholesterol on insulin binding to the insulin receptor in a membrane environment using several experimental models, including cultured cells, purified liver cell membranes, and a novel cell membrane model known as virus-like particles.

Cell culture studies were done on HepG2 cells, differentiated myotubes and CHO T10 cells, the latter a CHO cell line which overexpresses the insulin receptor (A isoform). The cholesterol content of the cells were either reduced or enriched by using methyl-β-cyclodextrin (MBCD) or cholesterol loaded- methyl-β-cyclodextrin (cMBCD), respectively. Interestingly, insulin binding decreased by about 2-fold as a function of cholesterol concentration irrespective of treatment with either 10 mM MBCD or 10 mM cMBCD. This suggests that there is an ideal concentration of cholesterol may be required to achieve optimal insulin binding.

The decreased binding of insulin observed in cells that were either depleted of or loaded with cholesterol was not due to a change in the affinity of the insulin receptors for insulin but rather, in each case, was due to about a 2-fold decrease in the number of available insulin receptors that were determined from detailed competition binding analyses. This observation was confirmed by quantitating cell surface insulin receptor expression using flow cytometry with a monoclonal antibody (83-7) directed against the α-subunit of the insulin receptor. This decrease in insulin receptor availability for insulin binding coincided with decreases in the autophosphorylation of insulin receptors and phosphorylation of Akt and GSK3β in HepG2 cells and differentiated myotubes but not in CHO T10 cells. One possible reason for this disconnect in insulin binding and signalling in CHO T10 cells could be due to the overexpression of the A-isoform of the insulin receptor, which predominantly signals through the ERK/MAPK pathway.

The impact of membrane cholesterol on insulin binding was confirmed *ex vivo* in plasma membrane purified from the livers of mice that were fed either a normal or

high-fat diet and treated with or without atorvastatin for 12 weeks. Remarkably, the cholesterol content of the purified plasma membranes decreased at least 5-fold in the mice fed the high-fat diet relative to those fed the normal diet. Concomitantly, insulin binding decreased about 3-fold in the liver plasma membranes of mice fed the high-fat diet. This parallel decrease in insulin binding coincides with the findings in the cell culture study. The decrease in plasma membrane cholesterol content was almost entirely accounted for by an increase in the microsomal cholesterol content in the mice fed the high-fat diet. The mechanism underlying the cholesterol distribution induced by the high-fat diet is unclear and it requires further exploration.

Total liver cholesterol was unaffected by either diet or atorvastatin treatment of the mice. However, the low cholesterol content of the plasma membrane associated with the high-fat diet was reversed by atorvastatin treatment to levels observed in mice fed the normal diet. This again coincided with an increased binding of insulin to the plasma membrane to the level that was observed in mice fed the normal diet. This correlated with the changes to the apparent number of available insulin receptors in the plasma membrane as determined from both detailed binding analyses and Western blots of the insulin receptor in the liver plasma membrane of the mice. These observations collectively reiterate the strong association between membrane cholesterol on insulin binding observed in the cell culture study.

Whilst the concomitant changes in plasma membrane cholesterol and insulin binding correlated with the decrease in the apparent number of available insulin receptors, it is difficult to explain how or why the availability of the receptors changes. This availability of the receptor cannot be explained by the downregulation of receptors because changes in cholesterol and insulin binding were also observed in purified plasma membranes or in VLPs, which were derived from the plasma membrane of cells in culture. Cholesterol is integral to lipid-raft structures in the membrane and altering cholesterol levels in the plasma membrane disrupts these structures. This in turn may influence the localization of insulin receptors in various membrane micro-domains or potentially lead to the clustering of receptors and thus, affect insulin binding. The mechanisms describing the apparent availability of insulin receptors remain a mystery but should form a focus for future research.

Studies were also conducted on a novel membrane model known as virus-like particles (VLPs) generated from expression of lenti-viral Gag protein in CHO T10 (overexpressing insulin receptor) and wild type CHO cells (CHO K1). Insulin receptor bearing VLPs derived from CHO T10 cells were highly uniform in size distribution with an average diameter of about 150 nM as estimated by dynamic light scattering analysis and scanning electron microscopy. Insulin receptors in VLPs generated from CHO K1 and CHO T10 cells bound insulin with a similar affinity to that observed with their corresponding parental cell lines as described by competition binding analyses. The changes in membrane cholesterol following MBCD or cMBCD treatment and its effects on insulin binding in VLPs followed a similar pattern to that observed in their corresponding parental cell lines.

Almost all of the insulin receptors in CHO K1 cells (about 98%) were recovered in the VLPs generated in this particular cell line. Interestingly and by contrast, only 2% of the total insulin receptors in CHO T10 cells were recovered in the VLPs generated in these particular cells. Indeed, no significant difference in insulin receptor content was observed between VLPs derived from CHO K1 and CHO T10 cells as determined by Western blot analysis. As insulin receptors, upon activation by insulin binding, accumulate to the lipid rafts in the plasma membrane, it may be possible that the number of lipid-raft structures in CHO T10 cell membrane is inadequate to account for the enormous number of insulin receptors overexpressed in CHO T10 plasma membrane. Hence, by this postulate, the VLPs that egress from the lipid-raft regions in the plasma membrane harbour only those receptors that are localized in these regions of the membrane. Given that the insulin receptors function normally in the lipid rafts in the plasma membrane, the limitation in the localization of the insulin receptors in lipid-rafts could be one another possible reason for the observed disconnect in downstream signalling pathway in CHO T10 cells. Thus, the impact of receptor distribution in lipid rafts and other membrane micro-domains must be considered whilst employing overexpressing cell models for studying receptor function, especially for those receptor proteins that are associated with these micro-domains in the plasma membrane for their normal function such as the insulin receptors.

In conclusion, this Thesis demonstrated a strong influence of cell membrane cholesterol content on insulin binding to insulin receptors in numerous experimental

models including several cultured cell models, liver plasma membranes of high fat fed and atorvastatin treated mice, and insulin receptor bearing VLPs. The generation, characterization and application of the latter as a suitable model for study of insulin-insulin receptor interactions in context of the complexity of a cell membrane environment represents another novel aspect of this Thesis. The Thesis also discusses possible mechanisms underlying these findings and their implications in understanding insulin-insulin receptor interactions in the membrane's native environment. Additional and novel observations discussed in this Thesis also include the limitations of overexpressing cell models in receptor-ligand interaction studies, cell-type specific effects on insulin binding in response to changes in membrane cholesterol content, the effect of high-fat diet on plasma membrane cholesterol content and insulin binding.

ABBREVIATIONS

℃	Degress Celsius
AF	AlexaFlour
AKT	Protein Kinase B
BSA	Bovine serum albumin
B_{max}	Maximum binding
CPM	Counts per minute
DLS	Dynamic light scattering
ER	Endoplasmic reticulum
ERK	Extracellular related kinase
ELISA	Enzyme-linked immunosorbent assay
FBS	Fetal bovine serum
g	Gram
GAPDH	Glyceraldehyde 3-phosphate dehydrogenase
GLUT	Glucose transporters
GSK3β	Glycogen synthase kinase 3β
HMGCR	3-Hydroxy-3-Methylglutaryl-CoA Reductase
^{125}I	Iodine-125
IC_{50}	Half maximal inhibitory concentration
IR	Insulin receptor
IRS-1	Insulin receptor substrate-1
KDEL	K – Lysine; D – Aspartate; E – Glutamate; L – Leucine
K_D	Dissociation constant
kDa	Kilodalton
L	Litre
M	Molar

mM	Millimolar
MAPK	Mitogen activated protein kinase
mg	Milligram
ml	Millilitre
Na+/K+ - ATPase	Sodium-potassium adenosine triphosphatase
nM	Nanomolar
PAM	Plasma membrane associated membrane
PI3K	Phosphatidylinositol-3-kinase
pM	Picomolar
RTK	Receptor tyrosine kinase
SER	Serine
SDHA	Succinate dehydrogenase complex, subunit A
SEM	Scanning electron microscopy
SPR	Surface plasmon resonance
THR	Threonine
TYR	Tyrosine
VLP	Virus-like particles
µg	Microgram
µl	Microlitre
µM	Micromolar

1.0. LITERATURE REVIEW

Diabetes mellitus comprises of a group of metabolic disorders characterized by chronic hyperglycemia. According to the atlas of the International Diabetes Federation, 2017, there are approximately 415 million adults affected by this disease. The number is expected to increase to ~ 642 million by 2040 [1]. The rise in the number of cases and lack of cost-effective treatment make this global pandemic a serious health and economical issue. The disease is classified into two main types (Type 1 and 2 Diabetes Mellitus), a clear distinction between which was made in 1936 [2]. Although diabetes is one of the oldest diseases known to mankind, the complexity of this disorder is not yet fully understood.

1.1. Pathophysiology of diabetes mellitus

Type 1 diabetes mellitus is characterized by a failure of adequate insulin secretion by the pancreas in response to an increase in blood glucose. It is an autoimmune disorder that results in the destruction of the pancreatic β-cells which are responsible for insulin secretion [3]. The factors that initiate this autoimmune condition are not clearly understood, however, environmental and genetic factors contribute to its development [4].

Type 2 diabetes mellitus is the more commonly occurring form of the disease accounting for about 95% of all diabetics. It is characterized by decreased insulin sensitivity at target tissues as a result of insulin resistance as well as decreased production of insulin due to pancreatic β-cell dysfunction [5]. The development of type 2 diabetes mellitus involves a complex interplay between genetic and environmental factors. Risk factors can be categorized into modifiable factors such as diet and sedentary life-style and non-modifiable genetic factors [6].

1.2. Structure and function of insulin and insulin receptor

1.2.1. Insulin

Insulin, secreted by pancreatic β-cells, plays a pivotal role in the regulation of cell metabolism, growth and division. The molecular mass of insulin is 5808 Da. The molecular structure of monomeric insulin comprises of two chains; an A-chain that consists of 21 amino acid residues and a B-chain that consists of 30 amino acid residues. Amino acids such as leucine and isoleucine cluster in the middle forming

the hydrophobic core. Charged amino acids such as arginine and glutamate cover the surface, contributing to water solubility. The secondary structure of the A-chain and B-chain include three α-helices (amino acid residues A1 to A8, A12 to A18 and B9 to B19) [7]. The two chains are linked by two inter-chain (A7-B7 and A20 – B19) and one intra-chain (A6 – A11) disulphide bonds. These disulphide linkages were shown to be involved in the self-association of insulin and the binding of insulin to the insulin receptor [8].

The self-association of insulin is essential for the stability of the molecule during storage in pancreatic β-cells and when secreted into blood [9]. In 1926, the 3-dimensional structure of insulin was elucidated using X-ray crystallography and since then, the contribution of 2-D NMR studies led to development in the knowledge of monomeric and multimeric forms of insulin [10, 11]. Insulin dimerizes at micromolar concentrations and in the presence of zinc (10 mM Zn^{++}), and at favourable pH 6.0, it self-assembles into higher-order conformations such as hexamers [12]. Insulin is stored in pancreatic β-cells as granules consisting of insoluble crystalline hexamers, with the six molecules of insulin arranged as three dimers [13]. The antiparallel β-sheets at the carboxy-terminus of the B chain on each monomer play a key role in the formation of the dimeric form of insulin. While these β-sheets are exposed to the outer surface of the insulin dimers, two nonpolar surfaces at the interface of the dimers form the hydrophobic core. One of two nonpolar surfaces is buried by a β-pleated sheet structure and the other extensive surface becomes buried when dimers associate to form hexamers [11, 12]. The same surface that is involved in self-association is also shown to be involved in receptor binding [7, 14].

1.2.2. The insulin receptor

Insulin receptors are transmembrane signalling proteins that belong to the family of ligand-activated receptor tyrosine kinases (RTKs) [14]. The insulin receptor has a role in several important physiological functions such as cell growth, differentiation and metabolism. The additional role of the insulin receptor in regulating cell metabolism makes it unique from other families of receptor tyrosine kinases such as epidermal growth factor receptors and fibroblast growth factor receptors that are involved only in cell growth and/or differentiation. Structurally, the unique feature of the insulin and closely related receptors (eg; insulin-like growth factor receptor,

IGF-R) among other receptor tyrosine kinases is their ability to form covalently linked functional dimers facilitated by disulphide bonds [15]. The unique structure and sub-unit composition of the insulin receptor are detailed below.

The insulin receptor is comprised of two α subunits that lie completely in the extracellular region and two β subunits that extend from the extracellular region (segment involved in disulphide bond formation with α-subunits) through the plasma membrane to the intracellular region (segment that includes the tyrosine kinase domains) spanning the bilayer with a single transmembrane link [16]. Each α-subunit comprises 723 amino acids with a molecular mass of 130 kDa and each β-subunit comprises 620 amino acids with a molecular mass of 95 kDa [17]. Each α-subunit is linked with a β-subunit forming two αβ-monomers, which link to form functionally active $(\alpha\beta)_2$-homodimers. These linkages are facilitated by two different classes of disulphide bonds (S-S). Class I disulphide bonds link the α-subunits of the homodimer and can be reduced under mild reducing conditions to give two αβ-monomers. Interestingly, these αβ-monomers bind insulin but with lower affinity than the holoreceptor, a structurally complete and functional state of the receptor [18]. Class II disulphide bonds between αβ monomers require stronger reducing conditions to form individual α and β subunits [19, 20]. Following synthesis, each disulphide linked αβ monomer, that is heavily glycosylated (N-linked), is transported to the plasma membrane and positioned in such a way that the whole α-subunit and 194 residues of the β-subunit lie in the extracellular region and comprises the ectodomain (extracellular region) of the mature receptor [21].

Typically, the αβ ectodomain comprises six domains; L1 (large domain 1), CR (cysteine rich domain), L2, three FnIII (fibronectin type III) domains (Fn_{0-2}), an insert domain (ID) that splits the middle FnIII domain and includes the carboxy terminal of the α-subunit (α-CT) and the amino terminus (N-terminal) of each β-subunit [14]. The intracellular region of the β-subunit includes the juxtamembrane portion containing the kinase catalytic domain and docking sites for insulin receptor substrates. A carboxy-terminal tail of the β-subunits includes two phopshotyrosine binding sites [9].

1.2.3. Insulin receptor synthesis and its isoforms

The insulin receptor is encoded by a single 22-exon gene located on chromosome 19; the mature receptors exist in two different isoforms, the A and B isoforms resulting from an alternative splicing of the primary transcript [22, 23]. The maturation process of the receptor involves synthesis of α and β subunits as a single precursor polypeptide (proIR) [24]. In the process of maturation in golgi compartments, this precursor polypeptide is cleaved on the carboxyl side tetrabasic amino acid sequence (Arg-Lys-Arg-Arg735) located at the junction between two subunits [16]. Though there are several endoproteases being linked in the maturation of membrane proteins such as the insulin receptors, furin, a major pro-protein convertase that is found in the trans-golgi network is shown to be involved in the cleavage of protein precursors [25, 26].

The two isomeric forms (IR-A and IR-B) differ slightly in their amino acid composition and physiological functions [27], and their distribution is regulated in a tissue-specific manner [28]. The absence (A-isoform) or presence (B-isoform) of the additional 12 amino acid sequence encoded by exon 11 makes the isoforms structurally and functionally distinct [28]. Isolation and characterization of human insulin receptor cDNA predicted the sizes of proreceptors of A and B isoforms to be 1343 and 1355 amino acid residues, the difference in sizes being due to the absence or presence of a 12-amino acid segment at the carboxy-terminal end of the insulin receptor α-subunit [22, 29, 30]. The maturation process of both these isoforms *in vitro* by recombinant furin was very similar [31]. However, a detailed statistical analysis of furin cleavage sites investigated within the 3D crystal structure of the furin catalytic domain suggested that the cleavage sites for furin extend beyond the tetrabasic consensus sequence up to 20 amino acids [32]. The extended sequences identified as the cleavage sites for furin included 10 amino acids of IR-B exon 11 which suggest that the recognition sites for cleavage can differ from IR-A [33]. In addition to furin, there are other proprotein convertases reported to be involved in the maturation that are specific to the isoform of the insulin receptor. This distinction in the maturation process is thus linked to the structural and functional differences between the A and B-isoform of the insulin receptors [33].

It is widely accepted that alternative splicing of the insulin receptor can be specific to cell type. Additionally, the relative abundance of the two isoforms varies with

development, aging and different disease states [34]. The A-isoform, dominant during the fetal and early developmental stages, is ubiquitously present during adult stages, whereas the proportion of B-isoform is higher in liver, kidney, skeletal muscle, adipose tissue and pancreatic-beta cells [35]. The affinity of the B-isoform of the insulin receptor for insulin is about two-fold higher than that for the A-isoform. Additionally, a relatively higher rate of internalization and recycling has been observed for the A-isoform receptor compared to the B-isoform [36, 37], however this observation remains inconclusive with contradictory evidence [38]. The factors that determine the relative abundance of the isoforms across various tissue types are currently unknown.

Following the first report made on the insulin receptor isoforms [16], several studies emerged that investigated the significance of the structural differences to their functions and the consequence of defects in the maturation process of these isoforms in the development of diabetes [39-41]. Increasing knowledge about the differences in the function between these isoforms reveals a correlation with their distribution in various tissues [42].

1.3. Insulin – Insulin receptor interaction

Since the insulin receptor was first characterized biochemically using ^{125}I radioligand binding studies in the early seventies, numerous studies over several decades have helped unravel the downstream signalling mechanism of insulin [21]. However, the molecular events underlying this interaction and influences of the membrane environment on this interaction remain elusive. Though the latter aspect forms the basis of the current study, existing knowledge of the possible molecular events facilitating the insulin-insulin receptor interaction is briefly addressed below.

It is known that the insulin molecule binds the preformed dimeric insulin receptor with a sub-nanomolar affinity which leads to autophosphorylation of the receptor and subsequent initiation of the intracellular signalling events. However, knowledge about the molecular events involved in the insulin-insulin receptor interaction and conformational changes leading to autophosphorylation are still being studied. Insulin binding to cell membranes, as analyzed by Scatchard plots, showed curvilinear binding isotherms which was interpreted as an indication of negative cooperativity since there was limited knowledge available on the structure and

composition of the insulin receptor [43]. However, this interpretation led to several controversies which were mitigated soon after the realization of its possible capacity to bind two insulin molecules due to the dimeric structure of the functional insulin receptor [13].

Affinity labelling studies with insulin and its analogues identified only the α-subunits of the insulin receptor and therefore, the ligand-receptor complex was believed to occur in this subunit [13]. Studies based on three dimensional structure of the insulin receptor ectodomain using x-ray crystallography showed an "inverted V" arrangement of α-subunits where the first three domains; L1-CR-L2, form one leg and three FnIII domains of the α-subunit form the other leg [44, 45]. The domain arrangement derived from the crystal structure suggested two potential ligand binding sites with varying affinity for insulin (site 1: low affinity and site 2: high affinity) and that site 2 may involve one or more FnIII domains [46, 47]. This was later confirmed by a study based on four crystal structures of insulin bound to truncated insulin receptor constructs. This study showed minimal direct interaction between the L1 domain of the insulin receptor and the insulin molecule, and the hormone's propensity to engage with the α-CT segment.

The interaction of insulin with the insulin receptor leads to two structural transitions, one in the insulin molecule: the residues at the C-terminus in the insulin B-chain are inverted against the other residues and are displaced on binding to α-CT segment of the receptor [48]. The other structural modification to favour the interaction occurs in the insulin receptor: the apo structure of the receptor, i.e., during the unbound state, the α-CT linkage can only be seen with the L1 domain. On the event of insulin binding, this linkage encounters a conformational change to rearrange the α-CT helix such that it binds both L1 and insulin [7]. This understanding also explains the changes in conformation of the insulin-insulin receptor complex which limit the contact of insulin with the L1 domain of the insulin receptor to only insulin's B-chain residues [7]. The above-mentioned conformational changes in the receptor and formation of a hormone-receptor complex were demonstrated to be closely linked with initiating the cross-phosphorylation of the kinase domains of β-subunits in the juxtamembrane region [7, 48].

1.4. Limitations of currently used membrane models

The interaction of insulin with the insulin receptor has mostly been evaluated using detergent-solubilized or truncated insulin receptor constructs [15]. These conventional approaches provided information on (i) the interaction of insulin with the ligand binding sites on the insulin receptor, (ii) allosteric regulatory properties of insulin and (iii) the mode of receptor autophosphorylation, however, they did not consider the influences of dynamic associations of membrane lipids and cholesterol with the insulin receptor in the course of this interaction [15, 49]. Insulin receptors, like most other transmembrane proteins, when solubilized may likely lose potential interactions with other membrane proteins and lipids that may have some key regulatory functions [50, 51]. Therefore, it becomes essential to employ a model that enables us to consider the influence of the functional membrane lipid environment and the native conformation of receptor proteins while studying the characteristics of insulin-insulin receptor interaction.

1.4.1. Virus-like particles

Transmembrane proteins such as insulin receptors consist of an integral membrane component which is tightly associated with the dynamic lipid-bilayer [49]. There is evidence that failing to consider this protein-lipid interplay could make it difficult to study their molecular interaction or may lead to wrong conclusions [49, 52]. The recent use of a novel cell membrane model known as virus-like particles (VLPs) enables receptor-ligand interactions in a protein's native conformation [53], and could be employed to study insulin receptor function.

VLPs are uniform, nano-sized spherical particles that extrude from the cell membrane of a host cell in a manner similar to that of a retroviral budding process [54]. VLPs are generated by co-expressing the membrane protein of interest and a retroviral core protein (Gag) in mammalian cells. The Gag protein self-assembles to form multimers and extrudes from the host cell with an intact portion of the cell membrane, complete with receptors and other membrane proteins in their native conformation (Fig. 1) [55]. Thus, unlike other membrane models, preparation of VLPs does not involve mechanical disruption or the use of solubilizing detergents. VLPs were known to extrude from specific regions of the plasma membrane that are rich in cholesterol. The effects of plasma membrane cholesterol content on viral protein

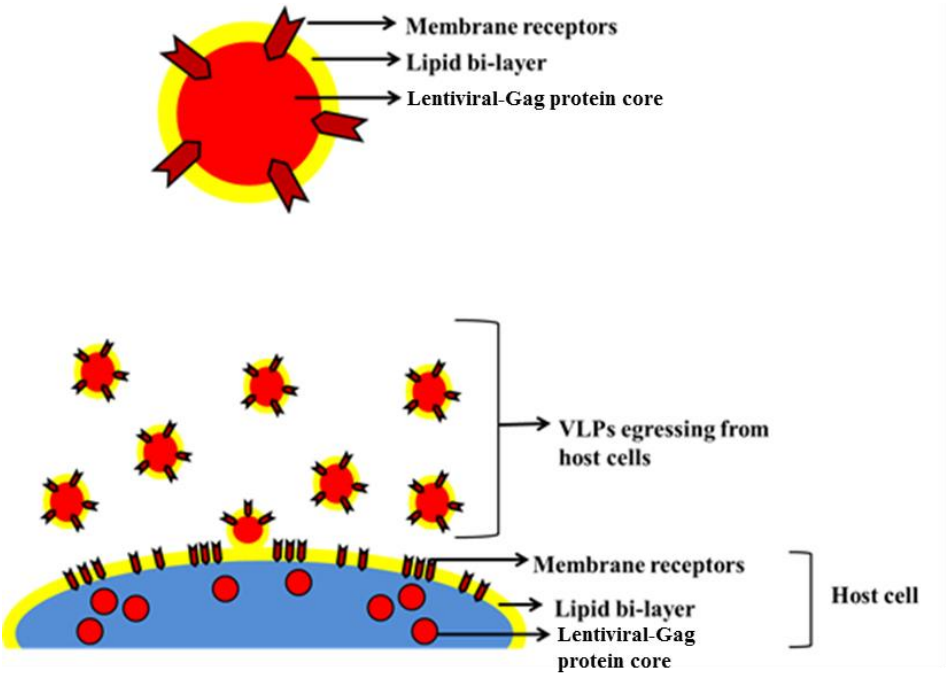

Figure 1. The generation of virus-like particles (VLPs) from cultured cells. VLPs consisting of an intact cell membrane portion with membrane proteins in their native conformation.

Picture adapted from the website of Integral Molecular. (http://www.integralmolecular.com/application-notes.php#tab_lipoparticle)

assembly, budding and, therefore on viral replication processes have been addressed in several studies [56-59]. VLPs offer many advantages over conventional models for studying membrane protein interaction mechanisms. VLPs are reportedly stable and viable at a range of different temperatures (-80 °C, – 20 °C, 4 °C or 25 °C) and have a considerably longer shelf-life. Furthermore, it was estimated that the target receptor protein concentration in the VLPs is 10 to 100 fold more than what can be found in cells [54]. VLPs are also uniform in size and shape making them a suitable candidate model for detailed receptor-ligand studies using optical biosensor platforms such as surface plasmon resonance (SPR) [53].

1.5. Insulin signalling

Insulin, secreted by pancreatic β-cells in response to a postprandial increase in blood glucose, mediates its effect by binding to the insulin receptor on the cell membrane of target tissues. This ultimately promotes numerous metabolic processes including glucose uptake for energy production or storage (Fig. 2) [60]. The signalling pathway is initiated by the binding of insulin to the extracellular domain of the insulin receptor [61]. Insulin binding to the receptor α-subunit triggers transphosphorylation between β-subunits at specific tyrosine residues, in an activation loop which results in an increase in kinase catalytic activity [62]. Additionally, the receptor also undergoes autophosphorylation at a number of specific tyrosine residues present in the juxtamembrane region of the β-subunit [61].

The binding of insulin to the insulin receptor and its subsequent activation further activates a family of membrane-associated insulin receptor substrate proteins (IRS1 to 4) by tyrosine phosphorylation. This further activates phosphatidylinositol-3 kinase (PI3K). This enzyme catalyzes the synthesis of phosphatidylinositol (3,4,5)-trisphosphate (PIP_3) by phosphorylation of phosphatidylinositol (4,5)-bisphosphate (PIP_2) [62]. The increase in PIP_3 levels leads to the recruitment of proteins containing pleckstrin homology (PH) domain, including phosphoinositide-dependent kinase 1 or PDK1 [63]. Activation of PDK1 is crucial for the activation of Akt (protein kinase B) which, after specific steps, leads to the translocation of a pool of glucose transporters (Glut) to the membrane and facilitates glucose uptake [64].

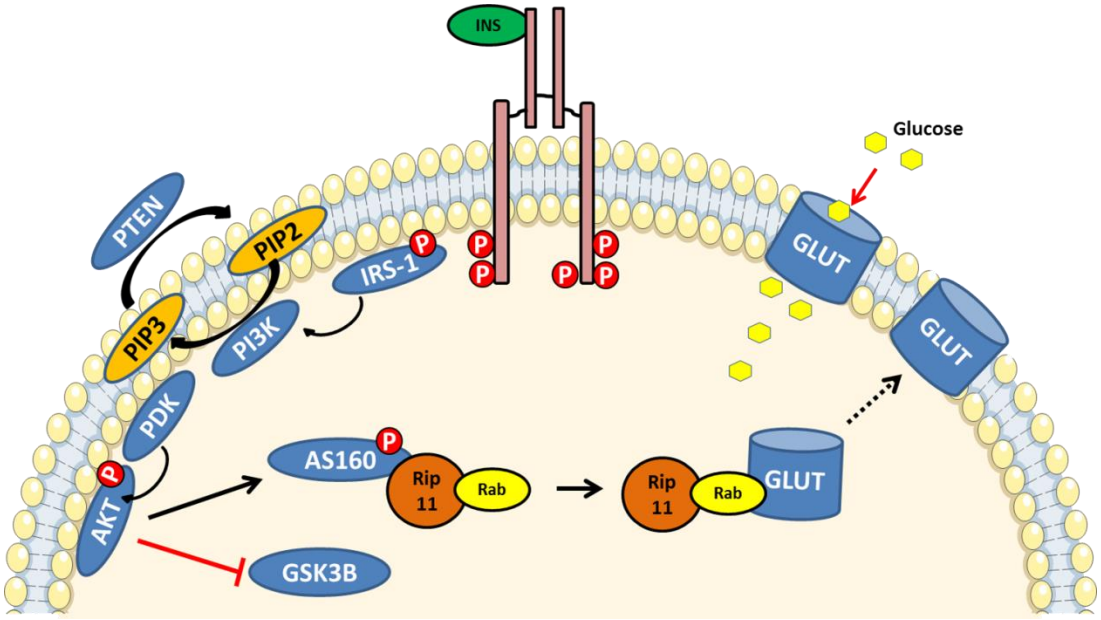

Figure 2. The key metabolic aspects of the insulin signalling pathway

The sequence of events is shown in an anti-clockwise direction. INS – insulin, IR – insulin receptor, p - phosphorylation, IRS-1 – insulin receptor substrate-1, PI3K – phosphotidyl-inositol 3 kinase, PTEN – phosphatase and tensin homolog, PDK-1 - phosphoinositide-dependent kinase 1, AKT – protein kinase B, GSK3β – glycogen synthase kinase 3β, PIP2 - phosphatidylinositol (4,5)-bisphosphate, PIP3 - phosphatidylinositol (3,4,5)-trisphosphate, AS160 – Akt substrate, Rip11 – Rab11 interacting protein, GLUT – glucose transporter.

While the above process describes the metabolic aspect of insulin signalling pathway, the other principal component of insulin signalling in cells is the regulation of growth-related gene expression via the Ras/MAP kinase pathway or the mitogenic aspect [65]. The growth signalling in cells in response to insulin binding to its receptor is initiated by the recruitment of adaptor/guanine nucleotide exchange factor (Grb2/SOS) complexes at Shc and insulin receptor substrates (IRS-1/2). This leads to the activation of small GTPase Ras which initiates a cascade of phosphorylation events resulting in the activation of MAP kinase. Activation of MAP kinase then leads to phosphorylation of various substrate proteins that promote the transcription of genes and synthesis of proteins involved in cell growth, differentiation and survival [42, 65]. Further to influences on receptor-ligand interactions, changes in membrane lipid composition also influence signalling events that occur in association with the plasma membrane. Some of the key signalling events pertinent to the insulin signalling pathway, such as activation by transphosphorylation at β-subunits of the insulin receptor, activation of IRS-1/2 and PI3K, conversion of PIP3 to PIP2, activation of Akt by PDK-1 and translocation of the glucose transporters that occur in or adjacent to the plasma membrane were found to be impaired as a consequence of alterations in membrane cholesterol content [49, 66, 67]. The importance of plasma membrane composition/environment is the central aspect of this Thesis and is thus discussed below.

1.6. The plasma membrane environment

The lipid bi-layer structure of the plasma membrane is a dynamic environment that enables constant movement of lipids and membrane associated proteins. It enables several vital physiological transport mechanisms and forms the cytoplasmic boundary for all cells. It acts as a physical barrier between cells and controls the movement of substances into or out of cells [68]. The structure and organization of plasma membrane can be explained by the ‘fluid mosaic model’, first described by Singer and Nicholson in 1972 [69].

According to this model, the principal components of plasma membrane are amphiphilic phospholipids which consist of a polar phosphate head group and non-polar tail group. Due to their amphiphilic nature, the phospholipids are spontaneously organized in a most thermodynamically stable configuration, with the polar head groups of the phospholipids facing the aqueous environment (intracellular or

extracellular side) and non-polar tail groups maximizing hydrophobic interactions [70]. This arrangement forms the basis of the phospholipid bi-layer structure of cell membrane.

1.6.1. Cell membrane phospholipid composition

The four main phospholipid components of cell membranes are phosphotidylcholine, phosphatidylethanolamine, phosphatidylserine and sphingomyelin. An additional fifth type known as phosphoditylinositol is a minor component [71]. However, the distribution of different types of phospholipids between the outer and inner leaflets of the lipid bi-layer is asymmetrical. Phosphotidylcholine and sphingomyelin compositions dominate the outer leaflet whereas the most prevalent phospholipids of the inner leaflet are phosphatidylethanolamine and phosphatidylserine [71, 72].

The distribution of different types of membrane lipids in the inner and outer leaflets of the cell membrane is determined by the difference in nature and structure of various lipids that form the bi-layer [73]. For example, phosphatidylserine and phosphoditylinositol, unlike sphingomyelin and phosphotidylcholine, carry negative charges in their phosphate heads and their distribution in the inner leaflet of the cell membrane is responsible for the overall negative charge in the cytosolic or inner leaflet. Differences in the arrangement and distribution of lipids contributes to the physical characteristics of the membrane such as the curvature of the membrane; for example, phosphotidylcholine that accounts for ~ 50% of the total phospholipid content of the cell membrane in most eukaryotes, has a near cylindrical geometry whereas phosphatidylethanolamine has a conical geometry in the bi-layer due to its smaller polar head groups relative to non-polar tails. Therefore, the distribution of phosphatidylethanolamine adjacent to phosphotidylcholine imposes a curvature stress on to the membrane that aids in vital cell to cell communications such as budding, cell fission and fusion [73, 74].

1.6.2. Cholesterol – structure and membrane topology

In addition to the above-mentioned lipids, mammalian plasma membrane also contains cholesterol, which is the major sterol in the body. The biosynthesis of cholesterol takes place in the endoplasmic reticulum (ER) of the cell and its transport to the plasma membrane is facilitated by numerous membrane associated proteins including caveolin [75]. A loss in the regulation of cell cholesterol distribution

between plasma membrane and other organelle membranes is associated with several metabolic disorders [76]. The vast majority of a cell's free cholesterol (i.e., unesterified cholesterol) is located in the plasma membrane and the remainder is found embedded in organelle membranes [77]. Structural aspects of the cholesterol molecule contributing to its overall hydrophobicity and the way these molecules interact with membrane phospholipids are addressed below.

The structure and function of cholesterol was not well understood until the late 19th century. Although first identified in 1789 in its solid form in gall stones, the complexities in its biosynthetic mechanisms and structural assembly were still being discovered throughout the 20th century [78, 79]. The polar region of this polycyclic amphipathic molecule consists of a single hydroxyl group. The remaining structure consists of four rigid hydrocarbon rings having a sterane backbone and an isooctyl sidechain that is strongly hydrophobic or non-polar [80]. The polar hydroxyl group of a cholesterol molecule is relatively smaller than the non-polar region and is thus unable to sufficiently protect the hydrophobic regions in an aqueous environment. For this reason, when introduced in aqueous solutions, free cholesterol molecules form cholesterol monohydrate crystals [81]. Therefore, despite its amphipathic nature, cholesterol molecules cannot form a bilayer in a biological environment and instead tend to interact with membrane lipids [82, 83]. The structure of the hydrophobic region of a cholesterol molecule possesses an asymmetry with two distinct faces, referred to as α and β faces [80, 84]. The β-face has a relatively significant irregular surface due to the presence of two methyl groups and a short eight carbon chain (iso-octyl chain) attached to C-17 of the sterane backbone whereas the α-face displays a flat or planar surface with no substituents [85, 86].

Structure – function relationship

The most important structural role of cholesterol in cellular membranes is its contribution to membrane strength and permeability. It not only limits membrane permeability to water and dissolved gases [87-89], but also controls the lateral diffusion of membrane lipids and proteins [90] by which it regulates the fluidity and phase transition properties of the membrane [91].

The importance of the structural arrangement of cholesterol and its associations with various membrane lipids have been identified in ordering and condensation of lipids

in the membrane [92, 93]. The structure of cholesterol includes a four ring steroid group out of which three are six-carbon rings and one is a five-carbon ring. The rings connected in *trans* orientation forms the flat, smooth and planar surface (α-face) while methyl substituents at the 10^{th} and 13^{th} position in relative *cis* orientation forms the rough surface (β-face), thus leading to an asymmetry in structure. The structure of cholesterol differs from structures of other sterols such as desmosterol and lanosterol in its limited addition of substituents to α and β faces and the presence of only one double bond between C-5 and C-6 in ring B [94].

1.6.3. Interaction of cholesterol with membrane lipids and proteins

The structural factors of phospholipids that influence cholesterol positioning in the bilayer are; head group structures, the length of hydrocarbon chains and the degree of unsaturation of the latter [95-97]. The orientation of cholesterol in the lipid bilayer is based on the interaction of its hydroxyl group and hydrophobic regions with the phosphate and hydrocarbon tail of the phospholipids, respectively [98]. The interactions of cholesterol with phosphatidylcholine and sphingomyelin, the most abundant phospholipids in cell membranes, have been well studied and the latter forms the basis of sphingolipid-cholesterol rich membrane microdomains known as lipid-rafts [99]. Studies on structural aspects of the interaction between cholesterol and phospholipids reveal there is a hierarchy to these interactions, with the interaction between cholesterol and sphingomyelin being more favourable than that with phosphatidylcholine due to the presence of saturated acyl chains and a *trans*-unsaturated sphingosine backbone which maximizes the Van der Waals interactions [100].

The umbrella model, proposed to explain cholesterol-lipid interactions, suggests that the four hydrocarbon rings of the cholesterol molecule that are strongly hydrophobic cannot be sufficiently shielded by the small, polar headgroup; therefore, association with large head-groups of phospholipids such as phosphotidylcholine and sphingomyelin becomes necessary for its positioning in the bi-layer [83]. Through these interactions, cholesterol also increases the order of saturated acyl chains of phospholipids therefore leading to a decrease in surface area of the lipids (lipid ordering effect) [85]. The surface area of the lipid bilayer in the presence of cholesterol is less than the sum of surface areas of individual components of the lipid

bilayer [101]. Also, cholesterol increases the surface density (condensing effect) of the membrane by decreasing its permeability [86, 102].

The bulky hydrophobic sterol rings and relatively smaller hydroxyl head group only confers a weakly amphipathic nature to the molecule [103]. A rise in cholesterol content of the bilayer results in an inadequate protection from the adjacent aqueous environment for the hydrophobic regions of the newly added cholesterol molecules. This consequently leads to the lateral redistribution of phospholipids and reorientation of their polar head-groups [82]. There exists a similar concept for lipid-protein interactions in the bilayer which is crucial for the stability and functioning of the membrane-bound proteins [104].

Similar to its interaction with lipids, cholesterol also interacts with proteins within transmembrane (TM) domains. The hydroxyl group of cholesterol can form hydrogen bonds with the polar group of the membrane protein whereas the aliphatic spikes on the rough β-face can bind to the side-chains of branched amino acids such as Ile, Val or Leu in the protein through Van der Waals interactions [105]. It is important to note that the association of cholesterol with a specific type of phospholipid in the bilayer can in turn influence its association with membrane proteins and thereby the functional aspect of that protein. For example, the interaction of cholesterol with phosphatidylcholine leaves both α and β faces available for interaction with the transmembrane domain of membrane proteins [84]. Additionally, the inadequate shielding for the hydroxyl group of cholesterol in phosphotidylcholine-cholesterol complexes favours its establishment of a hydrogen bond with the transmembrane domain of a membrane protein.

Alternatively, when complexed with sphingolipids (glycosphingolipids) cholesterol forms condensed lipids [106]. In this complex, the hydroxyl group of cholesterol forms a stable hydrogen bond with the polar head group of the sphingolipid whereas the smooth α-face of cholesterol interacts with the hydrophobic tails. The flexible acyl chain of phospholipids aligns effectively to complement the neighbouring cholesterol molecule to maximize the hydrophobic interactions and enable tight packing [107]. This leaves the rough β-face available for interaction with transmembrane domains of membrane proteins [108, 109]. Therefore, the difference in types of lipids between exofacial and cytoplasmic leaflets of the membrane and

preferential complexing of cholesterol with sphingolipids causes an asymmetry in the trans-bilayer distribution of cholesterol. This means that the accessibility of cholesterol for membrane protein interaction can be limited in the exofacial leaflet of the bilayer due to its higher sphingolipid content.

In addition to the advantages of cholesterol-lipid complexes in membrane protein-cholesterol interactions, the role of trans-bilayer cholesterol dimers leading to the activation of membrane protein by dimerization eg; G-protein coupled receptor, has been described [110]. Cholesterol dimerizes in the bilayer in two distinct ways through Van der Waals interactions; formation of trans-bilayer tail-to-tail dimers [111] and interaction of the planar α-faces leaving the β-faces of cholesterol molecules available for protein interactions [110]. Nevertheless, the membrane-spanning domain of the proteins and presence of cholesterol in both the leaflets in different orientations provides a large scope for specific interactions between cholesterol and cholesterol recognition motifs on the transmembrane domains of proteins in the bilayer [112].

1.7. Cholesterol synthesis and distribution in cells

Cholesterol biosynthesis

Cholesterol can be acquired by our body in two ways; either by *de novo* synthesis or from dietary intake. The production of cholesterol is highly regulated in the body such that when dietary intake of cholesterol is low, the *de novo* synthesis is upregulated and conversely, when the intake is high, excretion of cholesterol increases and the rate of synthesis decreases [78, 113]. In 1926, Heilbron, Kamm and Owens suggested that squalene is the precursor of cholesterol. However, Konrad, Bloch and Robert Langdon, in 1952, demonstrated that acetate is a more proximal precursor for both squalene and cholesterol. The biosynthesis of cholesterol is a complex process involving more than 20 enzymes and occurs in various subcellular regions such as cytosol, endoplasmic reticulum (ER) and peroxisomes. Due to the involvement of hydrophobic enzymes, substrates and products in the final steps of the biosynthetic pathway, synthesis partially occurs in the membrane environment [78].

The first phase of the cholesterol biosynthetic pathway involves the production of mevalonate from acetate. This occurs in the presence of an acetyl-coenzyme A

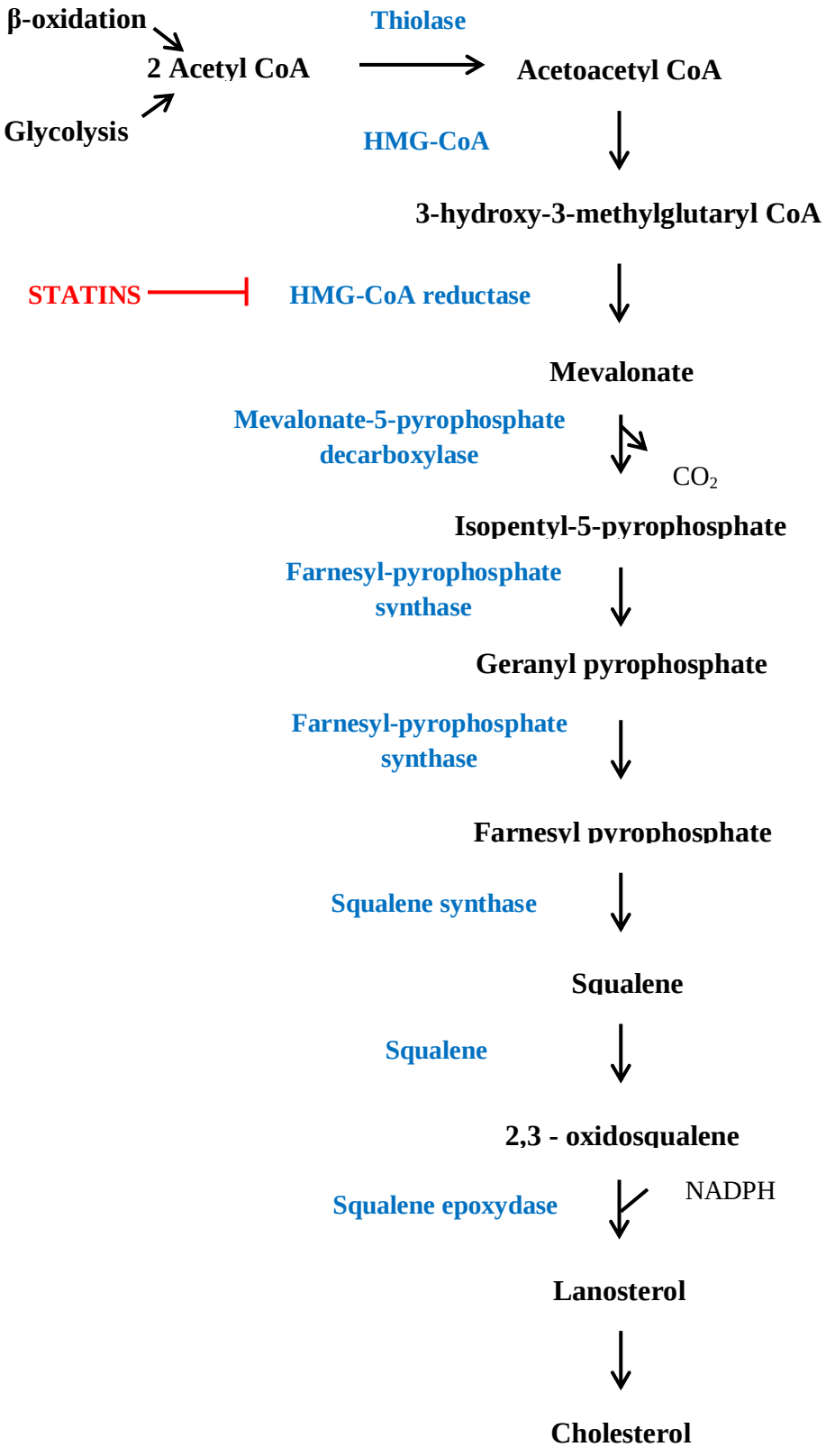

Figure 3. Cholesterol biosynthetic pathway

acetyltransferase (ACAT) enzyme known as thiolase, which catalyzes the condensation of two molecules of acetyl-coenzyme A (acetyl-CoA) to form acetoacetyl-CoA. HMG-CoA synthase catalyzes the addition of the third acetyl-CoA to acetoacetyl-CoA, which results in the formation of 3-hydroxy-3-methylglutaryl CoA (HMG-CoA). As a final step in the first phase, HMG-CoA is reduced to form mevalonate by HMG-CoA reductase (HMGCR) in the presence of the cofactor, NADPH. This reaction is catalyzed by HMGCR and is the rate limiting step in the biosynthetic pathway [78, 114].

Subsequently, mevalonate undergoes a series of phosphorylation steps and ATP dependent decarboxylation to form isopentynyl pyrophosphate (IPP), which is an activated isoprenoid molecule. Then, IPP undergoes 1:1 condensation with its isomer, dimethyl allylpyrophosphate (DMPP) to form geranyl pyrophosphate (GPP), which further condenses with one IPP molecule to generate farnesyl pyrophosphate (FPP). In the presence of squalene synthase and NADPH, head-to-tail condensation of two FPP molecules yields a 30-carbon molecule, squalene. Squalene, the precursor of all steroids, undergoes further cyclization processes, catalyzed by squalene monooxygenase and squalene 2,3-epoxidase enzymes, and this results in the formation of lanosterol [115]. Then, lanosterol undergoes a series of nineteen steps, in the presence of nine different enzymes, to form the 27 carbon molecule, cholesterol [116].

Cholesterol distribution in membranes

The preferential localization of cholesterol molecules in cellular membranes and their orientation dynamics with membrane lipids were discussed earlier in section 1.5.3. The distribution of cholesterol in cells and their trafficking within and between cells are tightly regulated by various cellular mechanisms. Cholesterol in cells is heterogeneously distributed among plasma membrane and other cellular membranes. While highly concentrated in plasma membranes, cholesterol is also found abundantly in intracellular vesicles, in increasing amounts from the cis to trans region of the golgi apparatus [117] and is in least abundance in the endoplasmic reticulum [118]. The processing steps of newly synthesized cholesterol are highly regulated and occur across various subcellular regions hence the transport of cholesterol between these regions is also crucial. The transport of cholesterol within

and between cells has been long known to occur via both vesicular and non-vesicular transport [119]. While a lot is known about endocytic, exocytic and luminal transport of cholesterol between and inside cells [120, 121], knowledge about the molecular mechanisms involved in the non-vesicular transport of cholesterol and lipids has not been well described [122-124]. However, over the last decade, knowledge has accrued on sterol binding proteins and their ability to transfer sterols in a membrane specific manner [125-128].

Compared to all other cellular membranes, the plasma membrane has the highest content of free or unesterified cholesterol [118]. Additionally, the amount of cholesterol relative to membrane lipids in plasma membrane was estimated to be ~ 35 mol% whereas it is ~ 5 mol% in endoplasmic reticulum (ER) [129]. The cholesterol content in intracellular membranes can be manipulated with exogenously applied interventions that alter plasma membrane cholesterol content such as desorption by cyclodextrins (CD) [130, 131]. Indeed, studies have suggested that reduction in plasma membrane cholesterol content could reflect on the ER cholesterol content, which may regulate a homeostatic mechanism upstream of ER so as to replenish the loss in plasma membrane [131, 132]. Lange *et al* (1999) demonstrated a concomitant reduction of ER cholesterol by 80% following a reduction in plasma membrane cholesterol by 25% when treated with 2% hydroxypropyl-β-cyclodextrin. Taken together, these findings may suggest that the changes in ER cholesterol levels as a consequence of changes in plasma membrane cholesterol content could be homeostatic mechanisms that occur to replenish the loss in plasma membrane cholesterol content.

1.8. Membrane cholesterol alterations by cyclodextrins

The preference of cells to maintain optimal plasma membrane cholesterol content at the cost of relative changes in intracellular membrane cholesterol content indicates the significance of cholesterol in plasma membrane functionalities. The influence of changes in plasma membrane cholesterol on membrane stability, receptor functioning and organelle functions have associations with the pathophysiology of metabolic disorders [133-135] and cancer [136-138]. This awareness of the physiological importance of plasma membrane cholesterol content eventually led to an increase in studies that involved manipulation of membrane cholesterol to study the impact on various aspects of membrane function [139].

The most common method to manipulate membrane cholesterol uses cyclodextrins, a class of pharmacological compounds known for their high affinity for cholesterol and ability to sequester cholesterol [140]. Cyclodextrins are cyclic oligosaccharides that are degradation products of starch. Their ability to completely dissolve in water and still sequester hydrophobic compounds accounts for their long recognition as effective carriers of hydrophobic drugs [140, 141]. Cyclodextrins exist as α (hexamer), β (heptamer) and ϒ (octomer) forms and their degree of oligomerization accounts for the size of the hydrophobic cavities, which in turn determines the overall hydrophobicity of different forms of cyclodextrins [141, 142].

β-cyclodextrins, compared to other forms, have the highest affinity for cholesterol [142, 143]. With a high affinity for cholesterol, β-cyclodextrin, among the three forms, is the least water-soluble form [140]. However, its solubility in water significantly increases in derivatives that include hydrophilic modifications such as methylated and 2-hydoxypropylated derivatives [141]. Therefore, in this study, methyl-β-cyclodextrin (MBCD), which features the highest affinity for cholesterol and complete solubility in water, was used to alter membrane cholesterol content of cells and model membranes (VLPs).

The ability of MBCD to effectively alter membrane cholesterol arises from a combination of its properties; high solubility in water, an ability to directly access the plasma membrane of cells, the presence of a hydrophobic core that has high affinity for cholesterol and their relatively smaller size that maximizes the frequency of collisions with free cholesterol molecules [144]. The degree of cholesterol depletion in cells depends on factors such as the concentration of MBCD used, duration of incubation and cell type [144-146].

While MBCD, due to its affinity for cholesterol, reduces cell membrane cholesterol, it can also be used to deliver and enrich cholesterol in cell membranes when pre-loaded with cholesterol [147, 148]. Sheets et al. [149] demonstrated that cholesterol content in mast cells, which were subjected to cholesterol reduction and enrichment conditions serially with MBCD and cMBCD, respectively, was 3.5 fold higher than the untreated cells. Consistent with this study, several studies confirm the ability of MBCD to deliver cholesterol to membranes in different cells, however, the degree of cholesterol repletion varies slightly with the type of cell and to a greater degree with

variations in the molar ratio of cholesterol and MBCD and period of incubation [150].

1.9. Statins

Increasing evidence linking elevated plasma cholesterol levels with cardiovascular diseases led to the search for drugs that could lower plasma cholesterol. There was particular interest in synthesizing compounds homologous to one or more intermediates in the cholesterol biosynthetic pathway that could block this multi-step process. The search resulted in several compounds which were found to be effective in animals; however only Triparanol, a synthetic cholesterol lowering drug was introduced into clinical use in the U.S. in 1959 [151]. Since this drug acts by inhibiting 24-dehydrocholesterol reductase, an enzyme that catalyzes the conversion of desmosterol to cholesterol [152], it resulted in increased tissue accumulation of desmosterol, causing several side-effects including increased risk of atherosclerosis [153]. For this reason, this drug was withdrawn from the market in 1962 [154, 155].

The search for compounds alternate to statins included those that interfere with intestinal absorption of cholesterol, however the efficacy of these drugs under *in vivo* conditions were significantly compromised and various deleterious side-effects became evident [156-158]. Soon after that, the focus turned towards the rate controlling enzyme in cholesterol biosynthesis, HMG-CoA reductase. In the early 1970s, A Endo et al., observed strong inhibitory effects of two compounds isolated from fungal culture broths on HMGCoA reductase activity [159]. However, one was associated with risk of renal toxicity [160] and the other led to concomitant increases in the expression of the enzyme following inhibition, which compromised its efficacy [161]. Following this, as a result of intense research and clinical trials spanning more than a decade, lovastatin became the first commercially available statin in 1987 [162]. The discovery of lovastatin subsequently led to the discovery of several other naturally occurring statins such as simvastatin and pravastatin and synthetically developed statins such as rosuvastatin, pitavastatin, fluvastatin, atorvastatin and cerivastatin [163].

1.9.1. Beneficial and adverse effects of statin therapy

Statins have become one of the most widely prescribed groups of drugs to treat hypercholesterolemia in patients globally [164]. A meta-analysis conducted in 2010

revealed that statin therapy significantly reduced major vascular risk events including myocardial infarction and ischaemic stroke [165]. Due to the accumulation of strong evidence supporting its use in patients, statin therapy is recommended as per the guidelines of the American Heart Association and the European Society of Cardiology [166, 167].

In addition to the cholesterol-lowering ability of statins, there is evidence for beneficial effects in patients with dementia, hepatocellular carcinoma and colonic neoplasia [168, 169]. In several population-based studies, statins were also shown to decrease the risk of developing oesophageal and gastric cancers [170, 171]. However, there are some concerns being expressed regarding the potential side-effects of statin therapy and use of statins for longer periods of time. Almost all of the statins were reported to be associated with musculoskeletal side-effects, although the severity of side-effects from current statin use are shown to be quite low [172].

There have been very few reports made on the association of statin therapy with hepatic dysfunction. Clinical trials have shown statins to be associated with increases in serum alanine aminotransferase (ALT) in 3% of patients on statin medication, which was considered to be clinically insignificant in the majority of instances [173]. Surprisingly, a study showed that atorvastatin treatment in patients with non-alcoholic fatty liver disease (NAFLD) and coronary artery disease not only reduced cardiovascular events significantly but also reduced mean serum ALT levels in these patients [174]. A similar study demonstrated that statin treatment in NAFLD patients significantly reduced the level of hepatic steatosis [175].

Elsewhere, a number of studies have demonstrated the influence of statins on key signalling events of the insulin signalling pathway and pancreatic beta cell function and therefore suggest a potential diabetogenic property for statins [176]. A number of other studies have also indicated that simvastatin and atorvastatin could induce insulin resistance and worsen glucose uptake in skeletal muscle cells and adipocytes, respectively, through completely different mechanisms [177, 178]. However, not all statins were shown to be associated with new onset diabetes and those that were shown to be associated had effects only at higher doses [179, 180]. Also, there is no strong evidence that suggests further complications due to the use of statins in diabetics. In summary, statins are believed to be safe and effective drugs with strong

evidence in cholesterol-lowering and cardio-protective effects outweighing the concerns about their side-effects which in most cases were not considered clinically significant [181]. In relevance to the current study, there is some evidence that supports the ability of statins to alter cholesterol in cellular membranes [135, 182] but the actual mechanisms involved in statin-mediated alterations in plasma membrane cholesterol remain largely unclear [183, 184].

1.10. Conclusion

The first event of insulin signalling is the interaction of insulin (INS) with the insulin receptor (IR) which then leads to a sequence of intra-cellular events in order to retain the glucose homeostasis. The IR is a heterodimeric transmembrane receptor with two extracellular α-subunits and transmembrane β-subunits belonging to the large class of receptor tyrosine kinases (RTKs). Each β-subunit spans the plasma membrane with a typical 22 amino acid lipophilic sequence. Thus, it is perhaps not surprising that there is strong evidence implicating imbalances in insulin receptor dysfunction with certain changes in lipid composition and distribution within plasma membrane of cells. This study principally focuses on the influence of plasma membrane cholesterol content on the interaction between insulin and the insulin receptor. It is evident from the literature that alterations in plasma membrane lipid composition impair key insulin signalling events but to date, the influence of cell membrane cholesterol on insulin-insulin receptor interaction has not been comprehensively studied. Therefore, this study aims to investigate:

- The influence of acute changes in plasma membrane cholesterol content using methyl-β-cyclodextrins (MBCD) on insulin-insulin receptor interactions and signalling in insulin sensitive cell types such as hepatocytes and skeletal muscle cells.
- The effects of chronic cholesterol reduction using a clinically relevant drug, atorvastatin on insulin-insulin receptor interaction and signalling in hepatocytes and skeletal muscle cells.
- The effects of diet and/or statin treatment on insulin-insulin receptor interaction in liver plasma membranes isolated from mice fed with high-fat diet and/or treated with atorvastatin.

- The use of a novel cell membrane model, virus-like particles (VLPs), to study the interaction of insulin with its receptor in its native cell membrane environment but in the absence of other cellular components.

2.0. MATERIALS AND METHODS

2.1. Materials

Chinese hamster ovary (CHO K1) and human hepatocarcinoma (HepG2) cell lines were purchased from the ATCC, Manassas, VA, USA. Human skeletal muscle cells and myoblasts (HSMM) and skeletal muscle cell growth media and supplements (SkGM-2 BulletKit) were purchased from Lonza, Basel, Switzerland. Fetal bovine serum, which was used to supplement the growth media, was purchased from HyClone®, VIC, Australia. NuncTM tissue culture flasks (25, 75 and 175 cm2) and penicillin/streptomycin (10,000 U/mL) for cell culture were purchased from ThermoFisher Scientific, MA, USA. Recombinant human insulin (dry powder), methyl-β-cyclodextrin (MBCD) powder, cholesterol powder and catalase solution were purchased from Sigma-Aldrich, CA, USA. Atorvastatin calcium trihydrate and dimethyl-sulfoxide (cell culture grade) were also purchased from Sigma-Aldrich. Amplex® Red cholesterol assay kit and PierceTM BCA protein assay kit were purchased from ThermoFisher Scientific. Phosphate buffered saline (PBS; 10 mM disodium phosphate (Na2HPO4) and 1.8 mM monopotassium phosphate (KH2PO4), pH 7.2 containing 137 mM sodium chloride (NaCl) and 2.7 mM potassium chloride (KCl)) was purchased from HyClone. RIPA buffer (25 mM Tris-HCl, pH 7.6 containing 150 mM NaCl, 1% NP-40, 1% sodium deoxycholate and 0.1% sodium dodecyl sulphate (SDS) was purchased from ThermoFisher Scientific. Protease and phosphatase inhibitor cocktails were purchased from Sigma-Aldrich. NuPAGETM LDS sample buffer, NuPAGETM sample reducing agent, NovexTM Sharp pre-stained protein standards, NuPAGETM MES SDS Running Buffer (20X), BoltTM 4-12% Bis-Tris Plus Gels (10-wells), Mini Gel Tank and iBlotTM transfer stacks were also purchased from ThermoFisher Scientific. Amersham ECL prime Western blotting detection reagent was purchased from GE Healthcare Life Sciences (IL, USA). Tyrosine A14 [125I] monoiodoinsulin (125I insulin) was purchased from PerkinElmer (#NEX196010UC, PerkinElmer, OH, USA). MembraneProTM functional protein expression kits and support kits (InvitrogenTM) for VLP generation were purchased from ThermoFisher Scientific. All antibodies were purchased from abcam, Cambridge, UK. Unless otherwise stated, all other growth media and reagents for cell culture were also purchased from Sigma-Aldrich. The major equipment used for this study include swinging bucket centrifuge (Allegra®

X-12R, BeckmanCoulter), Sorvall WX ultracentrifuge (ThermoScientific), an EnSpire Multimode Plate Reader (PerkinElmer®), 2470 WIZARD2TM gamma counter (PerkinElmer), BD LSRFortessaTM flow cytometer, Zetasizer Nano ZS (Malvern®) and field emission-scanning electron microscope (MIRA3-TESCAN).

2.2. Methods

2.2.1. Cell based study

2.2.1.1. Development of CHO T10 clone

Chinese Hamster Ovary (CHO) cells overexpressing human insulin receptor isoform – A (CHO T10) were previously developed in our laboratory using CHO K1 cells. Human insulin receptor cDNA (isoform-A) was donated by Dr Takashi Kadowaki, NIH, USA. The insulin receptor cDNA (5.2 kb) was inserted at the Hind III restriction site of pSV2neo, a mammalian transfection vector containing neomycin and ampicillin resistance. Briefly, CHO K1 cells were transfected with a mixture of lipofectamine and the aforementioned plasmid expressing the human insulin receptor. Cells were selected for neomycin resistance by supplementing the culture medium with geneticin. Single clones were isolated by limiting dilution and cells overexpressing insulin receptors were selected by measuring insulin binding to the cells. The cell line overexpressing insulin receptors used in this study was denoted as the CHO-T10 clone. CHO T10 cells or CHO K1 (wild-type) cells were used to generate VLPs.

Cells were either grown in RPMI-1640 or DMEM/F-12 (1:1) media supplemented with 10% fetal bovine serum and 100 U/ml penicillin/streptomycin. Cells were grown to form monolayers in 75 cm^2 or 25 cm^2 tissue culture flasks at 37 °C in a humidified incubator equilibrated with 5% CO_2. Cells were passaged or prepared for storage by decanting the culture media from tissue culture flasks and rinsing the cells twice with phosphate buffered saline (PBS). Adherent cells were detached from the culture plates by treatment with 0.25% trypsin at 37 °C for up to 15 min. After achieving cell detachment, trypsin action was neutralized by adding an equal volume of culture media supplemented with 10% fetal bovine serum to minimise further proteolytic effects of trypsin on the cells. Cell suspensions were then transferred to 15 ml falcon tubes and centrifuged at 1000 g for 5 min in a swinging bucket centrifuge (Allegra® X-12R, BeckmanCoulter) maintained at room temperature (~ 23

°C). The supernatants were discarded and pellets were dispersed in complete culture media. Cells were either subcultured in appropriate well-plates for experiments or processed for cryopreservation.

2.2.1.2. Cholesterol alteration in cells

Cells were seeded either in 48-well or 6-well cell culture plates. Cell seeding densities were kept constant across all cell types used for this study; 1.65 X 10^5 cells per well for 48-well plates and 5 X 10^5 cells per well for 6-well plates. The cells were allowed to adhere to plates for at least 8 h at 37°C. Methyy-β-cyclodextrin (MBCD) or cholesterol-loaded MBCD (cMBCD) stocks were diluted in appropriate fetal bovine serum-free media to prepare working concentrations ranging from 1 to 10 mM. The cells were then incubated for 30 min at 37 °C with either media containing no fetal bovine serum or MBCD or cMBCD. Alternatively, cholesterol reduction in cells was achieved by treating the cells with 10 µM atorvastatin for 48 h at 37 °C in DMEM or RPMI supplemented with 10% lipoprotein deficient serum (LPDS), which was prepared as described below in this section. Since atorvastatin stocks were made up in di-methyl sulfoxide (DMSO), the control group was treated with media containing DMSO (0.1% v/v) (volume of DMSO equivalent to the volume of 10 mM atorvastatin stock solution added to the media). The treatments were stopped by aspirating the media containing MBCD, cMBCD or atorvastatin and washing twice with PBS, pH 7.2.

Preparation of MBCD and cMBCD stocks

Methyl-β-cyclodextrin (MBCD) powder was dissolved in PBS, pH 7.2 to make a 100 mM stock and stored at – 20 °C. Methyl-β-cyclodextrin loaded with cholesterol (cMBCD), of molar ratio ~ 20:1 was prepared by vortexing MBCD powder and cholesterol powder in PBS, pH 7.0 for 10 min. A homogenous state was attained after sonication in a probe sonicator (Misonix s-4000, QSonica) at 50% vibration amplitude at which the amplitude is ~ 60 µm (as recommended by the manufacturer), for at least 30 min or until there were no visible suspensions. The homogenous samples were then filter sterilized using 0.2 µm syringe filters and stored at – 20 °C [185].

Preparation of atorvastatin stocks

Atorvastatin calcium trihydrate was prepared as 10 mM stocks in cell culture grade dimethyl-sulfoxide (DMSO) and stored as 20 µl aliquots at – 80 °C.

Lipoprotein deficient serum (LPDS)

The density of fetal bovine serum was adjusted to 1.21 g/ml which was achieved by dissolving sodium bromide to a final concentration of 3.4 M. The mixture was centrifuged for 2 min at 700 g, in a swinging bucket centrifuge maintained at room temperature (~ 23 °C) to remove air bubbles and non-dissolved sodium bromide. The mixture were then transferred to 11.5 ml polyallomer ultracrimp tubes and centrifuged for 20 h at 70000 g using a Sorvall T-1270 rotor in a Sorvall WX ultracentrifuge (ThermoScientific). LPDS was collected by making a hole near the neck of the tube for air flow and piercing the base of the tube with a butterfly needle. About 9.5 ml of LPDS was collected from the bottom in a fresh plastic tube leaving out the floating layer of lipoproteins in the centrifuge tube. The collected LPDS was then dialysed for 24 h with two changes of PBS, pH 7.2 at 4 °C. The dialysed samples were then sterilized by filtration through a 0.2 µm filter and stored as 10 ml aliquots at -20 °C.

2.2.1.3. Lipid extraction

Following treatment with MBCD, cMBCD or atorvastatin, media was aspirated and cells were washed twice with PBS, pH 7.2. A volume of 200 µl of hexane:2-propanol (3:2, v/v) was then added. After 2 to 3 min incubation, the mixture was aspirated and transferred to 'v'-bottomed 96-well plates, and dried in a fume hood. After complete evaporation, the precipitates were redissolved in 40 µl of 1:1 mixture of 1x reaction buffer (0.1 M potassium phosphate buffer, pH 7.4, containing 0.5 M sodium chloride, 5 mM cholic acid and 0.1% Triton® X-100) from the cholesterol kit described below, and 2-propanol, for cholesterol measurements [186].

2.2.1.4. Cholesterol quantification

Cholesterol was quantified using an Amplex® Red cholesterol assay kit (#A12216, ThermoFisher Scientific) with strict adherence to the manufacturer's protocol. In brief, the precipitates obtained from the step mentioned above were dissolved in 40 µl of a 1:1 (v/v) mixture of reaction buffer (Component E in the AmplexRed®

cholesterol assay kit, ThermoFisher Scientific; contains 0.1 M potassium phosphate, pH 7.4, 0.5 M sodium chloride, 5 mM cholic acid and 0.1% Triton® X-100) and 2-propanol. The dissolved samples were further diluted in the same mixture prior to assaying. A range of cholesterol standards were prepared by dilution of the calibrator provided in the kit as per the manufacturer's guidelines using the same buffer used for diluting the samples.

Since this assay measures the amount of hydrogen peroxide released from the oxidation of free cholesterol in the samples, catalase was added to eliminate any hydrogen peroxide generated by the partial oxidation of 2-propanol. Prior to the addition of samples and standards, 10 µl of 500 U/ml catalase was added to the wells of a black flat bottomed 96-well plate. Calibrators or diluted samples (40 µl) were then added to wells containing catalase and left for incubation at 37 °C for 15 min [186]. Subsequently, 50 µl of working reagent (prepared as per manufacturer's guidelines) was added to the wells containing samples or calibrators and incubated for 30 min at 37°C. The fluorescence was then measured in an EnSpire Multimode Plate Reader (PerkinElmer®) set to an excitation of 560 nm and emission wavelength of 590 nm. The linear relationship between the concentration of the calibrators and the corresponding fluorescence values were ensured using a line of best fit. This standard curve was then used to estimate cholesterol content in the samples.

2.2.1.5. Cell viability assay

Cells were seeded at a seeding density of 3 X 10^4 cells per well in 96-well plates and incubated overnight at 37 °C. The cells were either treated with MBCD/cMBCD or atorvastatin for 30 min or 48 h, respectively. The treatment was stopped by aspirating the media and washing twice with PBS, pH 7.2. The viability of cells was then evaluated using an alamarBlue® cell viability assay (#DAL1025, ThermoFisher Scientific) with strict adherence to the manufacturer's protocol. Briefly, media (100 µl) containing 1x alamarBlue® reagent was then added to all wells except the wells used for background correction and incubated at 37 °C for 3 h. The resulting fluorescence was measured using an EnSpire Multimode Plate Reader (PerkinElmer®) set to an excitation wavelength of 570 nm and emission wavelength of 580 nm.

2.2.1.6. Protein quantification

The effects of various treatments on protein content of cells were estimated using BCA protein assay kit with strict adherence to the manufacturer's protocol. Briefly, well plates were placed on ice and cells lysed in 1x RIPA buffer. The lysates and bovine serum albumin standards from the kit were diluted appropriately in lysis buffer. Cell lysates or standards (25 µl) were pipetted in to a clear, flat-bottomed 96-well plate. Working reagent was prepared as per manufacturer's guidelines. Working reagent (200 µl) was added to wells containing lysates or standards and briefly mixed on a plate shaker. The plates were covered and incubated at 37 °C for 30 min. The plates were equilibrated to room temperature and the absorbance was measured at 562 nm using an EnSpire® Multimode Plate Reader (PerkinElmer®). The linear relationship between the concentration of the calibrators and the corresponding absorbance values were ensured using a line of best fit. This standard curve was then used to estimate protein content in the samples.

2.2.1.7. Insulin binding assay

Insulin stocks

Unlabelled insulin stocks were prepared as 206 µM stocks as described: 12 mg of recombinant human insulin powder was weighed, transferred to a 15 ml falcon tube and dissolved in 450 µl of 0.02 M HCl. This solution was immediately made up to 10 ml with 50 mM HEPES (4-(2-hydroxyethyl)-1-piperazineethanesulfonic acid), pH 7.6 containing 0.1% bovine serum albumin. The preparations were then filtered through a 0.2 µm syringe filter and aliquots stored at -20 °C. Typically, for binding assays, ~ 150 Bq/mmol of A14 [^{125}I] monoiodoinsulin (^{125}I-insulin; specific activity of 370 KBq/mmol) prepared in a binding buffer comprising 50 mM HEPES, pH 7.6 and 0.1% bovine serum albumin was used.

Insulin binding was evaluated by measuring the binding of ^{125}I insulin to the insulin receptors on cells in the presence of a range of unlabelled human insulin concentrations (0 to 20.6 µM) using a 2470 WIZARD2 ^{TM} gamma counter (PerkinElmer). Briefly, cells were grown and treated in 48-well plates (except for HSMMs, which were grown, differentiated and treated in 6-well plates). Following treatments, media was aspirated and cells were washed twice with PBS, pH 7.2. The treated cells were then incubated overnight at 4°C with media containing unlabelled

and labelled insulin. After the incubation, media was aspirated from the cells, which were then gently washed three times with ice-cold PBS, pH 7.2. The cells were lysed in 1% SDS for ~ 5 min and the lysates were then transferred to 3DT tubes for count estimations. Radioactivity in the tubes was measured using 2470 gamma counter. The displacement of ^{125}I-insulin by increasing concentrations of unlabelled insulin was plotted and non-linearly fitted to a one-site fit model using GraphPad® PRISM. Non-specific binding of ^{125}I-insulin, as determined based on the best-fit values, was used to calculate its specific binding by subtracting it from the binding values obtained at each concentration (0 to 20.6 µM) of unlabelled insulin. The best-fit values (top and bottom values for total and non-specific binding respectively and affinity (K_D) were used to derive maximal binding (B_{max}) and estimate the effects of various treatments on these parameters.

2.2.1.8. Flow cytometry

The effect of changes in cell cholesterol on insulin receptor density on the cell surface was studied using flow cytometry (BD LSRFortessa™ – BD Biosciences). Following cholesterol altering treatments, the cells were detached from the culture flasks by treating with 0.25% trypsin for not more than 5 min. Following detachment, the cells were recovered by centrifugation at 700 g for 5 min and cell pellets were resuspended in ice-cold Tris-buffered saline or TBS (50 mM Tris-HCl buffer, pH 7.5, containing 150 mM NaCl) and cell counts were estimated using a hemocytometer. The cells were aliquoted to 'U' bottomed 96-well plates at a density of 1 x 10^6 cells per well. The plates were then chilled on ice and centrifuged at 700 g for 4 min at 4 °C. The pelleted cells were resuspended and washed twice in cell staining buffer (BioLegend®), again at 4 °C.

A Zombie NIR™ fixable viability kit (BioLegend®) was used to quantify dead cells in all treatment groups. The lyophilized Zombie NIR™ dye was reconstituted in 100 µl of DMSO and stored at – 20 °C as a stock solution. Prior to use, this was diluted 1:500 in TBS with no added fetal bovine serum or bovine serum albumin. Staining of cells involved resuspension of the cells in 100 µl of this working solution and a 10 min incubation at room temperature, prior to removal of the staining solution by centrifugation at 700 g for 4 min at 4°C. For the immunostaining procedure, optimized dilutions of primary and secondary antibodies were made up in cell staining buffer. The cell pellets were resuspended in 100 µl of mouse anti-insulin

receptor alpha antibody and incubated for 45 min at room temperature (~ 23°C). The plates were centrifuged again at 700 g for 4 min at 4°C, supernatants aspirated and cell pellets were washed twice with 150 µl of cell staining buffer. The cell pellets were then resuspended in 100 µl of goat-anti-mouse IgG antibody (#ab150113, abcam) and incubated for 30 min at room temperature (~ 23°C). The plates were then centrifuged at 700 g for 4 min at 4°C to remove media containing secondary antibody and the cell pellets were then washed twice with 150 µl of cell staining buffer and finally resuspended in 100 µl of the same buffer for FACS analysis. A control group with no staining was prepared for all cell types to correct for autofluorescence. The samples were analyzed in a BD LSRFortessa™ flow cytometer using BD FACSDIVA™ software. After priming the system with double distilled water, the samples were transferred to 3DT tubes and docked to the system ensuring the probe was completely immersed into the sample. The system was assigned to count a maximum of 50,000 events and this was kept constant for all the treatments and replicates in all experiments. The gating for live/dead cells and insulin receptor positive events was done using the gating tool in the software. Median fluorescence intensities in various treatments were measured and compared using Flowlogic™ 7.2 software (Inivai Technologies™) or FLOWJO (BD Medical Technology).

2.2.1.9. Western blotting for cultured cells

Sample preparation

Cells were grown and treated in 6-well plates. The treatments were stopped by removing the media and washing the cells with TBS. The plates were placed on ice and 100 µl of ice-cold RIPA buffer containing protease and phosphatase inhibitor was added to all wells and allowed to incubate for 2 min. The wells were scraped with a 1 ml micropipette tip with the end cut off and the lysed samples were collected in pre-chilled 1.5 ml Eppendorf tubes. In order to achieve complete cell disruption and lysis, the lysates were then sonicated in a Bioruptor® Plus bath sonicator (diagenode™) with six successive 15 second cycles including a five second break between each cycle. The lysed samples were then centrifuged in a microfuge at 14000 g for 10 min at 4 °C. The supernatants containing proteins were transferred to fresh tubes. About 15 to 20 µl of lysates were used for protein quantification using a

BCA assay as described in section 2.1.6. The remaining lysates were stored at – 80 °C for Western blotting.

SDS-PAGE

Lysates containing ~ 30 µg of protein were mixed with NuPAGE™ LDS sample buffer and NuPAGE™ sample reducing agent. The mixture was heated in a heat block at 95 °C for 3 min and briefly spun for 30 s in a mini-centrifuge to retrieve the condensates generated in the heating step. The solubilized samples were separated by electrophoresis in a Bolt™ 4-12% Bis-Tris Plus Gel along with Novex™ Sharp pre-stained protein standards. Electrophoresis was carried out in a Mini Gel Tank filled with 1x NuPAGE™ MES SDS Running Buffer for 80 min at a constant voltage of 120 V. The proteins were electrophoresed. The separated proteins were then transferred to a nitrocellulose membrane in a dry blotting system.

Protein transfer by electroblotting

Following electrophoresis, the gels were layered along with iBlot™ transfer stacks according to the manufacturer's guidelines for dry transfer of proteins to a nitrocellulose membrane. The dry transfer was carried out in an iBlot™ gel transfer device. Briefly, the gels were layered on top of the nitrocellulose membrane fixed to the anode of the transfer stacks. A filter paper pre-soaked in double-distilled water was layered on top of the gels and air bubbles between the layers were removed with the help of a "debubbling" roller. Finally, the anode stack was placed on the top and the stacking was completed by putting the disposable sponge in place and the assembly was compressed by closing the lid. A preset program (20 V for 7 min) was chosen for transfer of proteins to the nitrocellulose membrane. After the run, the stacks were dismantled and the membrane containing transferred proteins was retrieved for the blocking step. In the blocking step, the membranes were incubated in blocking buffer comprising Tris-buffered saline, pH 7.6 containing 3% bovine serum albumin and 0.2% Tween-20 for 1 h at ~ 23 °C.

Immunoblotting

After the blocking step, the membranes were incubated in primary antibodies, prepared in the same buffer used in the blocking step, on a rocker for at least 8 h at 4 °C. Following incubation with the primary antibodies, the membranes were then

Table 1. List of protein targets and their respective antibodies used in Western blot analyses

Protein targets	Primary antibody	Secondary antibody
Insulin receptor	ab5500	ab6721
Insulin receptor-α-subunit	ab36550 monoclonal (83-7)	ab150113
Phosphorylated (tyr 1361) in the β-subunit of insulin receptor	ab60946	ab6721
Phosphorylated GSK 3β (Ser9)	ab131097	ab6721
Akt	ab126811	ab6721
Phosphorylated Akt (Thr308)	CST #4056	ab6721
HMGCR	ab174830	ab6721
MyoD	CST #13812	ab6721
Lentiviral-Gag	ab100970	ab6721
β actin	ab8227	ab6741
GAPDH	ab8245	ab6789
Na+/K+ ATPase	ab76020	ab6721
Syntaxin - 6	ab140607	ab6721
SDHA	ab139181	ab6721
KDEL	ab176333	ab6721

incubated for 1 h at room temperature with horseradish peroxidase (HRP) conjugated secondary antibody prepared in blocking buffer. Specific details on protein targets, corresponding primary and secondary antibodies are listed in Table 1. Finally, the membranes were given a minimum of three 5 min washes using 1x Tris-buffered saline, pH 7.6 containing 0.2% Tween-20. The membranes were then incubated for 5 min in ~ 150 µl freshly prepared 1:1 mixture of luminol enhancer (solution A) and peroxide solution (solution B) provided in the Amersham ECL prime Western blotting detection reagent kit. The membranes were transferred to a ChemiDoc™ MP system (Bio-Rad) for imaging and densitometry analyses were performed using ImageLab® software (Bio-Rad).

2.2.2. Animal studies

2.2.2.1. Diets and treatments

In this study, liver tissue samples were opportunistically collected from mice used for a related project from my supervisor's laboratory which was originally designed to investigate the effects of high-fat diet and statin treatment on pancreatic β-cell function. The liver tissue samples obtained from mice were used to investigate the effects of the same on insulin-insulin receptor interaction characteristics in plasma membrane and insulin signalling. Male C57B1/6J mice aged 8 weeks were obtained from the Animal Resource Centre, Murdoch, Western Australia. The mice were delivered to the animal facility, Curtin University and left to acclimatise for a week. Following acclimatisation, mice were randomly assigned to two diet groups: normal (ND) and high-fat diet (HFD) (Speciality Feeds, Glen Forrest, Western Australia), then each diet group was subsequently assigned to two treatment groups; A – atorvastatin and P - pravastatin treated groups, making 6 groups in total including controls. The original study and procedures involved in handling the animals were carried out in strict accordance with the guidelines of the National Health and Medical Research Council of Australia as approved by Curtin Animal Ethics Committee (AEC_2016_17) for the project titled "Statins & islet function".

2.2.2.2. Harvesting of mouse liver

Mice were administered 200 µl of either water or atorvastatin or pravastatin (suspended or dissolved in water, respectively) at 10 mg/kg/day by gastric gavage daily from weeks 4 to 16. Following completion of the treatment period, mice were

starved for 6 h and anaesthetized in an isoflurane chamber before euthanized by cervical dislocation. Liver samples were collected in pre-chilled 1.5 ml Eppendorf tubes and snap-frozen either in dry ice or liquid nitrogen upon removal from the carcass. The tissue samples were stored at – 80 °C for later use. A protocol described

by JM Suski et al., 2014 was adapted to process the liver tissue samples and collect various sub-cellular fractions for the study of effects of high-fat diet and statin treatment on cholesterol content and insulin signalling [187].

2.2.2.3. Liver tissue homogenization

The glassware used in this process were autoclaved and rinsed with double distilled water. The pH adjustments for all reagents and buffers used in this procedure were done at 4 °C. The general reagents used to prepare buffers were 1M Tris-HCl, pH 7.4, 0.5 M HEPES, pH 7.4, 100 mM EDTA, pH 7.4 and 100 mM EGTA, pH 7.4. Liver tissues were retrieved from -80 °C storage and weights of wet tissue samples were recorded. The tissue samples were washed at least thrice with ice-cold starting buffer comprising 30 mM Tris-HCl (pH-7.4), 225 mM mannitol and 75 mM sucrose. The washed tissue samples were then transferred to a 10 ml glass/Teflon Potter-Elvehjem homogenizer containing 5 ml of ice-cold isolation buffer-1 (0.5% (wt/vol) bovine serum albumin and 0.5 mM EGTA and 1% (v/v) protease and phosphatases inhibitor cocktail in starting buffer) and homogenized manually by 18-20 strokes. The homogenates were then transferred to 15 ml centrifuge tubes and centrifuged at 800 g at 4 °C for 5 minutes in a Beckman Coulter swinging bucket centrifuge. The supernatants were centrifuged again under identical conditions and the pellets were discarded. A small volume of the crude homogenates were collected and stored at -80 °C for cholesterol and protein estimation, and Western blotting.

2.2.2.4. Isolation of plasma membrane from mice liver samples

Crude mitochondrial isolation

The supernatants from the step above were then transferred to fresh thick-wall 10 ml polypropylene tubes and centrifuged at 10000 g for 10 minutes in a 70.1 Ti rotor and Beckman Coulter ultracentrifuge. The supernatants containing crude plasma membrane and cytosolic fractions were transferred to a fresh tube. The crude mitochondrial pellet was carefully resuspended in 5 ml of ice-cold starting buffer

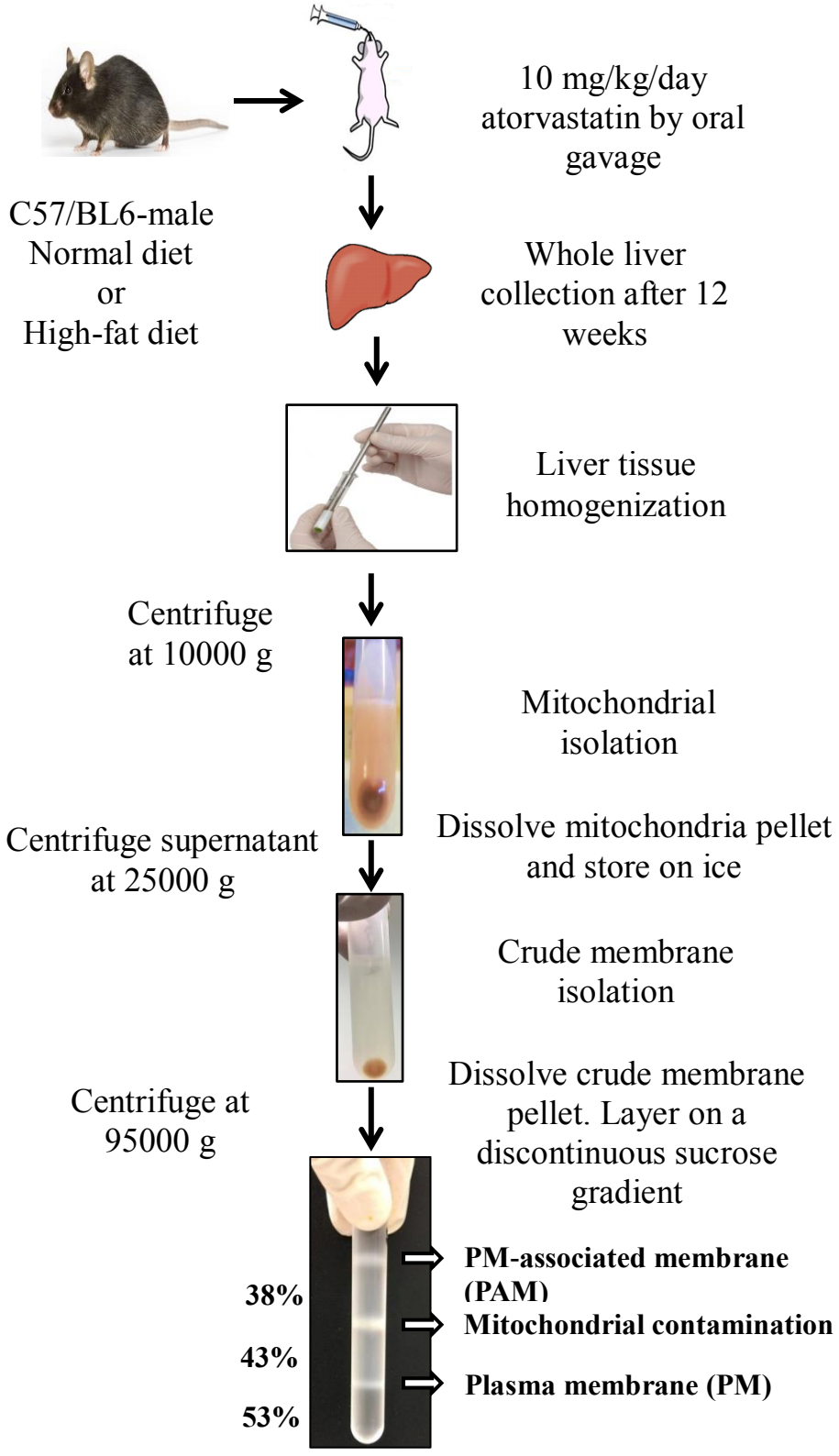

Figure 4. A schematic representation for plasma membrane isolation from mouse liver

with a 1 ml micropipette with the tip cut off. The tubes were then centrifuged using similar conditions to wash the mitochondrial fraction. The mitochondrial pellets were then resuspended in 500 µl of mitochondrial resuspension buffer comprising 5 mM HEPES (pH 7.6), 250 mM mannitol, 0.5 mM EGTA and 1% (v/v) proteases and phosphatases inhibitor cocktail and stored at – 80 °C.

Crude plasma membrane isolation

The supernatant containing plasma membrane and cytosolic fractions were transferred to fresh tubes and centrifuged at 25000 g for 20 min at 4 °C. The supernatants containing the cytosolic fraction were collected and stored on ice. The cytosolic fraction was processed later together with the sucrose gradient centrifugation step mentioned below. The pellet containing crude plasma membrane was resuspended in 10 ml of ice cold starting buffer and centrifuged again using similar conditions to remove microsomal and cytosolic contamination. After discarding the supernatant, the crude plasma membrane pellet was resuspended in 1 ml of ice-cold plasma membrane resuspension buffer comprising 5 mM Bis-Tris powder and 0.2 mM EDTA (adjusted for pH 6.0 using KOH or HCl).

Sucrose gradient centrifugation

A discontinuous sucrose gradient was set up in a 14 ml thin-walled polyallomer ultracentrifuge tube. Sucrose solutions were prepared as described above in the reagent set-up section. The tubes were serially filled with increasing concentrations of sucrose solutions in the following way; 3 ml of 53% sucrose solution was added to the tube followed by layering 4 ml each of 43% and 38% sucrose solutions. The resuspended plasma membrane pellet and the cytosolic fractions collected previously were then layered on top of individual discontinuous sucrose gradients. Approximately, 2 ml of ice cold PMRB was added to fill up to the neck of the tubes, which were then weight matched. The tubes were centrifuged in an SW 40 Ti rotor at 95000 g for 2.5 h. This step resulted in three dense bands; band 1) on top of 38% sucrose gradient containing plasma membrane associated membranes or PAMs, band 2) at the interface between 38% and 43% sucrose gradient solutions containing mitochondria tightly interacting with plasma membranes and band 3) at the interface between 43% and 53% sucrose gradient solutions containing plasma membrane. The

bands 1 and 3 were carefully collected using a transfer pipette and transferred to fresh tubes. The tubes were filled completely with ice-cold starting buffer and centrifuged at 95000 g as previously for 1 h at 4°C.

The supernatants containing cytosolic fractions were included in the sucrose gradient centrifugation step mentioned above to separate microsomes. After high speed centrifugation, the supernatants containing cytosolic fractions were transferred to fresh tubes and microsomal pellets were resuspended in 10 ml of ice-cold starting buffer and re-centrifuged with bands 1 and 3 mentioned above. PAM and plasma membrane pellets were resuspended in 100 µl of ice-cold IB-2 containing 1x protease and phosphatase inhibitor cocktail and microsomal pellets were resuspended in 500 µl of ice-cold IB-2 and all were stored at – 80 °C.

2.2.2.5. Protein and cholesterol estimation

All fractions obtained from whole liver tissues of mice from various treatment groups were estimated for total protein and cholesterol content using bicinchoninic (BCA) assay and AmplexRed® cholesterol assay respectively. Briefly, liver fractions were solubilized in 1% SDS in PBS and quantified for total protein content using BCA assay kit as described in Section 2.2.1.6. Liver fractions were diluted in 1x reaction buffer (Component E provided in the AmplexRed® cholesterol assay kit, ThermoFisher Scientific) containing 0.1 M potassium phosphate, pH 7.4, 0.5 M sodium chloride, 5 mM cholic acid and 0.1% Triton® X-100 and total cholesterol contents were estimated as described in Section 2.2.1.4.

2.2.2.6. Insulin binding assay

Insulin binding analyses in liver fractions were done using competition binding analysis. Liver fractions were diluted in binding buffer containing 50 mM HEPES, pH 7.6 and 0.1% bovine serum albumin and incubated with ^{125}I insulin and unlabelled insulin in 3DT tubes for ~ 18 h at 4 °C. Following incubation, a mixture of 20% polyethylene glycol (PEG) and 0.4% bovine gamma globulin (5:1, v/v) was added to the tubes and gently vortexed. The tubes were then placed on ice for 15 min and centrifuged for 25 min at 10,000 *g* at 4° C in a refrigerated centrifuge (Avanti® J-E). The 3DT tubes were placed in polycarbonate adapters to fit in a fixed angle rotor (JA 20.1) and to avoid breaking during centrifuge. Following centrifugation, the supernatants were discarded and the pellets were read for ^{125}I counts in a gamma

counter (2470-WIZARD$_2^{TM}$ PerkinElmer). The data from the displacement of ^{125}I insulin by increasing concentrations of unlabelled insulin (~ 40 pM to 20.6 µM) was fitted to a one-site fit model using GraphPad® PRISM software and the best-fit values were used to estimate maximal binding and affinity of insulin receptors for insulin.

2.2.2.7. Insulin signalling by Western blotting

The effects of diet and statin treatments on hepatic insulin signalling of mice were estimated using Western blot analysis. Approximately, 20 – 25 µg of total protein, as measured by BCA assay, was loaded onto each well of a 10-well, 1 mm thick, 4 – 12% Bis-Tris gradient gel and electrophoresed as per conditions mentioned and Western blot analyses were conducted as described in section 2.1.9. Separate loading controls were used for membrane (Na^+/K^+ - ATPase) and cytosolic fractions (GAPDH).

2.2.3. Model membrane - virus-like particles (VLPs)

2.2.3.1. VLP generation

CHO T10 or CHO K1 cells were grown to 85% confluence in T-175 tissue culture flasks in RPMI-1640 containing 10% fetal bovine serum and 1 % penicillin/streptomycin. After achieving 85% confluence, CHO T10 or CHO K1 cells were fed with fresh RPMI-1640 containing 4% fetal bovine serum and incubated overnight at 37°C, in an atmosphere equilibrated with 5% CO_2. From this point, the cells were maintained in an antibiotic-free media. VLP generation was carried out over a three day period. Following overnight incubation, the transfection procedure for VLP generation was carried out in CHO T10 or CHO K1 cells and according to the manufacturer's protocol.

In brief, the cells were fed with 25 ml of fresh RPMI-1640 containing 4% fetal bovine serum and the prepared transfection mixture was then added dropwise and incubated overnight at 37°C. The transfection mix was prepared as follows: A 9 ng/mL solution of the lentiviral Gag protein was prepared by gently adding and mixing 36 µl of MembranePro^{TM} reagent containing 1 µg/ml of lentiviral Gag protein, to 4 ml of freshly prepared RPMI-1640 containing 2% fetal bovine serum in a 15 ml centrifuge tube. In a separate 15 ml centrifuge tube, a solution containing 45

µg/ml of the provided cationic lipid solution was prepared by gently mixing 180 µl of 1 mg/ml Lipofectamine® 2000 in 4 ml of RPMI-1640 containing 2% fetal bovine serum. The mixtures were then combined in one 15 ml centrifuge tube and incubated for 20 min at room temperature to allow formation of Gag protein-Lipofectamine® 2000 complexes. After ~18 h of incubation, the media containing the transfection mixture was decanted and cells were either fed with fresh RPMI-1640 containing 4% fetal bovine serum, or for insulin stimulatory studies, fresh RPMI-1640 containing 4% fetal bovine serum and insulin at a final concentration of 100 nM. After a 24 h incubation, the VLP-containing media was collected in 50 ml centrifuge tubes and cells were again fed with fresh RPMI-1640 containing 4% fetal bovine serum. From this point, media (~ 32 ml) was collected every 24 h for up to a 72 h time point. The collected media was briefly centrifuged in a swinging bucket centrifuge at 800 g for 5 min at ~ 23 °C to remove debris. A volume of 30 ml was transferred to a fresh centrifuge tube using a serological pipette, whilst avoiding collection of the last few mL close to the debris. After careful transfer of the suspensions, 6 ml of MembranePro™ precipitation mix was added and mixed gently by inverting the tubes several times and incubated overnight at 4 °C. This was then centrifuged at 2800 g for 1 h at 4 °C. The supernatants were carefully discarded without dislodging the pellets containing VLPs. VLP pellets were then washed with 5 ml of MembranePro™ reagent: PBS, pH 7.2 (1:5, v/v) and centrifuged at 2800 g at 4 °C for 15 min. The supernatants were discarded and pellets were resuspended in 50 mM HEPES, pH 7.6 and stored at - 80 ^{o}C.

2.2.3.2. Dynamic light scattering analysis for VLPs

VLPs were diluted in PBS, pH 7.2 and transferred to plastic disposable cuvettes and analyzed in a Zetasizer Nano ZS (Malvern®) which uses dynamic light scattering to determine particle size and size uniformity. This system uses a standard 4 mW laser operating at a wavelength of 633 nm and the observed intensity of the scattered light resulting from the dispersity of VLPs due to Brownian motion in suspension was used to determine particle size and size uniformity. The analysis was performed with the help of Malvern® software.

2.2.3.3. Electron microscopy for VLPs

The size and morphology of the VLPs were also examined by field emission-scanning electron microscopy (FE-SEM) using a MIRA3 (TESCAN). Sample

preparation involved formalin fixation and ethanol dehydration. A volume of 100 µl of VLPs and 4% paraformaldehyde was sequentially pipetted on to a glass cover slip mounted on an aluminium stub. The sample was then left overnight for fixation at room temperature. Following fixation, samples were dehydrated by serial treatment with increasing concentrations of ethanol: specifically, by treatment with 150 µl each of 10, 20, 40, and 90% ethanol solutions for 10 min at each concentration. After complete evaporation, the glass slide was mounted on the aluminium stub using sticky carbon conductive tape. The imaging was performed in the Microscopy and Microanalysis Facility located within the John de Laeter Centre, Curtin University, Bentley, WA.

2.2.3.4. Insulin binding assays for VLPs

The presence of functional insulin receptor in VLPs generated from cells was examined by competition binding analysis. The assay set-up was designed in a similar fashion to that in cell models but with slight alterations; the assays were carried out in 3DT tubes as opposed to multi-well plates since VLPs tend to remain suspended in solution and the retrieval process involved a polyethylene glycol precipitation step. The reaction mixture consisted of 50 µl VLPs, 25 µl each of ^{125}I-insulin (~ 2.5 to 3 pM) and increasing concentrations (0 to 20 µM) of unlabelled insulin prepared as described in Section 2.2.1.7. The tubes were capped and incubated at 4°C for approximately 18 h. Following incubation, a mixture of 20% polyethylene glycol (PEG) and 0.4% bovine gamma globulin (5:1, v/v) was added to the tubes, which were then gently vortexed. The tubes were then placed on ice for 15 min and centrifuged for 25 min at 10,000 *g* at 4° C in a refrigerated centrifuge (Avanti® J-E). The supernatants were discarded and the pellets were analyzed by radio-counting on a gamma counter (2470-WIZARD$_2$™ PerkinElmer).

2.2.3.5. Insulin receptor quantification

Receptor concentration was approximated in cells and VLPs based on a method described by DeBlasi et al., 1989 [188], the equation for which is shown below.

$$B_{max} = B_0 * [K_D/L]$$

In this equation, B_{max} represents the maximum binding, B_0 represents the difference between the highest and lowest values of the one-site model fit, K_D represents the affinity of insulin for insulin receptors and L represents the concentration of ^{125}I-

insulin [188]. The number of insulin receptors present per cell was estimated using the following equation:

$$\text{Receptor number per cell} = B_{max} * [6.023 \times 10^{23} / \text{Number of cells}]$$

In this equation, B_{max} represents the maximum binding of insulin and 6.023×10^{23} is the Avogadro's constant.

2.2.3.6. Cholesterol and protein estimation

To measure cholesterol content, VLPs were extracted for non-polar lipids with a mixture of hexane/2-propanol (3:2, v/v) in 'v-bottom' 96 well plates. A volume of 50 µl of VLP suspension derived from CHO T10 or CHO K1 cells, diluted 1:4 in 50 mM HEPES, pH 7.6, was added to 'v-bottom' 96-well plates. A volume of 150 µl of hexane/2-propanol (3:2, v/v) mixture was then added to all the wells containing VLPs and left to evaporate in a fume hood. After complete evaporation, the dried extracts were dissolved in a 1:1 mixture of the assay 1x reaction buffer (component E in the AmplexRed® cholesterol assay kit, ThermoFisher Scientific; contains 0.1 M potassium phosphate, pH 7.4, 0.5 M sodium chloride, 5 mM cholic acid and 0.1% Triton® X-100) and 2-propanol and used for cholesterol quantification using the Amplex® Red cholesterol assay (Section 2.1.4). For protein quantification, 50 µl of VLPs, diluted 1:4 in 50 mM HEPES, pH 7.6 was solubilized in 50 µl of 1% SDS in PBS and quantified for total protein content using the BCA protein assay (Section 2.1.6).

2.2.3.7. Western blotting of virus-like particles

The presence of insulin receptors was also confirmed by Western blot analysis. VLPs were solubilized in 1% SDS in PBS and estimated for total protein content using BCA assay. Solubilized VLP samples containing ~ 20 µg of total protein were mixed with loading buffer containing 1 x Laemmli buffer and 1.42 M 2-mercaptoethanol as the final concentration. These mixtures were then heated at 95 °C for 2 min. The samples were loaded onto 10-well, 1 mm thick, 4-12% Bis-Tris gradient gels for SDS-PAGE. Western blotting was carried out in a similar manner to that used for whole cell models (Section 2.1.9). The membranes were incubated overnight at 4 °C in anti-insulin receptor, anti-Gag, anti-Na+/K+ ATPase or anti-GAPDH primary antibodies followed by 1 h incubation at room temperature (~ 23 °C) with respective horseradish peroxidase conjugated secondary antibodies. Both primary and

secondary antibodies were prepared in Tris-buffered saline, pH 7.6 containing 0.2% Tween-20 and 3% bovine serum albumin. After incubation, the membranes were washed thrice with TBS, pH 7.6 containing 0.2% Tween-20. The membranes were then imaged and densitomery analyses were conducted as described in section 2.1.9.

2.2.3.8. Modulation of membrane cholesterol content in VLPs

Alterations in membrane cholesterol content of VLPs were achieved by treatment with 10 mM methyl-β-cyclodextrin (MBCD) or cholesterol loaded-MBCD (cMBCD) for 30 min at room temperature (~ 23 °C). VLPs were then pelleted by centrifugation in the presence of MembranePro^{TM} reagent (1 in 5 dilution). The VLP pellets were resuspended in 30 µl of hexane/2-propanol (3:2, v/v) and added to 'v-bottom' 96 well plates. The effects of MBCD or cMBCD treatments on insulin-insulin receptor interactions, cholesterol and protein content, and were examined in VLPs as described in Sections 2.2.3.6.

3.0 RESULTS

3.1. Effect of cyclodextrins and statins on cholesterol content and insulin action in cultured cells

Chinese Hamster Ovary cells over-expressing the insulin receptor (CHO T10), human hepatocarcinoma cells (HepG2), human skeletal muscle cells and myoblasts (HSMM) differentiated into myotubes were treated with either MBCD or cMBCD, as an approach to manipulate membrane cholesterol levels or with atorvastatin to reduce cholesterol biosynthesis in cells (see Methods, Section 2.2.1.2). The viability of each of these cell lines was not significantly affected by treatment with up to 10 mM MBCD (Fig 5A, 5C and 5E) [1]. However, whilst up to 10mM cMBCD also did not affect the viability of CHO T10 cells (Fig 5B), a slight but significant increase and decrease in cell viability was observed as a function of cMBCD concentration in HepG2 and HSMM cells, respectively (Fig 5D and 5F). Atorvastatin treatment did not affect the viability of CHO T10 cells (Fig. 6A), however, it significantly decreased the viability of HepG2 cells ($P < 0.05$) and undifferentiated HSMMs ($P < 0.0001$) (Fig. 6B and 6C).

Cell cholesterol decreased significantly in each cell type following an acute 30 min treatment with increasing concentrations of MBCD (Fig. 7A - C). [1] Cell cholesterol decreased by about a 2-fold ratio in each cell type following treatment with the maximal dose of 10 mM MBCD. Conversely, cholesterol levels increased in each cell type following an acute 30 min treatment with increasing concentrations of cMBCD (Fig. 7A - C). The concentration of cholesterol increased by about 2-fold in each cell type following treatment with the maximal dose of 10 mM cMBCD. Cell cholesterol content also decreased significantly in all three cell models after they were treated for 48 h at 37 °C with 10 μM atorvastatin in the presence of lipoprotein deficient serum (Fig. 8A – C).

The specific binding of ^{125}I-insulin to all three cell models decreased significantly in a concentration-dependent manner following treatment with either MBCD or cMBCD (Fig. 9A – C).[1] This suggests that there may be an optimal cholesterol

[1]A linear fit is only used to fit data herein to illustrate the correlation between increasing concentrations of MBCD, cMBCD or atorvastatin on viability of cells, cell cholesterol content or insulin binding.

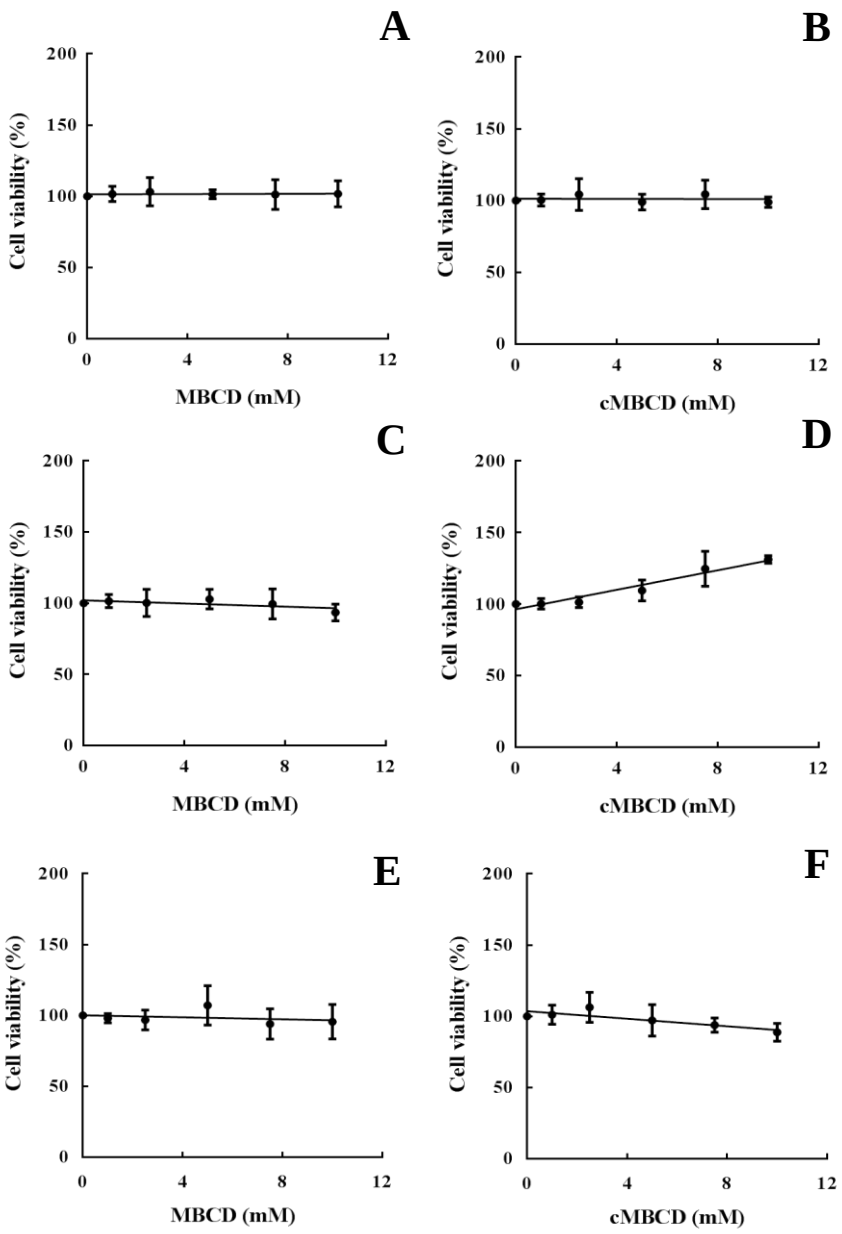

Figure 5. Effect of MBCD or cMBCD treatment on cell viability. CHO T10 (A and B), HepG2 (C and D) and undifferentiated HSMM (E and F) cells were treated for 30 min at 37 °C with increasing concentrations of MBCD or cMBCD. Following treatment, cell viability was measured as described in section 2.2.1.5. The resulting fluorescence values were normalized relative to the untreated cells. The experiment was conducted three times in triplicate but only one representative data set is illustrated, with each data point shown as the mean ± SD (n=3).

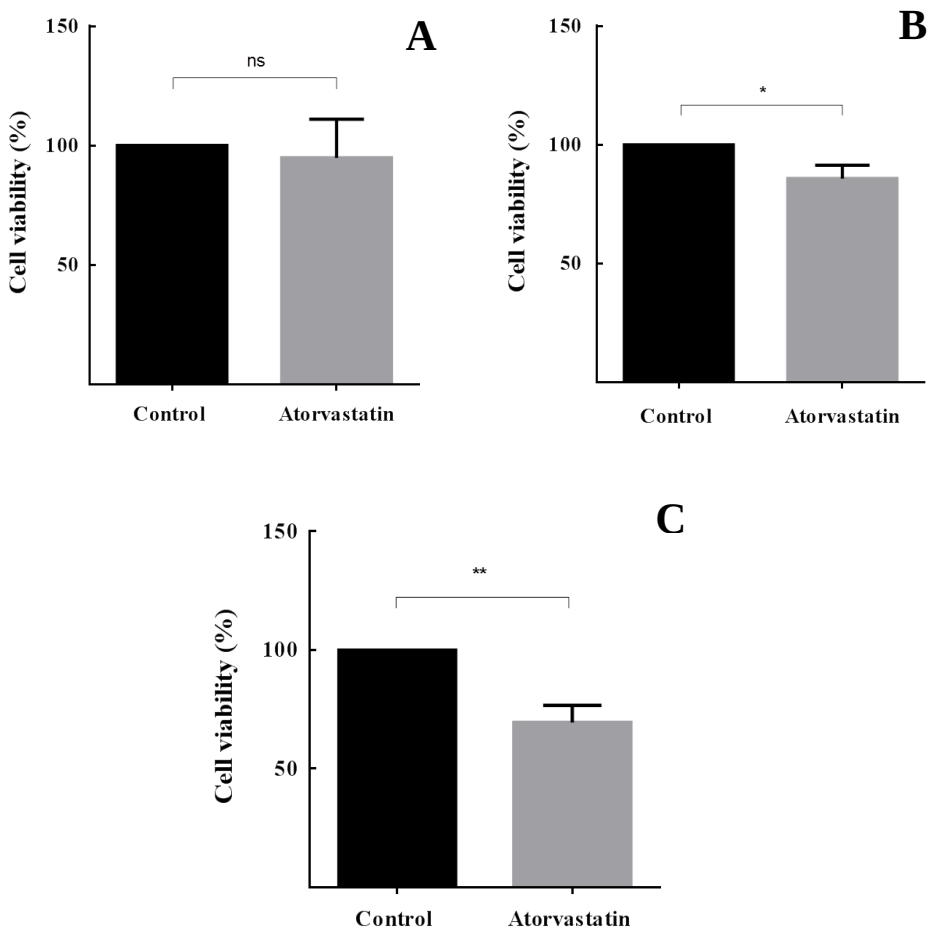

Figure 6. Effect of atorvastatin treatment on cell viability. CHO T10 (A), HepG2 (B) and undifferentiated HSMM (C) cells were treated for 48 h at 37 °C with atorvastatin in the presence of lipoprotein deficient serum. Following treatment cell viability assay was conducted as described in Section 2.1.5. The resulting fluorescence was measured in all cell types and values normalized to their respective control groups were plotted. The resulting fluorescence values were normalized relative to the untreated cells. The experiment was conducted three times in triplicate but only one representative data set is illustrated, with each data point shown as the mean ± SD (n=3). Data from all three experiments were used for statistical analysis (Paired t-test: ns – not significant, * $P < 0.05$, ** $P < 0.01$, $n = 9$).

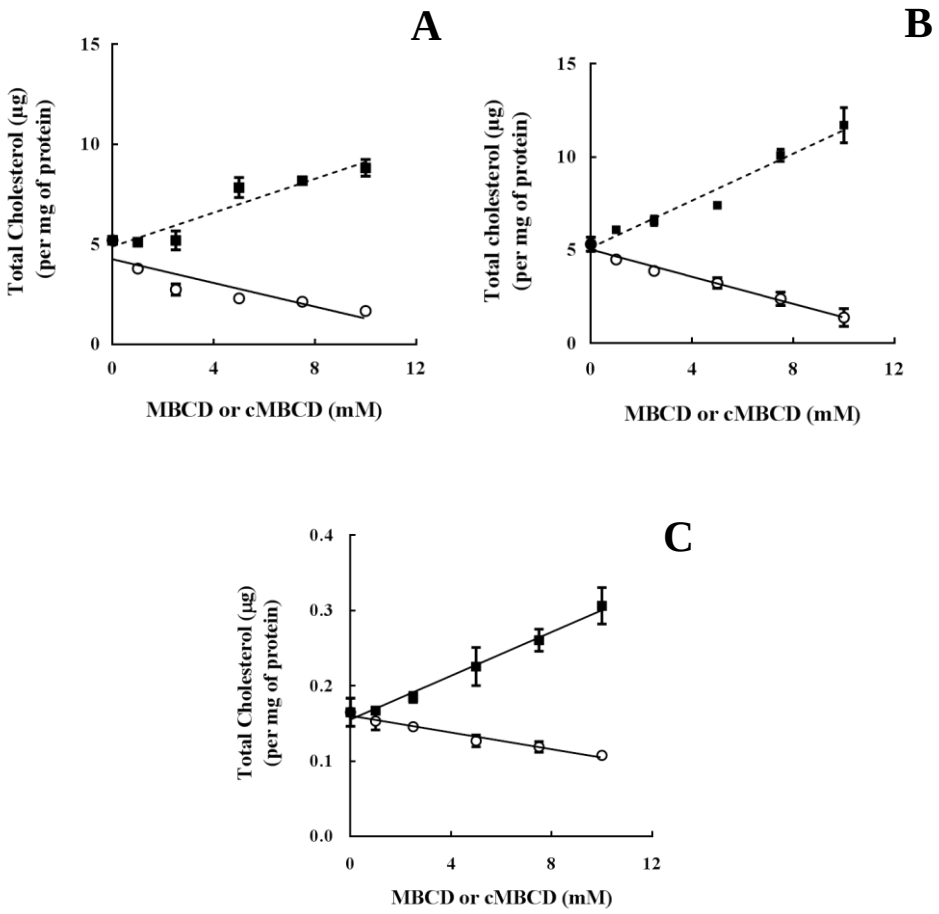

Figure 7. Effect of MBCD or cMBCD treatment on cholesterol content of cells in culture. CHO T10 (A) and HepG2 (B) cells, and differentiated myotubes (C) were treated for 30 min at 37 °C with increasing concentrations of MBCD (-⊖-) or cMBCD (-■-). Following treatments, cholesterol was extracted from cells and measured as described in the Methods, section 2.2.1.3 and 2.2.1.4, respectively. The experiment was conducted three times in triplicate but only one representative data set is illustrated, with each data point shown as the mean ± SD (n=3).

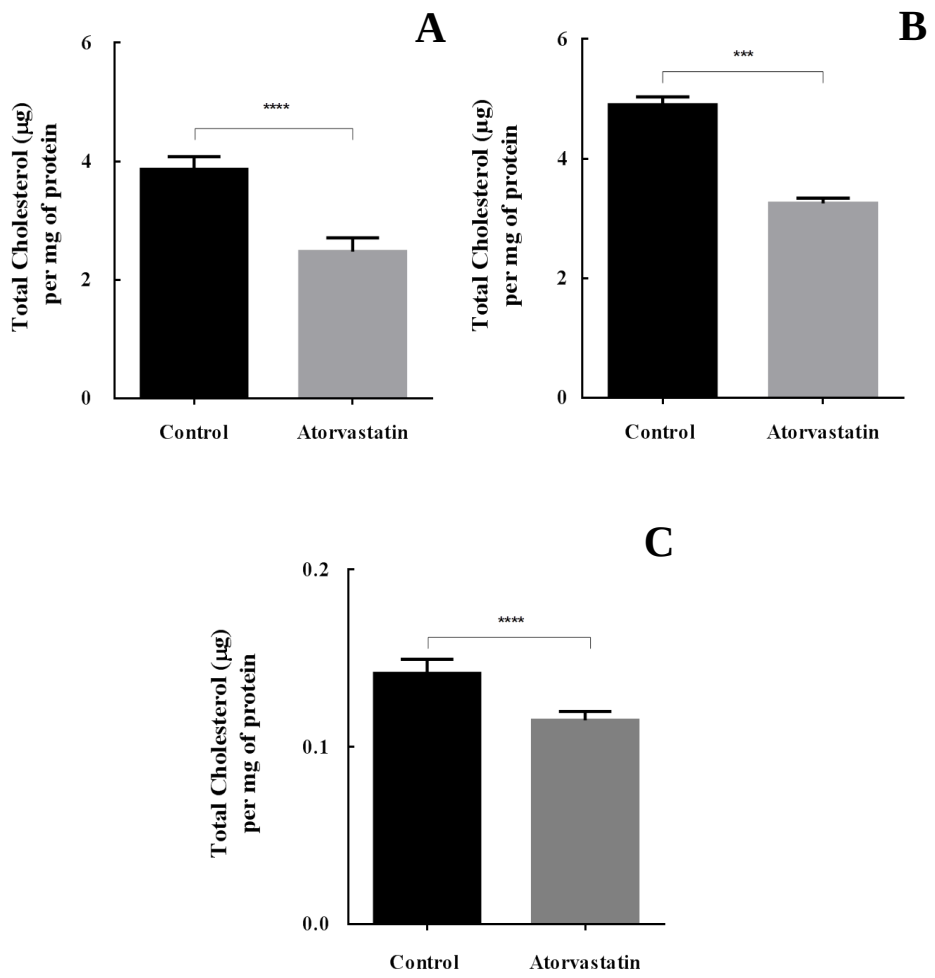

Figure 8. Effect of atorvastatin treatment on cholesterol content of cells in culture. CHO T10 (A) cells, HepG2 (B) cells and differentiated myotubes (C) were treated for 48 h at 37 °C with 10 µM atorvastatin in the presence of lipoprotein deficient serum. Following treatments, cholesterol was extracted from cells and measured as described in the Methods, section 2.2.1.3 and 2.2.1.4., respectively. The experiment was conducted three times in triplicate but only one representative data set is illustrated, with each data point shown as the mean ± SD (n=3). Data from all three experiments were used for statistical analysis (Paired t-test: *** $P < 0.001$, **** $P < 0.0001$, n=9).

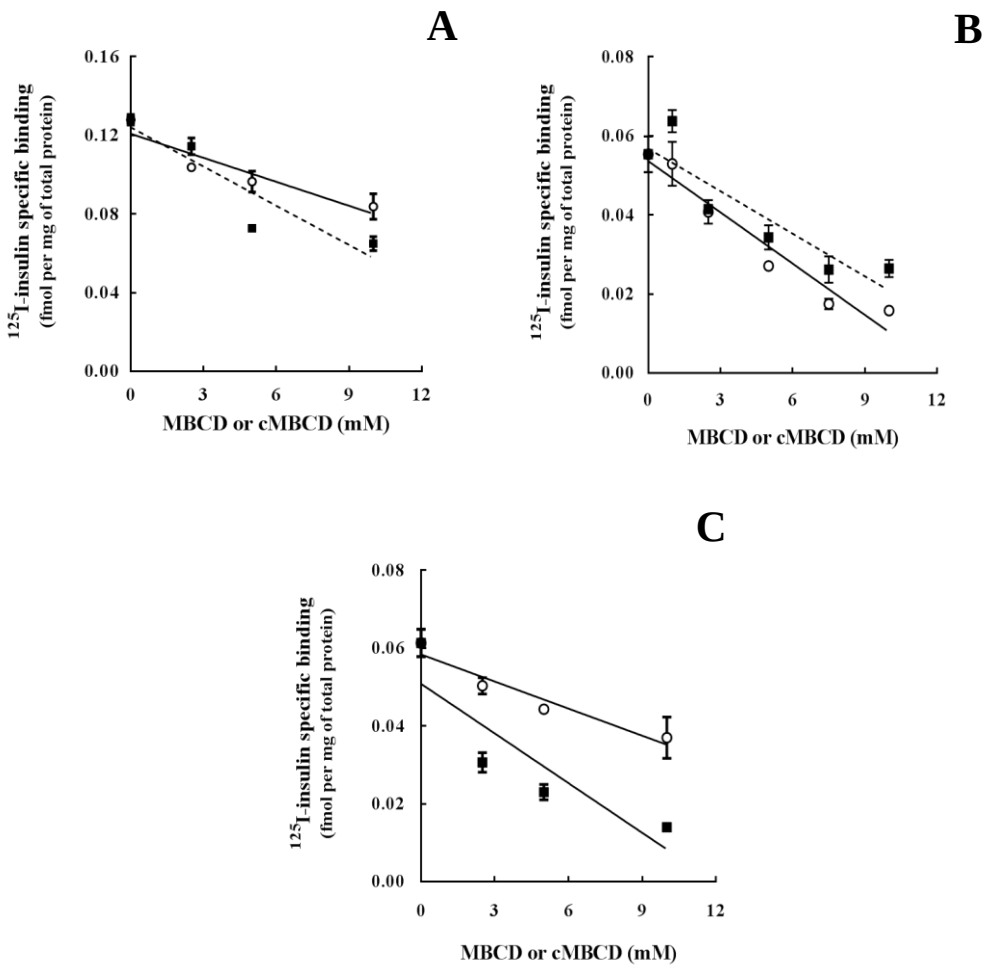

Figure 9. Effect of MBCD or cMBCD on ^{125}I-insulin binding in cultured cells. CHOT10 (A) cells, HepG2 (B) cells and differentiated myotubes (C) were treated for 30 min at 37 °C with increasing concentrations of MBCD (⊖) or cMBCD (■). Following treatments, insulin binding assays were conducted as described in the Methods, Section 2.1.7. The experiment was conducted three times in triplicate but only one representative data set is illustrated, with each data point shown as the mean ± SD (n=3).

concentration in cells supporting maximal insulin binding. The effect of acute treatment with MBCD and cMBCD on decreasing insulin binding to CHO T10 and HepG2 cells was evaluated in greater detail using radio-ligand competition binding studies conducted over a wide range of competing unlabelled insulin concentrations (Fig. 10)[2]. Analysis of the competitive binding plots (Table 2) suggested that MBCD or cMBCD treatment decreased in insulin binding in CHO T10 cells by decreasing the number of available cell surface insulin receptors (MBCD or cMBCD, $P < 0.0001$); there was no apparent change in the affinity of insulin to insulin receptors in CHO T10 cells (MBCD, $P = 0.3$; cMBCD, $P = 0.2$). Similarly, based on competitive binding analysis, MBCD or cMBCD treatment decreased insulin binding in HepG2 cells by decreasing the number of available cell surface insulin receptors (MBCD: $P < 0.01$; cMBCD: $P < 0.05$); no apparent change in the affinity of insulin to the insulin receptors was observed (MBCD, $P = 0.4$; cMBCD, $P = 0.5$). It is notable that in HepG2 cells, the largest decrease in binding was observed with MBCD treatment while in CHO T10 cells the largest decrease in binding was observed with cMBCD treatment. Thus, the impact of cholesterol loading or depletion in the membrane on insulin binding appears to be cell type specific.

As a more direct approach to evaluate the influence of cyclodextrins on the number of insulin receptors on the surface of cells, CHO-T10 and HepG2 cells were first treated with either 10 mM MBCD or cMBCD and then insulin receptors were detected by incubating the cells serially with a monoclonal antibody raised against the α-subunit of the anti-insulin receptor (83-7) and then a fluorophore (Alexaflour-488) conjugated secondary antibody (see Methods, Section 2.2.1.8). The effects of the treatments on cell surface insulin receptor density in CHO T10 and HepG2 cells were then detected by flow cytometry. Treatment with either MBCD or cMBCD significantly decreased the density of insulin receptors on the surface of CHO-T10 and HepG2 cells (Fig. 11 A and B respectively). It is interesting to note cMBCD treatment had a greater effect on decreasing the apparent number of insulin receptors in CHO T10 cells than in HepG2 cells. This observation is consistent with the trends observed for the specific binding of ^{125}I-insulin to CHO T10 and HepG2 cells as

[2] For binding analyses, it was assumed that there is a single class of binding sites for ligand binding and that there was no cooperativity between the ligand binding sites.

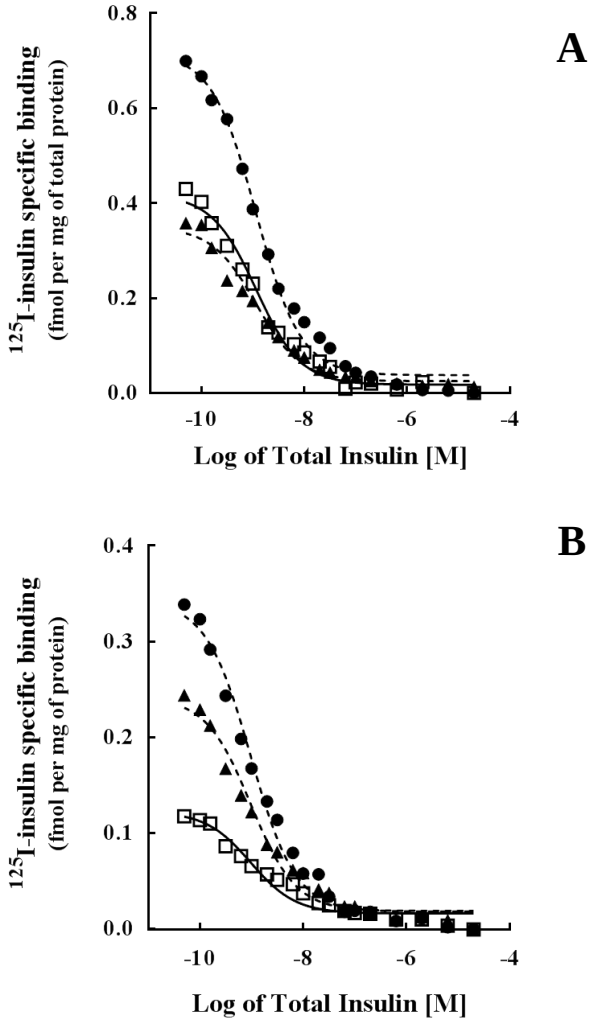

Figure 10. Effect of MBCD or cMBCD treatment on the competitive binding of ^{125}I-insulin to CHO T10 and Hep G2 cells. Following treatment with either 10mM MBCD (⊟), 10 mM cMBCD (-▲·) or untreated (-●·), CHO T10 (A) and HepG2 (B) cells were incubated for 18 h at 4 °C with a wide concentration range of competing unlabelled insulin (0 to 20.6 μM,) and a single concentration of ^{125}I-insulin (approximately 3 pM) as described in the Methods, section 2.1.7. The binding data were fitted to a one site-fit model and compared using GraphPad PRISM®. The experiment was conducted three times in duplicate but only one representative data set is illustrated, with each data point shown as the mean of duplicates.

Table 2. The effect of MBCD and cMBCD treatments on membrane insulin receptor number and affinity in CHO T10 and HepG2 cells.

Cell Models	Treatments	Affinity K_D (nM)	Receptor number per cell ($\times 10^5$)
CHO T10	Control	1.8 ± 0.4	5.3 ± 0.2
	MBCD	1.1 ± 0.5 (ns)	3.1 ± 0.1***
	cMBCD	1.3 ± 0.6 (ns)	2.3 ± 0.4****
HepG2	Control	1.1 ± 0.4	0.41 ± 0.05
	MBCD	1.7 ± 0.3 (ns)	0.18 ± 0.02***
	cMBCD	1.1 ± 0.3 (ns)	0.28 ± 0.02*

The affinity and receptor number values were estimated based on non-linear curve fitting analysis of the competition binding curves shown in Fig.12. The reported p-values for treatments are based on the comparisons with respective controls (ANOVA- Dunnette's multiple comparison test: ns – not significant, *P < 0.05, *** P < 0.001, **** P < 0.0001).

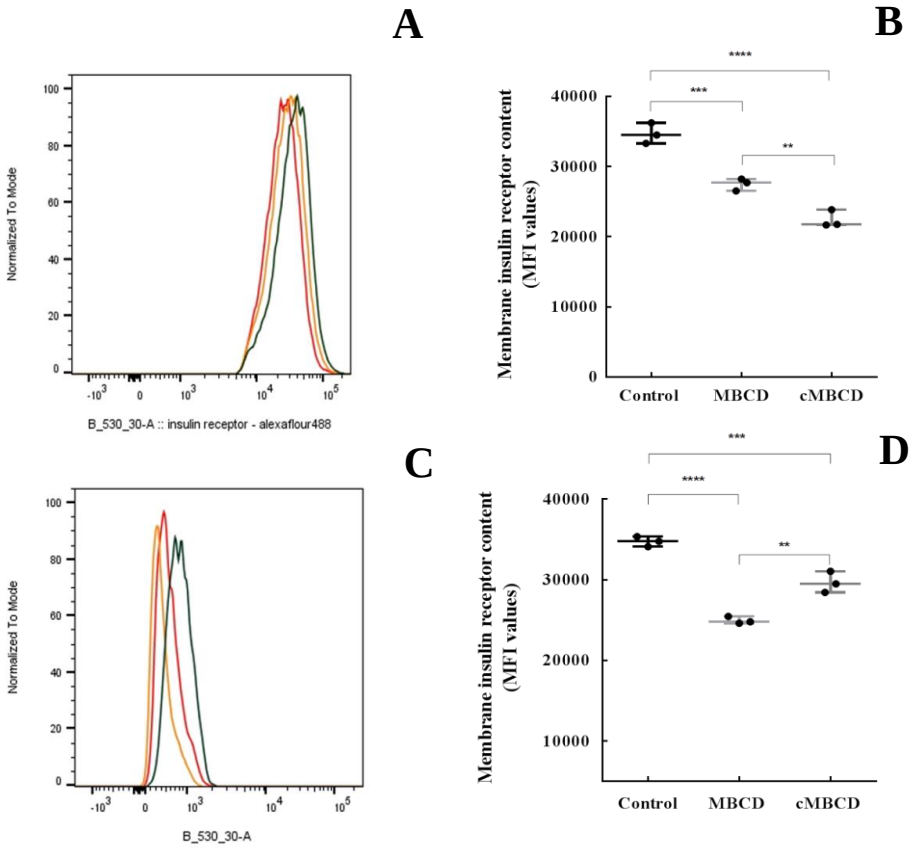

Figure 11. Effect of MBCD or cMBCD treatment on cell surface insulin receptor density in CHO T10 and HepG2 cells. Following treatments with MBCD or cMBCD, CHO T10 and HepG2 cells were incubated with anti-insulin receptor-α antibody and respective secondary antibody, and flow cytometry analysis was conducted as described in the Methods, section 2.2.1.8. One representative histogram out of three separate experiments is shown in plots A (CHO T10) and C (HepG2) that depicts the insulin receptor positive events in control (green), 10 mM MBCD (orange) and 10 mM cMBCD (red) treated groups. Comparative plots of median fluorescence intensity (MFI) values of insulin receptor positive events obtained from the histograms are illustrated in plots B (CHO T10) and D (HepG2). The experiment was conducted three times in triplicate but only one representative data set is illustrated as mean ± SD (n=3). Data from all three experiments were used for statistical analysis (Tukey's multiple comparisons test: ** $P < 0.01$, *** $P < 0.001$, **** $P < 0.0001$, n=9).

shown in Fig. 10. This reinforces the apparent cell-specific nature of the impact of cholesterol loading or depletion on insulin binding and the apparent insulin receptor number detected.

The association between cholesterol content and insulin binding in cultured cells was further examined using two approaches. In the first approach, the cells were allowed to "naturally" recover from MBCD or cMBCD mediated alterations in cell cholesterol, by maintaining the cells in complete media, i.e., media supplemented with 10% fetal bovine serum for a period of 24 h following treatments. In CHO T10 and HepG2 cells, a substantial increase or decrease in cell cholesterol content, approaching the level observed in the control cells, was observed after 24 h following MBCD or cMBCD treatment respectively (Fig. 12A and 12B). Contrastingly, in differentiated myotubes, no considerable change in cell cholesterol was observed after the recovery period following MBCD treatment; however, a substantial decrease in cell cholesterol, approaching the level observed in the control cells, was observed after the recovery period following cMBCD treatment (Fig. 12C). The specific binding of ^{125}I-insulin increased substantially in all three cell types after the recovery period following either MBCD or cMBCD treatment, approaching the level observed in control (untreated) cells (Fig. 13). Interestingly, no considerable change in binding was observed in differentiated myotubes after the 24 h recovery period following MBCD treatment (Fig. 13C), in which the cholesterol content was also observed to be unaltered (Fig. 12C).

As an alternative approach to evaluate the association between cholesterol and insulin binding, CHO T10 cells were treated sequentially with MBCD and then cMBCD or vice versa, and their effects on cell cholesterol content and insulin binding were estimated. The effects of MBCD or cMBCD on cell cholesterol content in CHO T10 cells were reversed by the sequential treatment with cMBCD or MBCD, respectively (Fig. 14A), in each case approaching the level observed in the control cells. As would be expected if membrane cholesterol and insulin binding were linked, the specific binding of ^{125}I-insulin in CHO T10 cells was also normalized towards the control level when sequentially treated with MBCD and then with cMBCD or vice versa (Fig. 14B). Thus, the decrease in insulin binding in cells treated with MBCD or cMBCD is not likely due to a secondary effect of the

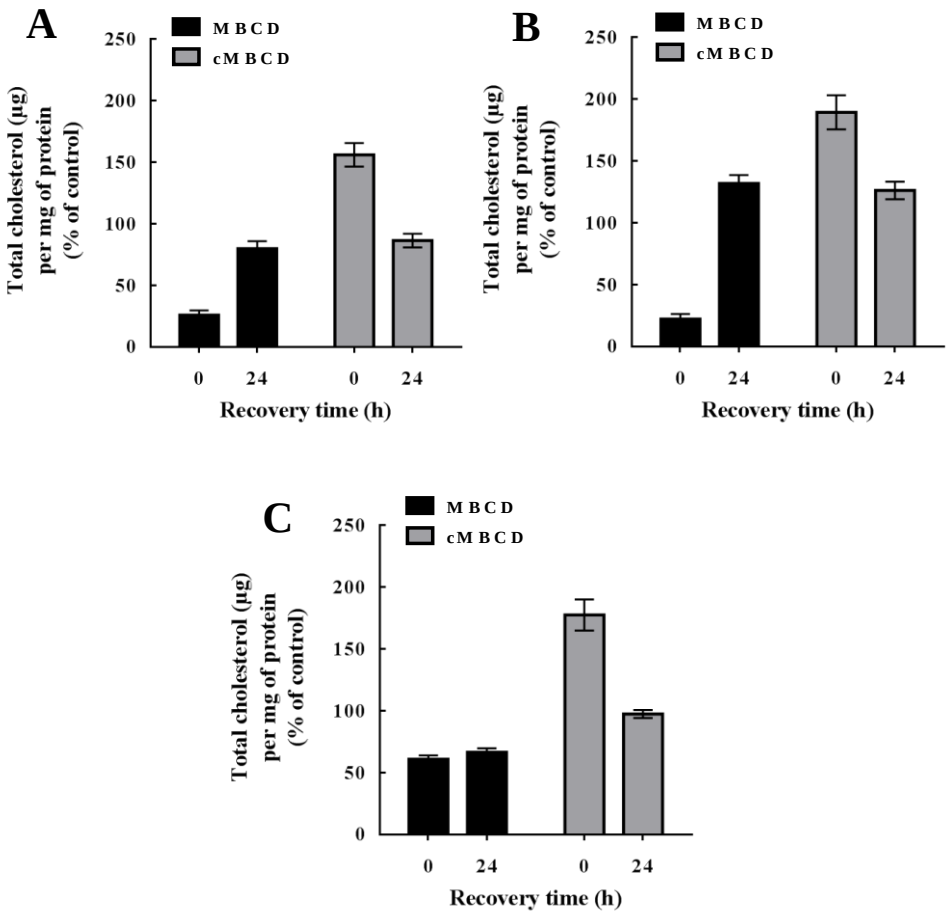

Figure 12. Normalization of cell cholesterol content by cultured cells following MBCD or cMBCD treatment. CHO T10 cells (A), HepG2 cells (B) and differentiated myotubes (C) were treated for 30 min at 37 °C with media alone (control), 10 mM MBCD or 10 mM cMBCD. The cells were then washed twice with PBS and cultured for a further 24 h at 37 °C in fresh media containing fetal bovine serum. A separate batch of cells was cultured for 24 h prior to treatment for 30 min with either MBCD or cMBCD (0 h recovery). Cells were extracted for cholesterol and protein as described in Methods, section 2.2.1.3, 2.2.1.4 and 2.2.1.6 respectively. Changes in cell cholesterol were normalized to total protein content and reported as percentages of control. The experiment was conducted three times in triplicate but only one representative data set is illustrated as mean ± SD (n=3).

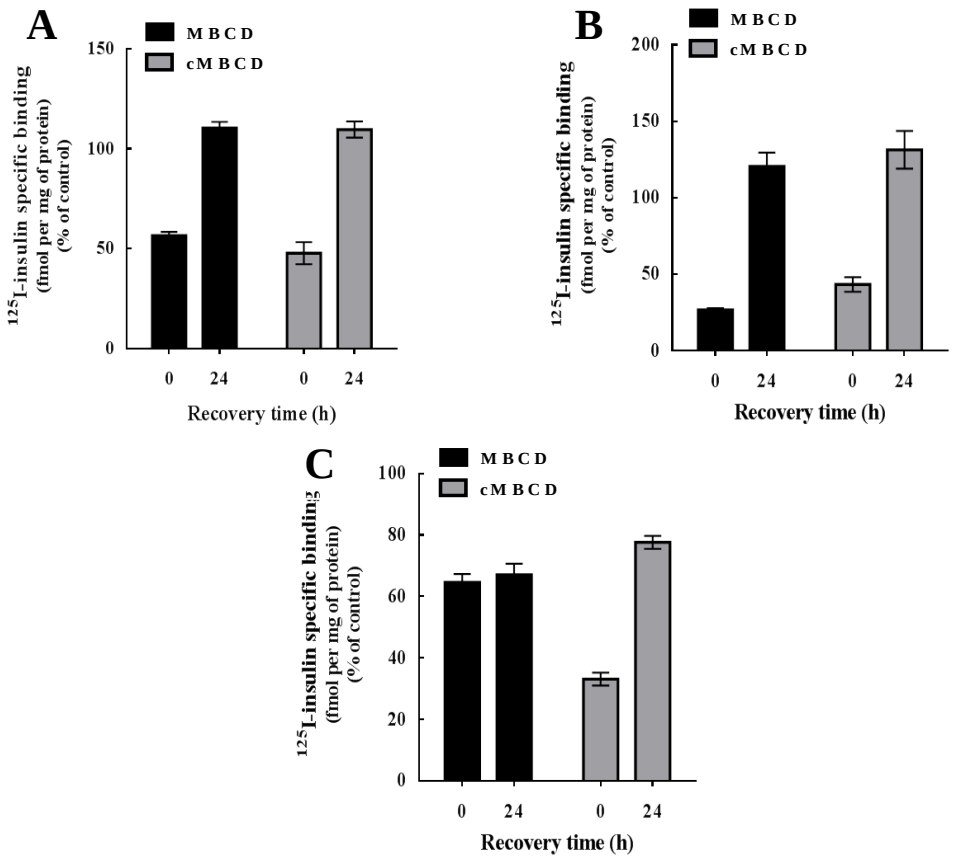

Figure 13. Normalization in ^{125}I-insulin binding in cultured cells following MBCD or cMBCD treatment. CHO T10 cells (A), HepG2 cells (B) and differentiated myotubes (C) were treated for 30 min at 37 °C with media alone (control), 10 mM MBCD or 10 mM cMBCD. The cells were then washed twice with PBS and cultured for a further 24 h at 37 °C in fresh media containing fetal bovine serum. A separate batch of cells was cultured for 24 h prior to treatment for 30 min with either MBCD or cMBCD (0 h recovery). Insulin binding assays were then conducted on treated cells as described in the Methods, section 2.2.1.7. Changes in insulin binding were normalized to total protein content and reported as percentages of control (untreated). The experiment was conducted three times in triplicate but only one representative data set is illustrated.

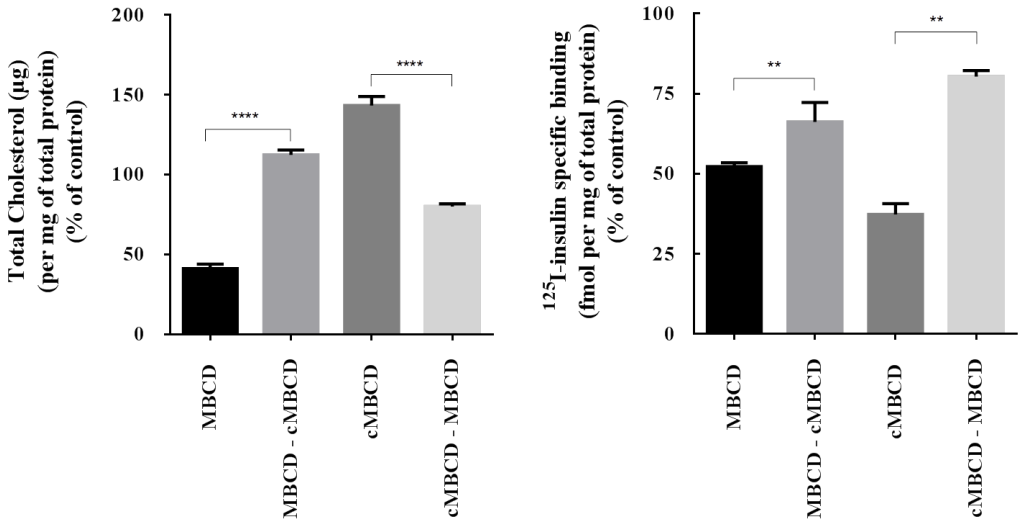

Figure 14. Effect of sequential treatment with MBCD and cMBCD on cholesterol content and ^{125}I- insulin binding. CHO T10 cells were treated for 30 min at 37 °C in media containing 10 mM MBCD in the absence of fetal bovine serum (control). A separate batch of cells was sequentially treated for 30 min at 37 °C in media first containing 10 mM MBCD and then in media containing 10 mM cMBCD or vice versa. Following treatments, suspension media containing MBCD or cMBCD was removed and the wells were rinsed twice with PBS. Cholesterol measurements and binding assay were then conducted as described in the Methods, sections 2.2.1.3 and 2.2.1.7 respectively. Changes in cholesterol (A) and insulin binding (B) were normalized to total protein content and reported as percentages of the control. The experiment was conducted two times in triplicate but only one representative data set is illustrated. Data from all experiments were used for statistical analysis (Tukey's multiple comparisons test: ** $P < 0.01$, **** $P < 0.0001$, n=6).

treatment. Rather, the observations (Fig. 13 and 14) support the conclusion that the changes in cholesterol content are directly linked with the changes in insulin binding and apparent insulin receptor number in cultured cells.

The influence of a 48 h atorvastatin treatment on insulin binding in CHO-T10 and HepG2 cells was also evaluated. Despite atorvastatin lowering cholesterol levels in each cell type (Fig. 8), it had no effect on insulin binding in either CHO T10, HepG2 (Fig. 15) or differentiated myotubes (data not shown). Analysis of the competitive binding data in Fig. 15A and B, assuming a one-site model, confirmed that there was no apparent effect of atorvastatin on either the affinity of insulin for insulin receptors or the number of insulin receptors present in CHO T10 cells or HepG2 (Table 3). These results were somewhat surprising given the clear effect of MBCD mediated cholesterol alteration on insulin binding in these cell types. Possible reasons for this apparent conundrum are further detailed in the Discussion section 4.1 of this Thesis. A summary of the effects of the MBCD, cMBCD or atorvastatin treatment in CHO T10, HepG2 and differentiated myotubes on insulin binding and receptor content is shown in Table 4.

The effects of various treatments on the total insulin receptor content phosphorylation of the β-subunit of the insulin receptor, Akt and GSK3β were evaluated (Fig. 16 - 21). There was no significant effect of MBCD or cMBCD on the total insulin receptor content in CHO T10, HepG2 or differentiated myotubes (Fig. 16B, 17B and 18B). This may appear at odds with the earlier observations based on the binding and flow cytometry analyses, which suggests that MBCD and cMBCD decreases insulin binding in CHO T10 and HepG2 cells by decreasing the apparent number of insulin receptors on the surface of cells. However, it should be noted that the quantitation of insulin receptors in the Western blots herein were based on the total cell lysates whereas quantitation based on binding and flow cytometry analysis would have measured cell surface insulin receptors and not total cellular receptor levels.

The treatment of CHO T10 cells with MBCD resulted in a significant decrease in phosphorylation of the β-subunit of the insulin receptor and Akt (Fig. 16C and D; $P < 0.001$ in both cases), despite having no effect on total insulin receptor content. These decreases coincided with the binding data shown in Fig.10; however, no

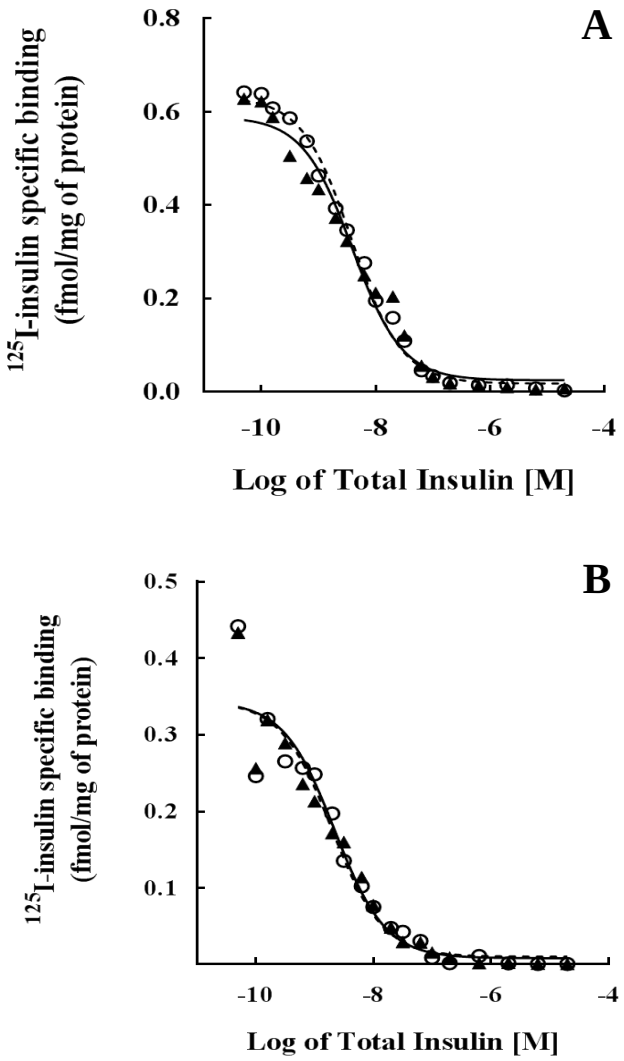

Figure 15. Effect of atorvastatin treatment on the competitive binding of ^{125}I-insulin to CHO T10 and HepG2 cells. Following 48 h treatment at 37 °C with 10 μM atorvastatin CHO T10 (A) and HepG2 (B) cells were incubated for 18 h at 4 °C with a wide concentration range of competing unlabelled insulin (0 to 20.6 μM) and a single concentration of ^{125}I-insulin (approximately 3 pM) (see Methods, section 2.2.1.7 for assay procedure). The specific binding of ^{125}I-insulin in control (⊖) and atorvastatin treated groups (▲) were fitted to a one site-fit model and compared using GraphPad PRISM®. The experiment was conducted three times in duplicate but only one representative data set is illustrated, with each data point shown as the mean of duplicates.

Table 3. The effect of atorvastatin treatment on insulin receptor number and affinity in CHO T10 and Hep G2 cells.

Cell Models	Treatments	Affinity K_D (nM)	Receptor number per cell (x 10^5)
CHO T10	Control	3.8 ± 1.1	4.9 ± 0.7
	Atorvastatin	3.9 ± 1.2 (ns)	4.5 ± 0.6 (ns)
HepG2	Control	2.2 ± 1.4	0.14 ± 0.04
	Atorvastatin	1.9 ± 1.3 (ns)	0.16 ± 0.03 (ns)

The affinity and receptor number values were estimated based on non-linear curve fitting analysis of the competition binding curves to one-site fit binding model using GraphPad PRISM® (see Methods, Section 2.2.1.7). The reported p-values for treatments in CHO T10 cells and HepG2 cells are based on the comparisons with the respective controls (An F-test was used for affinity comparisons with the control and unpaired t-test (two-tailed) was done for comparing receptor number; ns – not significant).

Table 4. A summary of the effects of MBCD, cMBCD or atorvastatin treatment on insulin binding and insulin receptor content in cultured cells.

	Cholesterol content			Insulin binding			Receptor content estimated by binding assay			Receptor content estimated by flow cytometry		
Treatments	**CHO T10**	**HepG2**	**Myotubes**	**CHO T10**	**HepG2**	**Myotubes**	**CHO T10**	**HepG2**	**Myotubes**	**CHO T10**	**HepG2**	**Myotubes**
10 mM MBCD	↓	↓	↓	↓	↓	↓	ns	ns	*	↓	↓	*
10 mM cMBCD	↑	↑	↑	↓	↓	↓	ns	ns	*	↓	↓	*
10 µM Atorvastatin	↓	↓	↓	ns	ns	nd	ns	ns	*	*	*	*

The effects of MBCD or cMBCD or atorvastatin treatment on cell cholesterol content, insulin binding and receptor content estimation by binding assay and flow cytometry were summarized in this table (↓ denotes a decrease, ↑ denotes an increase, ‘ ns ‘ denotes no significant change, ‘nd’ denotes ‘not determined’ and ‘ * ’ denotes ‘not examined’).

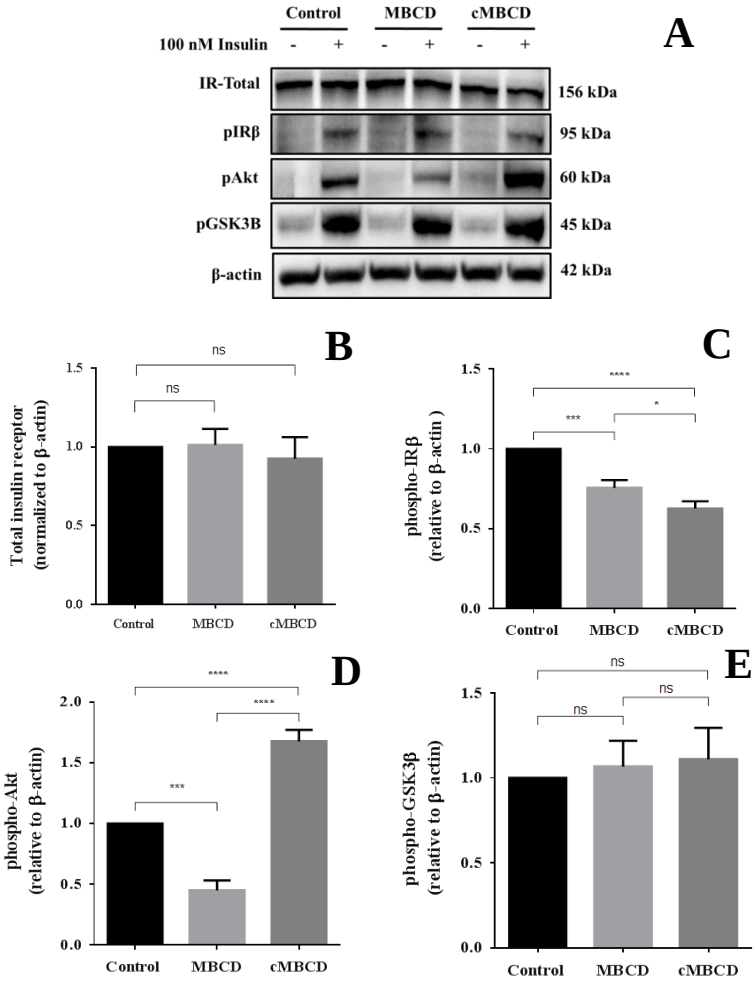

Figure 16. Effect of MBCD and cMBCD treatments on insulin signalling in CHO T10 cells. Cells were treated for 30 min with 10 mM MBCD or 10 mM cMBCD and then for 7 min at 37 °C with 100 nM insulin. Following treatments, the cells were lysed in RIPA buffer and Western blot analysis was conducted as described in the Methods, section 2.2.1.9. One representative Western blot image out of three separate experiments is shown in (A). Bands representing total insulin receptor expression (B), the phosphorylation of IR-β (Tyr 1361) (C), phosphorylation of Akt (Tyr 308) (D) and phosphorylation of GSK3β (Ser 9) (E) were quantitated by densitometry analysis and normalised to β-actin expression. Data from all three experiments were plotted as mean ± SD (Tukey's multiple comparisons test: ns – not significant, * $P < 0.05$, ** $P < 0.01$, **** $P < 0.0001$, $n = 3$).

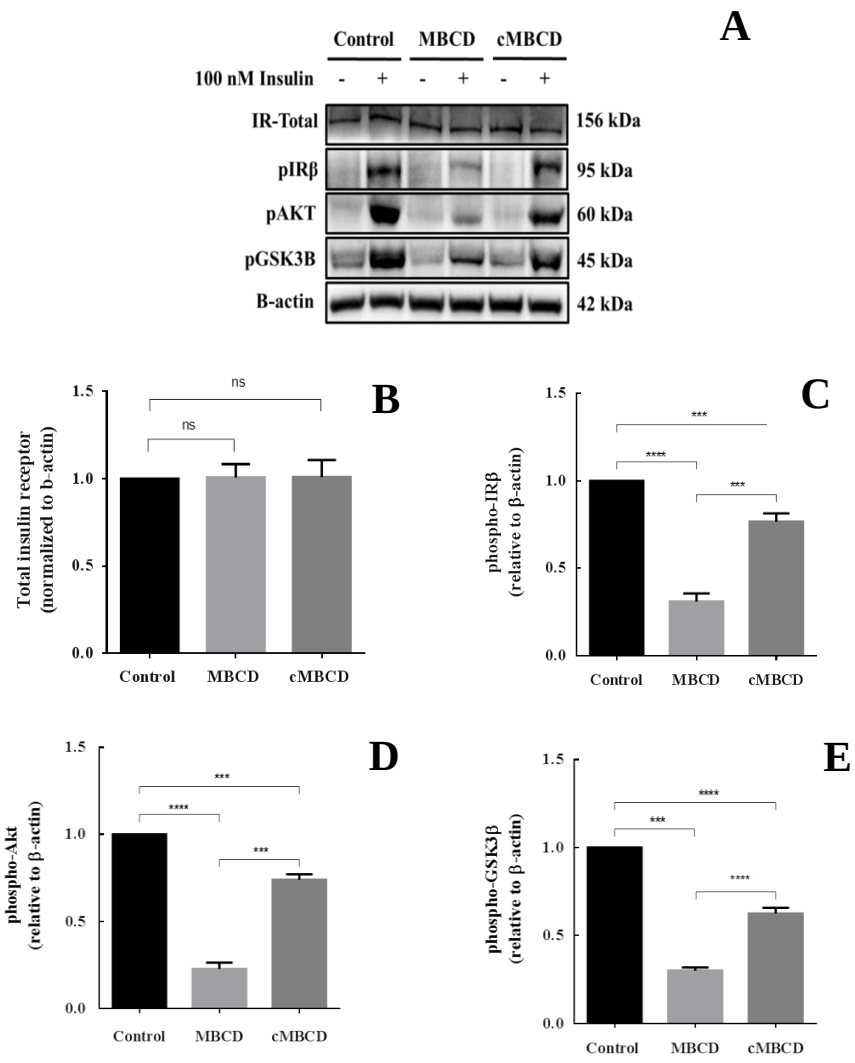

Figure 17. Effect of MBCD and cMBCD treatments on insulin signalling in HepG2 cells. Cells were treated for 30 min with 10 mM MBCD or 10 mM cMBCD and then for 7 min at 37 °C with 100 nM insulin. Following treatments, the cells were lysed in RIPA buffer and Western blot analysis was conducted as detailed in Methods, Section 2.2.1.9. One representative Western blot image out of three separate experiments is shown in (A). Bands representing total insulin receptor expression (B), the phosphorylation of IR-β (Tyr 1361) (C), phosphorylation of Akt (Tyr 308) (D) and phosphorylation of GSK3β (Ser 9) (E) were quantitated by densitometry analysis and normalised to β-actin expression. Data from all three experiments were plotted as mean ± SD (Tukey's multiple comparisons test: ns – not significant, * $P < 0.05$, ** $P < 0.01$, **** $P < 0.0001$, $n = 3$).

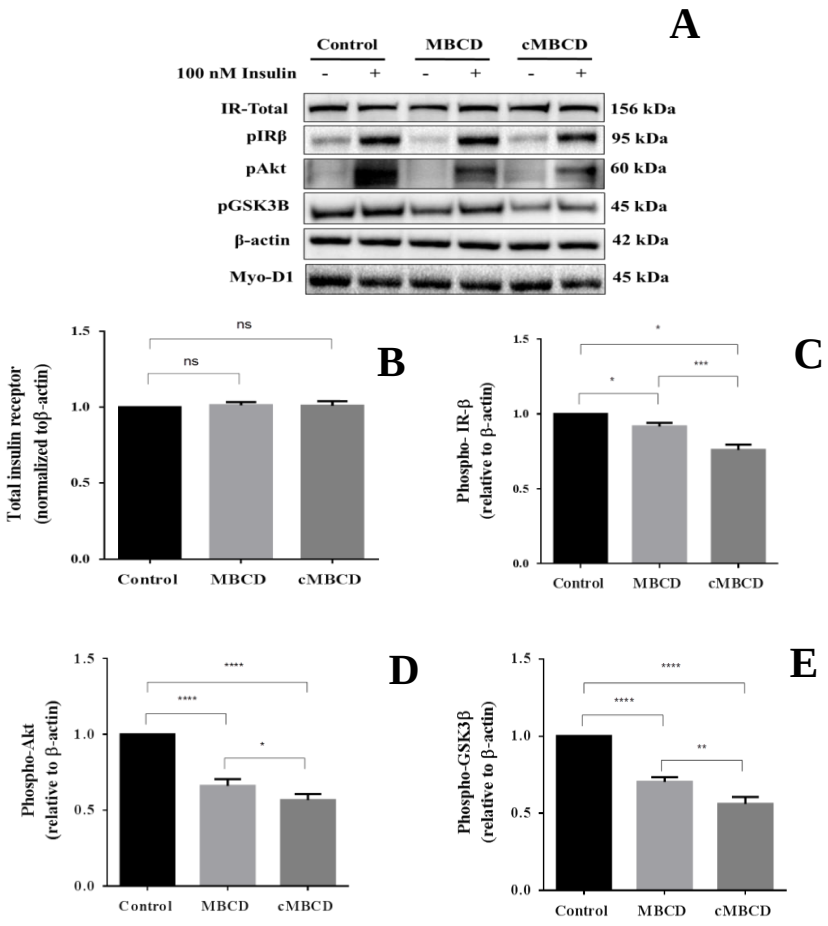

Figure 18. Effect of MBCD and cMBCD treatments on insulin signalling in differentiated myotubes. Differentiated myotubes were treated for 30 min with 10 mM MBCD or 10 mM cMBCD and then for 7 min at 37 °C with 100 nM insulin. Following treatments, myotubes were lysed in RIPA buffer and Western blotting analysis was conducted as described in Methods, Section 2.2.1.9. One representative Western blot image out of three separate experiments is shown in (A). Bands representing total insulin receptor expression (B), the phosphorylation of IR-β (pTyr 1361) (C), phosphorylation of Akt (pTyr 308) (D) and phosphorylation of GSK3β (Ser 9) (E) were quantitated by densitometry analysis and normalised to β-actin expression. Data from all three experiments were plotted as mean ± SD (Tukey's multiple comparisons test: ns-not significant, * $P < 0.05$, ** $P < 0.01$, *** $P < 0.001$, **** $P < 0.0001$, $n = 3$).

significant effect was observed in phosphorylation of GSK3β (Fig. 16E). Whilst the proportion of phosphorylated insulin receptors was significantly decreased following cMBCD treatment (Fig. 16C, $P < 0.0001$), the amount of pAkt detected was substantially increased (Fig. 16D; $P < 0.001$). As was observed with MBCD treatment of CHO T10 cells, there was no corresponding change in the phosphorylation of GSK3β (Fig. 16E; $P = 0.1$) after cMBCD treatment. Thus, there does not appear to be a clear link between the decreased autophosphorylation of the insulin receptors in CHO T10 cells following treatment with either MBCD or cMBCD and its downstream signalling outcomes in Akt and GSK3β phosphorylation. Some possible reasons for these somewhat counterintuitive results are detailed in the Discussion of this Thesis in section 4.1.

In contrast to the observations made in CHO T10 cells, there appears to be a clear link between the effect of insulin binding and insulin signalling outcomes in both HepG2 and differentiated myoblasts (Fig. 17 and 18, respectively). The proportion of insulin receptors that were autophosphorylated decreased significantly when HepG2 or differentiated myoblasts were treated with either 10 mM MBCD or cMBCD (Fig. 17C and 18C), coinciding well with the decreased insulin binding. Moreover, the changes observed in autophosphorylation of the insulin receptor in the presence of either MBCD or cMBCD corresponded with the changes observed in the expression of either pAkt or pGSK3β in HepG2 cells and myotubes (Fig. 17 and 18).

The expression of total insulin receptor protein was unaffected in CHO T10, HepG2 or differentiated myoblasts following treatment with atorvastatin (Fig. 19, 20 and 21). Whilst decreasing cholesterol levels in CHO T10, HepG2 and differentiated myotubes (Fig. 8A - C), atorvastatin treatment did not impact insulin binding to these cells (Fig. 15). This finding contrasts with the effect of MBCD in decreasing cholesterol levels (Fig. 10A and B), which corresponded with the decreased insulin binding to these cells (Table 2). Given that atorvastatin had minimal if any effect on insulin binding to these cells in culture, it was expected that it would have little impact on the autophosphorylation of insulin receptors and downstream signalling pathways. Indeed, atorvastatin treatment of CHO T10 and Hep G2 cells appeared to have minimal impact on the activation of their insulin receptors, Akt or GSK3β (Fig. 19 – 20). On the other hand, atorvastatin did substantially impact autophosphorylation of insulin receptors, Akt and GSK3β in differentiated myotubes

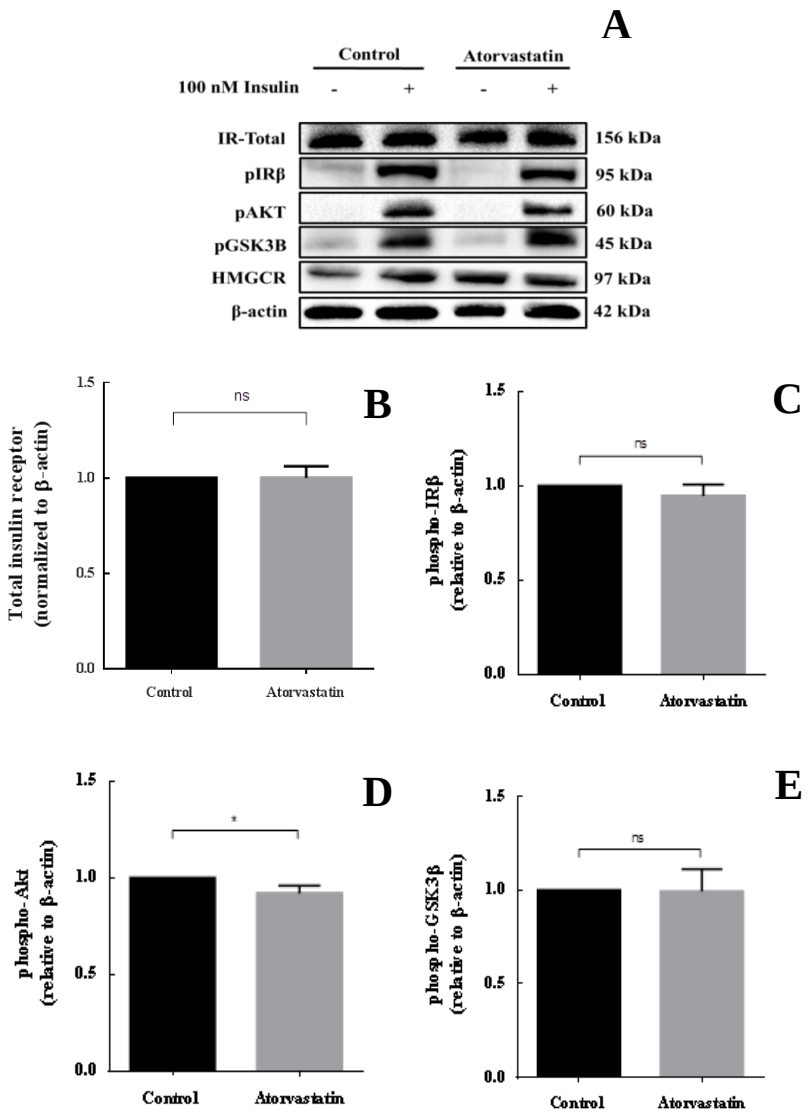

Figure 19. Effect of atorvastatin on insulin signalling in CHO T10 cells. Cells were treated for 48 h with 10 µM atorvastatin and then treated for 7 min at 37 °C with 100 nM insulin. Following treatments, the cells were lysed in RIPA buffer and Western blot analysis was conducted as described in the Methods, section 2.2.1.9. One representative Western blot image out of three separate experiments is shown in (A). Bands representing total insulin receptor expression (B), the phosphorylation of IR-β (Tyr 1361) (C), phosphorylation of Akt (Tyr 308) (D) and phosphorylation of GSK3β (Ser 9) (E) were quantitated by densitometry analysis and normalised to β-actin expression. Data from all three experiments were plotted as mean ± SD (Paired t-test: * $P < 0.05$, ns – not significant, n = 3).

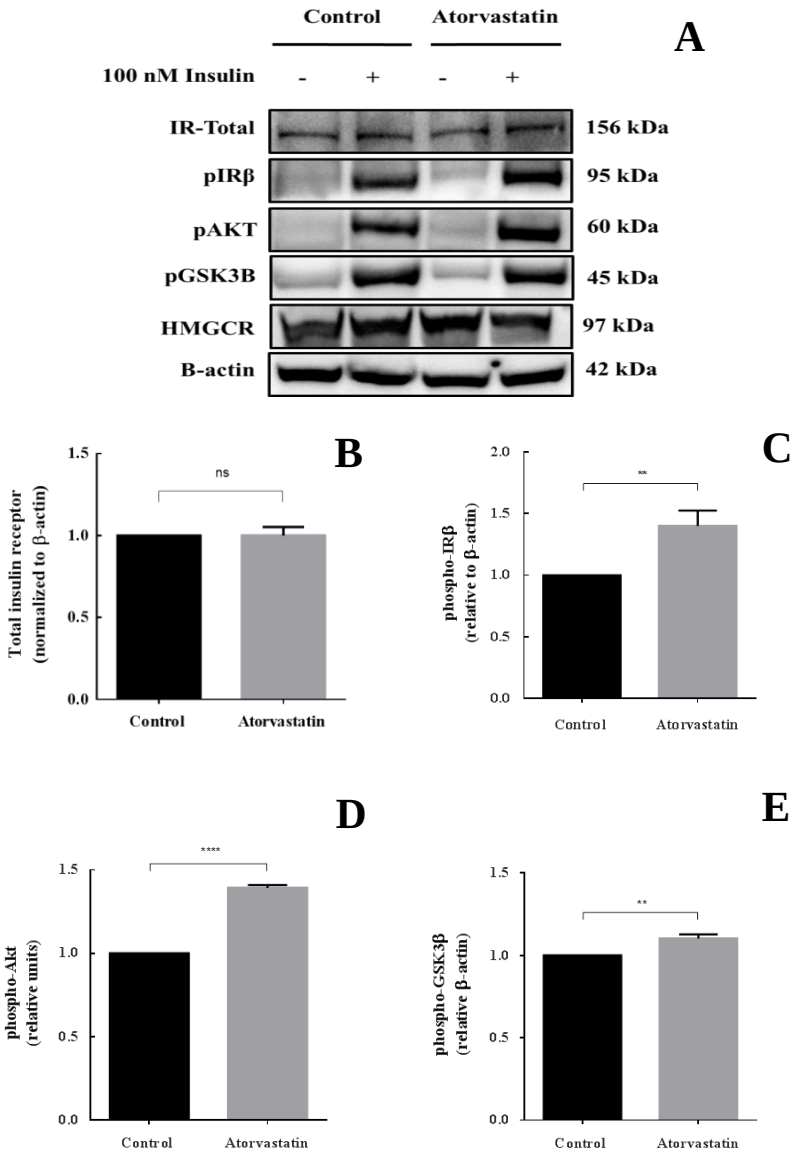

Figure 20. Effect of atorvastatin on insulin signalling in HepG2 cells. Cells were treated for 48 h with 10 μM atorvastatin and then treated for 7 min at 37 °C with 100 nM insulin. Following treatments, the cells were lysed in RIPA buffer and Western blot analysis was conducted as described in the Methods, section 2.2.1.9. One representative Western blot image out of three separate experiments is shown in (A). Bands representing total insulin receptor expression (B), the phosphorylation of IR-β (Tyr 1361) (C), phosphorylation of Akt (Tyr 308) (D) and phosphorylation of GSK3β (Ser 9) (E) were quantitated by densitometry analysis and normalised to β-actin expression. Data from all three experiments were plotted as mean ± SD (Paired t-test: * $P < 0.05$, ** $P < 0.01$, $n = 3$).

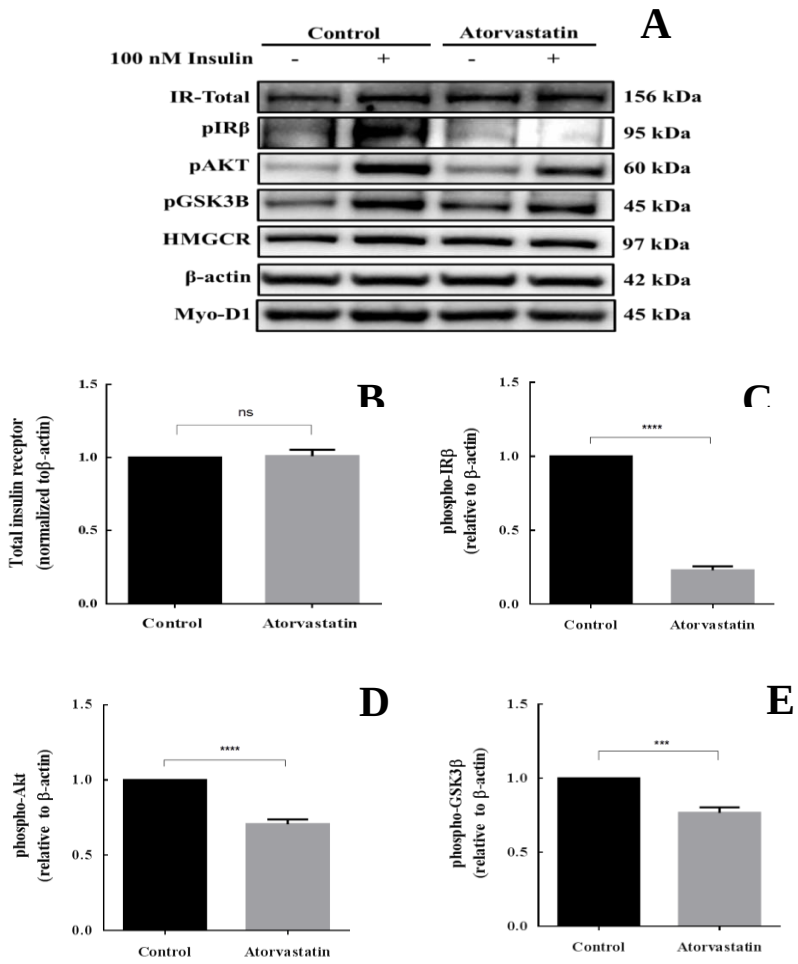

Figure 21. Effect of atorvastatin on insulin signalling in differentiated myotubes. Differentiated myotubes Cells were treated for 48 h with 10 µM atorvastatin and then treated for 7 min at 37 °C with 100 nM insulin. Following treatments, the cells were lysed in RIPA buffer and Western blot analysis was conducted as described in the Methods, section 2.2.1.9. One representative Western blot image out of three separate experiments is shown here (A). Bands representing total insulin receptor expression (B), the phosphorylation of IR-β (Tyr 1361) (C), phosphorylation of Akt (Thr 308) (D) and phosphorylation of GSK3β (Ser 9) (E) were quantitated by densitometry analysis and normalised to β-actin expression. Experiment was conducted three times and data from all three experiments were plotted as mean ± SD (Paired t-test: * $P < 0.05$, ** $P < 0.01$, $n = 3$).

Table 5. A summary of the effects of MBCD, cMBCD or atorvastatin treatment on insulin signalling events in cultured cells.

	Total IR			pIRβ			pAKT			pGSK3β		
Treatments	**CHO T10**	**HepG2**	**Myotubes**	**CHO T10**	**HepG2**	**Myotubes**	**CHO T10**	**HepG2**	**Myotubes**	**CHO T10**	**HepG2**	**Myotubes**
10 mM MBCD	ns	ns	ns	↓	↓	↓	↓	↓	↓	ns	↓	↓
10 mM cMBCD	ns	ns	ns	↓	↓	↓	↑	↓	↓	ns	↓	↓
10 µM Atorvastatin	ns	ns	ns	ns	↑	↓	ns	↑	↓	ns	↑	↓

The effects of MBCD or cMBCD or atorvastatin treatment on cell cholesterol content, insulin binding and affinity, and surface insulin receptor content were summarized in this table (↓denotes a significant decrease, ↑denotes a significant increase, ‘ ns ‘ denotes no significant change and ‘ * ’ denotes ‘not examined’).

(Fig. 21). A summary of the effects of the MBCD, cMBCD or atorvastatin treatment in CHO T10, HepG2 and differentiated myotubes on insulin signalling events is shown in Table 5.

3.2. Effects of a high fat diet and atorvastatin treatment on cholesterol content and insulin action in mouse liver

Mice were fed for 12 weeks with either a normal or high-fat diet in the presence or absence of atorvastatin as described in Methods, Sections 2.2.2.1. Whole livers were then collected, and various membrane and cytosolic fractions were isolated from the tissue samples as described in Methods, Section 2.2.2.2. Each fraction obtained from the liver tissue samples was characterized by Western blotting analysis based on the presence or absence of characteristic protein markers. The plasma membrane fractions isolated for this study were enriched in Na^+/K^+ ATPase and were largely free of contamination by mitochondrial (SDHA) and endoplasmic reticulum (KDEL) protein markers (Fig. 22). However, the presence of syntaxin-6 in the plasma membrane fraction suggests some contamination by golgi membranes. The presence of the insulin receptor was found to be significantly higher in the plasma membrane fraction compared to all other fractions (Fig.22). Likewise, the specific binding of ^{125}I insulin was also highest in the plasma membrane fractions, irrespective of diet and atorvastatin treatment (Fig. 23). Taken together, these findings suggest that the membrane fraction isolated for this study was highly enriched in plasma membranes and that they contained functional insulin receptors that specifically bound insulin.

The total cholesterol content of liver homogenates was unaffected by high-fat feeding (Fig. 24 and 25). Interestingly, and by contrast, atorvastatin treatment generally resulted in an increase in cholesterol content in all fractions examined including liver homogenate, plasma membrane and cytosolic fractions, reaching statistical significance in all but the plasma membrane fraction for mice on a normal diet (Fig. 25). In contrast to results on homogenate, there was a substantial decrease in the cholesterol content of the plasma membrane and cytosolic fraction of mice that were fed a high-fat diet (HFD) (Fig. 24 and 25). Interestingly, when mice were fed the high fat diet and also treated with atorvastatin (HFD-A), the cholesterol content of their cytosolic and plasma membrane fractions increased substantially and were

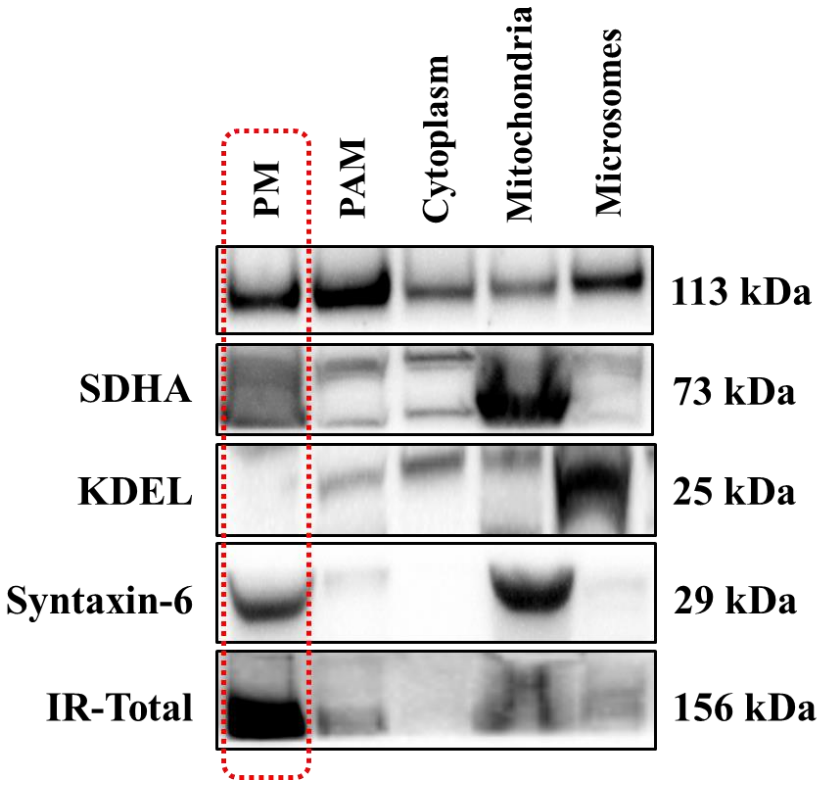

Figure 22. Characterization of mouse liver fractions based on specific protein markers. Total protein content in liver fractions was estimated using a BCA assay as described in the Methods, section 2.2.3.5. Protein (20 µg) was separated by SDS-PAGE and Western blot analysis was conducted as described in the Methods, section 2.2.3.7. A representative Western blot image illustrating the specific marker-based characterization of liver fractions is shown here; plasma membrane (PM); plasma membrane-associated membrane (PAM); cytoplasm; mitochondria, and microsomes. The presence of membrane-specific markers was monitored in each fraction: Na^+/K^+ - ATPase (plasma membrane marker); succinate dehydrogenase (SDHA - mitochondrial membrane marker); endoplasmic reticulum c-terminal tetrapeptide (Lys-Asp-Glu-Leu; represented as KDEL) and syntaxin-6 (golgi apparatus membrane marker); and the insulin receptor (IR-Total).

Figure 23. Specific binding of ^{125}I-insulin in mouse liver fractions. Insulin binding to liver fractions was determined as described in the Methods, section 2.2.3.6. In brief, liver fractions were diluted in binding buffer and incubated for 18 h at 4°C with approximately 3 pM of ^{125}I-insulin in the presence (non-specific binding) or absence (total binding) of unlabelled insulin (~20 µM). Specific binding was calculated in each fraction from the difference between the total and non-specific binding of the ^{125}I-insulin. Insulin binding was evaluated in plasma membrane (PM), plasma membrane-associated membrane (PAM), cytoplasm, mitochondria and microsomes obtained from three randomly selected mice from each group (ND, ND-A, HFD and HFD-A). The experiment was conducted three times in triplicate and the mean values of each fraction obtained from each mouse within the same group were pooled, with data shown as mean ± SD (one-way ANOVA: **** $P < 0.0001$, $n = 3$).

NORMAL DIET (ND)

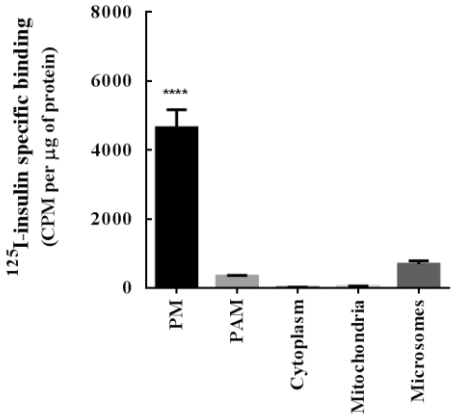

NORMAL DIET-ATORVASTATIN (ND-A)

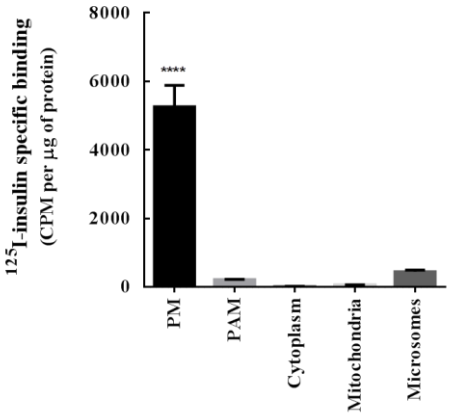

HIGH-FAT DIET (HFD)

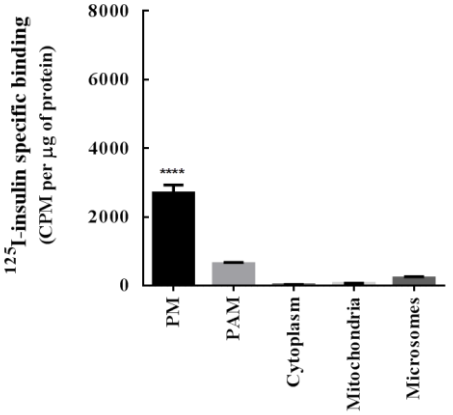

HIGH-FAT DIET-ATORVASTATIN (HFD-

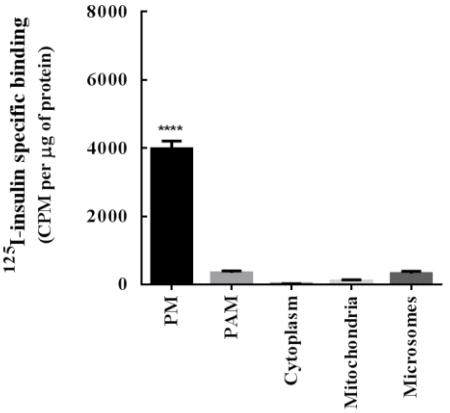

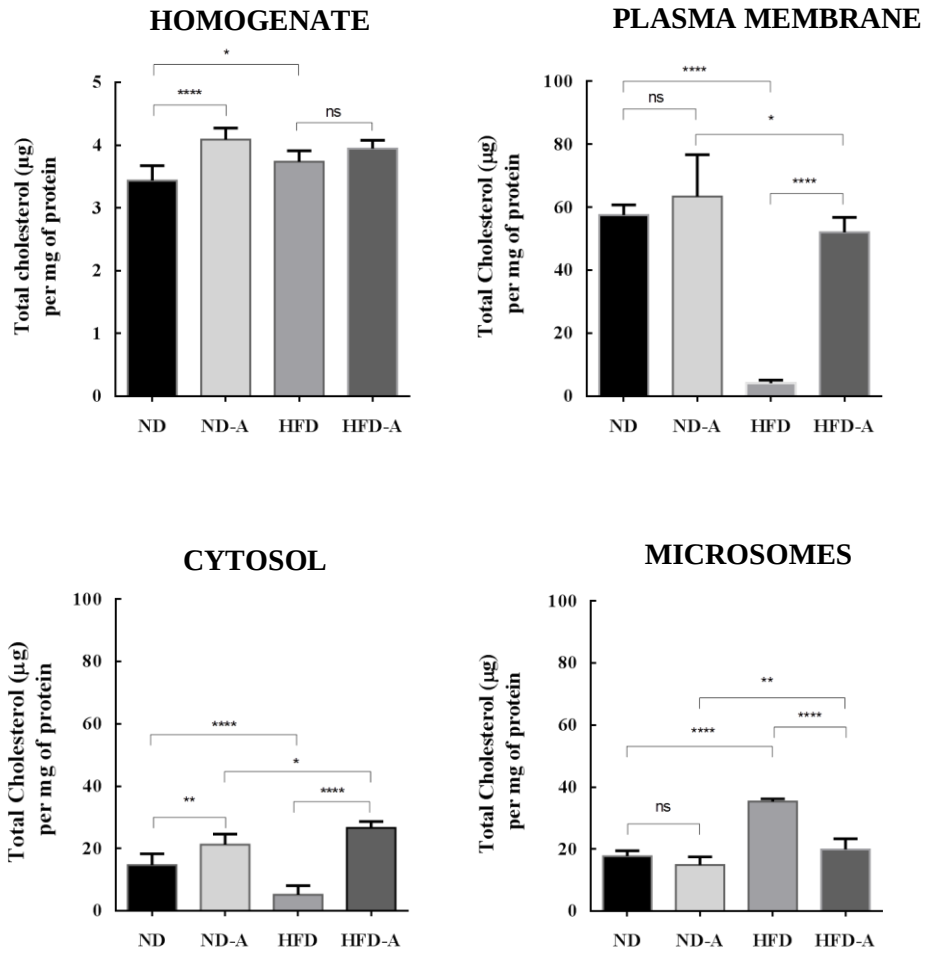

Figure 24. Effect of diet and atorvastatin treatment on cholesterol content per milligram of protein. Mice were fed for 12 weeks with either a normal diet (ND), a high fat diet (HFD), a normal diet whilst treated with atorvastatin (ND-A) or a high fat diet whilst treated with atorvastatin (HFD-A) as described in Methods, section 2.2.3.1. Livers from each of seven mice in each group were individually fractionated as described in Methods, section 2.2.3.3 and 2.2.3.4. The cholesterol content in each fraction from each mouse was then determined in triplicate as described in Methods, section 2.2.3.5 and normalised to total protein content. The data is shown as the mean ± SD of cholesterol levels determined from the seven mice in each group. A Tukey's multiple comparison test was performed to determine the levels of statistical difference between groups: ns – not significant; * $P < 0.05$ ** $P < 0.01$; *** $P < 0.001$; **** $P < 0.0001$.

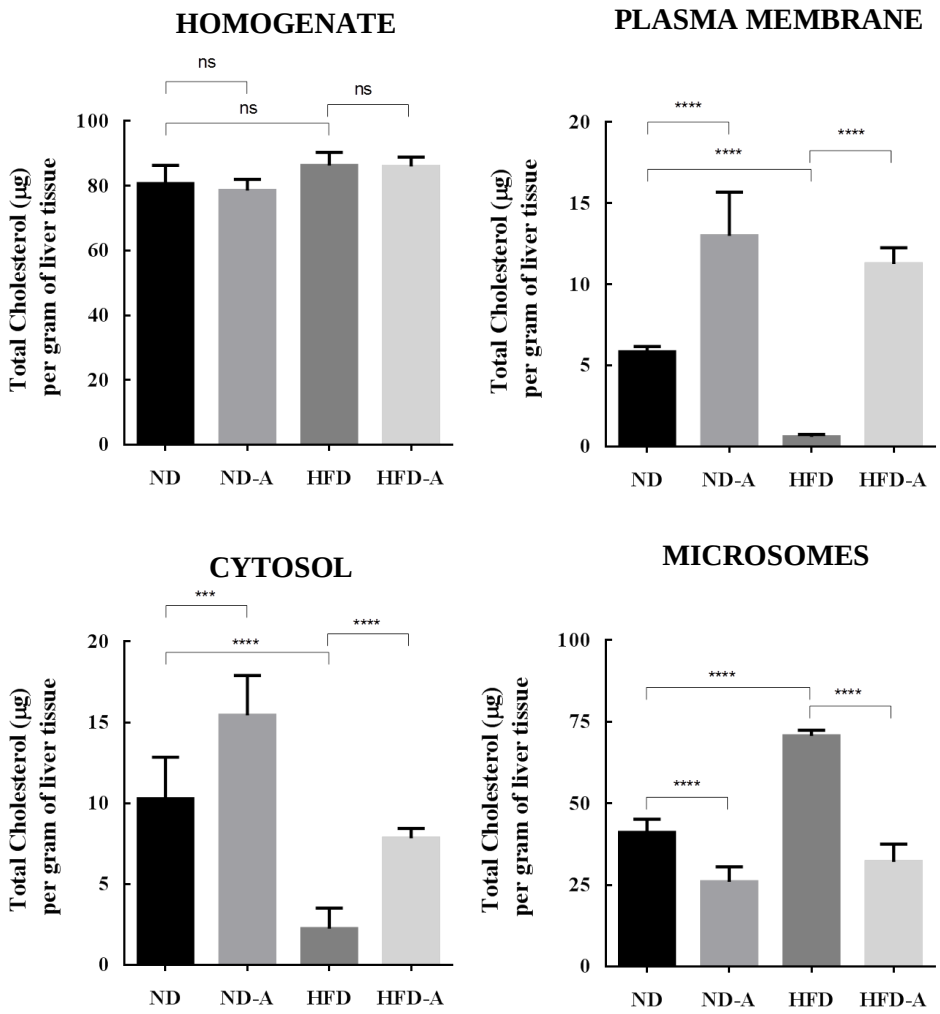

Figure 25. Effect of diet and atorvastatin treatments on total cholesterol content per gram of liver tissue. Mice were fed for 12 weeks with either a normal diet (ND), a high fat diet (HFD), a normal diet whilst treated with atorvastatin (ND-A) or a high fat diet whilst treated with atorvastatin (HFD-A) as described in Methods, section 2.2.3.1. Livers from each of seven mice in each group were individually fractionated as described in Methods, section 2.2.3.3 and 2.2.3.4. The cholesterol content in each fraction from each mouse was then determined in triplicate as described in Methods, section 2.2.3.5 and the changes in total cholesterol content were illustrated here. The data is shown as the mean ± SD of cholesterol levels determined from the seven mice in each group. A Tukey's multiple comparison test was performed to determine the levels of statistical difference between groups: ns – not significant; **** $P < 0.0001$.

essentially indistinguishable from those fed a normal diet (ND) (Fig. 24 and 25). The other notable finding, and in contrast to the observations in plasma membrane and cytosolic fractions of mice that were fed a high-fat diet (HFD), was a substantial increase in the cholesterol content of the microsomal fraction in HFD group compared all other groups (Fig. 24D and 25D). These findings were somewhat counterintuitive and unexpected and are discussed in greater detail in the Discussion section 4.2 of this Thesis.

The competitive binding of ^{125}I-insulin to plasma membranes isolated from mice that were fed a normal or high fat diet and the effect of atorvastatin treatment in each group is illustrated in Fig. 26 for each of seven animals in each treatment group (Fig. 26 A-G). The specific binding of ^{125}I-insulin in mice that were fed the high-fat diet (HFD) was markedly decreased in the plasma membrane fraction isolated from each mouse from that group compared to mice that were fed the normal diet (ND) (Fig 26). This appeared to be due to the substantial decrease ($P < 0.0001$) in membrane insulin receptors content in mice that were fed the high fat diet (Fig. 28) and not as a consequence of the slight decrease in the affinity of insulin for insulin receptors (Fig. 26 and Table 6, $P < 0.01$).

The effect of the high fat diet in reducing the specific binding of insulin was ameliorated in each of the seven mice by atorvastatin treatment (Fig. 26). Analysis of the competitive binding data suggest that this recuperative effect is due to an almost 10-fold increase in affinity of insulin for insulin receptor and at least a 5-fold decrease in available insulin receptors (Table 6). Perhaps, atorvastatin recruits a small class of high affinity receptors to the plasma membranes in the mice fed a high fat diet. Alternatively, as eluded to previously when evaluating insulin binding in the cell culture models used in this study, the binding model used to analyse the data may not adequately describe the data. Indeed, Western blot analysis clearly illustrates that atorvastatin most likely ameliorates the loss of insulin binding in mice that were fed a high-fat diet by increasing the number of insulin receptors available to bind insulin (Fig. 28). Whilst atorvastatin ameliorated the loss of insulin binding in plasma membranes from mice fed a high fat diet, it is notable that atorvastatin had little effect on the specific binding of insulin receptors in any of the seven mice that were fed the normal diet (Fig. 26). Indeed, compared to the control (ND) group, no

Figure 26. Effect of diet and atorvastatin treatments on the competitive binding of ^{125}I-insulin to plasma membranes obtained from mouse liver. Plasma membranes were individually isolated from livers of mice that were fed either a normal diet (ND, n=7, ⊖), a normal diet whilst simultaneously being treated for 12 weeks with atorvastatin (ND-A, n=7, -●·); a high-fat diet (HFD, n=7, -⊟·), or a high-fat diet whilst simultaneously being treated for 12 weeks with atorvastatin (HFD-A, n=7, -■-), as described in detail in Methods, section 2.2.2.2. The binding of ^{125}I-insulin to the membranes isolated from each animal was determined as described in Methods, section 2.2.2.6. Each competitive displacement curve was fitted to a one-sit fit model using GraphPad PRISM®. The binding data for one of the seven animals from each of the four groups is shown in each plot (A to G). Each data point in each plot is a mean of duplicate determinations.

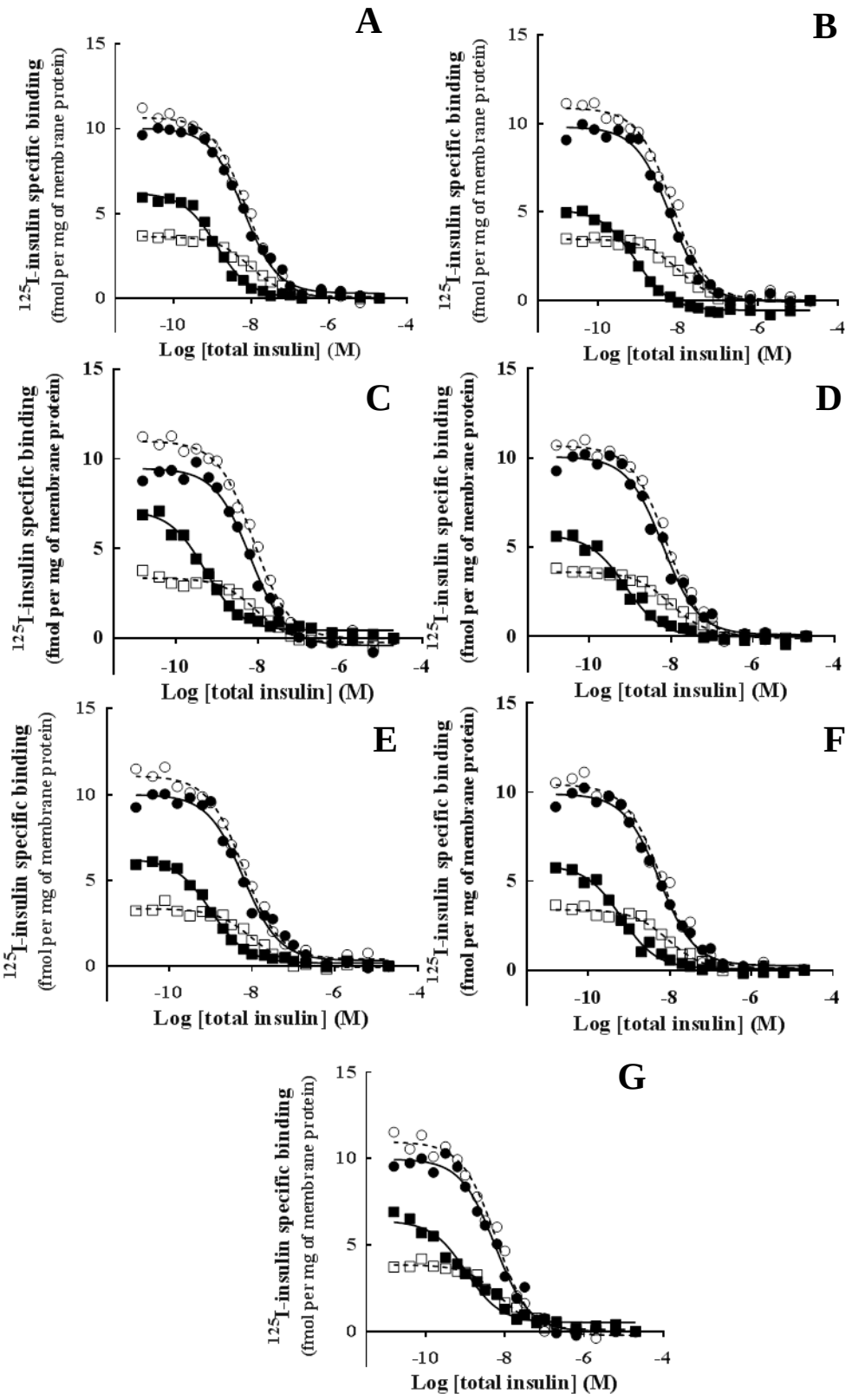
A
B
C
D
E
F
G
^{125}I-insulin specific binding
(fmol per mg of membrane protein)
Log [total insulin] (M)
15
10
5
0
-10
-8
-6
-4

Table 6. Effect of diet and atorvastatin treatments on insulin binding parameters in plasma membrane isolated from mice liver tissue.

Treatment groups	Affinity (K_D) (nM)	Receptor number per mg of plasma membrane protein (X 10^9)
ND	6.9 ± 0.8	1.3 ± 0.2
ND-A	6.1 ± 0.4	1.03 ± 0.07
HFD	9.4 ± 0.9	0.57 ± 0.04
HFD-A	0.9 ± 0.3	0.09 ± 0.03

The affinity (K_D) values and receptor numbers in each of the treatments were determined from the competitive binding plots shown in Fig. 27 using a one-site fit model. The data shown as the mean ± SD of data obtained from the seven animals for each treatment group. Statistical analyses, as shown below, was conducted using ANOVA - Tukey's multiple comparison test.

Affinity (K_D)
ND vs ND-A, ns- not significant, P = 0.3
ND vs HFD, ** P < 0.01
ND-A vs HFD-A, ****P < 0.0001
HFD vs HFD-A, ****P < 0.0001

Receptor number
ND vs ND-A, P = 0.1, ns
ND vs HFD, ***P < 0.001
ND-A vs HFD-A, ****P < 0.0001
HFD vs HFD-A, ****P < 0.0001

significant difference could be observed in either the affinity (P = 0.3) of insulin receptors for insulin or in the number of insulin receptors present per mg of membrane protein (P = 0.1) in mice that were fed the normal diet and treated with atorvastatin (ND-A). In context of the influence of membrane cholesterol content on insulin binding, treatment of liver plasma membranes of mice that were fed a normal diet, with 10 mM MBCD or cMBCD, also decreased insulin binding to these membranes (Fig. 27), in a manner similar to that observed in cultured cells and VLPs. This is interesting because unlike cultured cells, purified plasma membranes and VLPs lack a cytoplasmic organization to account for the possibility of receptor internalization or recycling process. Thus, it may suggest that the observed decrease in insulin binding following changes in membrane cholesterol may not be due to a decrease in the apparent number of receptors present in the membrane but could likely be due to a decrease in the availability of these receptors for the binding of insulin or antibodies directed towards their extracellular domains. This point is further expanded in the Discussion, section 4.1.

The influences of diet and atorvastatin on insulin receptor expression and its phosphorylation in the plasma membrane fraction, and, Akt and GSK3β phosphorylation in the cytosolic fraction were assessed by Western blot analysis. It is clear from Fig. 28 that both diet and statin treatment influenced the apparent total insulin receptor content in the plasma membrane fraction and its phosphorylation. Insulin receptor expression and its phosphorylation were decreased substantially in mice that were fed the high-fat diet (HFD), compared to mice that were fed a normal diet (ND) (Fig. 28). The decrease in insulin receptor number and phosphorylation in the plasma membrane observed in high-fat diet feeding was recovered by atorvastatin treatment; compared to the HFD group, ~ 2-fold and 4-fold increases in insulin receptor expression and phosphorylation, respectively, were observed in the HFD-A group (Fig. 28). These results are consistent with the observations from the binding analysis (Fig. 27). Atorvastatin treatment had no such effect on mice that were fed the normal diet, with the insulin receptor expression and its phosphorylation being very similar in the ND-A and ND groups. No difference was observed in total Akt expression across all four treatments (Fig. 29B) as a function of diet and/or atorvastatin treatment. However, total GSK3β expression varied significantly between the treatment groups (Fig. 29E). While there was no effect of high-fat diet

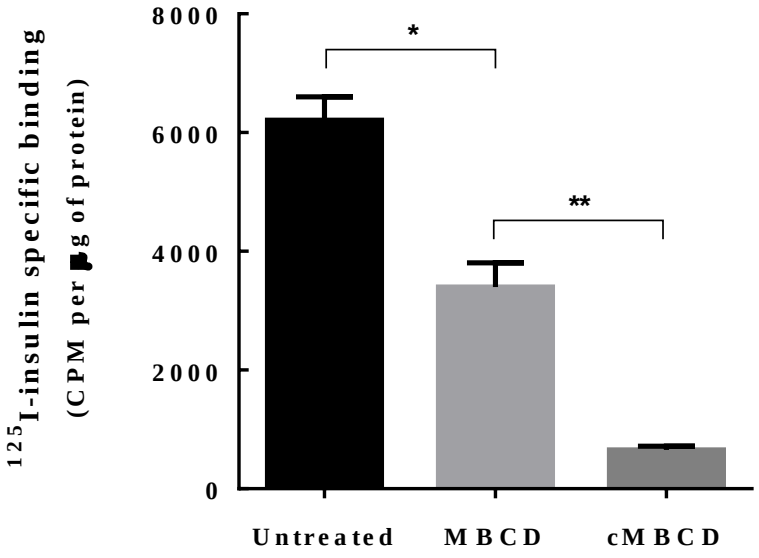

Figure 27. Effect of MBCD or cMBCD treatment on insulin binding to plasma membranes obtained from mouse liver. Plasma membranes were isolated from liver tissues of mice that were fed a normal diet (ND) for 12 weeks as described in Methods, section 2.2.3.4. Membranes were treated with either 10 mM MBCD or cMBCD for 30 min at room temperature (~ 23°C) and insulin binding assay was conducted as described in Methods, section 2.2.2.6. Total protein content of the membranes following treatment with either MBCD or cMBCD was determined using a BCA assay as described in section 2.2.3.5. The experiment was conducted two times in triplicate using membranes from a different mice in every instance but only one representative data-set is illustrated as mean ± SD (n = 3). Data from both the experiments was considered for statistical analysis (Dunnett's multiple comparisons test: * $P < 0.05$, **$P < 0.01$).

Figure 28. Effect of diet and atorvastatin treatments in mice on membrane insulin receptor content and its phosphorylation status. Plasma membrane fractions from liver tissue were isolated from mice that fed either a normal diet (ND) or a high fat diet (HFD) or a normal diet whilst treated for 12 weeks with atorvastatin (ND-A) or a high fat diet whilst treated for 12 weeks with atorvastatin (HFD-A) as described in Methods, section 2.2.3.4. Total protein content in each fraction was determined using a BCA assay as described in section 2.2.3.5. Total membrane protein (20 µg) was separated using SDS-PAGE and Western blot analysis was conducted as described in section 2.2.3.7. A representative Western blot image is shown in (A). Bands representing total insulin receptor content (B) and its phosphorylation status (Tyr 1361) (C), were quantitated by densitometry analysis and normalised to Na^+/K^+ - ATPase expression. The ratio of phosphorylated insulin receptor-β to total insulin receptor is shown in (D). Data shown as mean ± SD is from seven separate experiments conducted for all the animals in each group (Tukey's multiple comparisons test: ns – not significant, **** $P < 0.0001$, $n = 7$ animals per group).

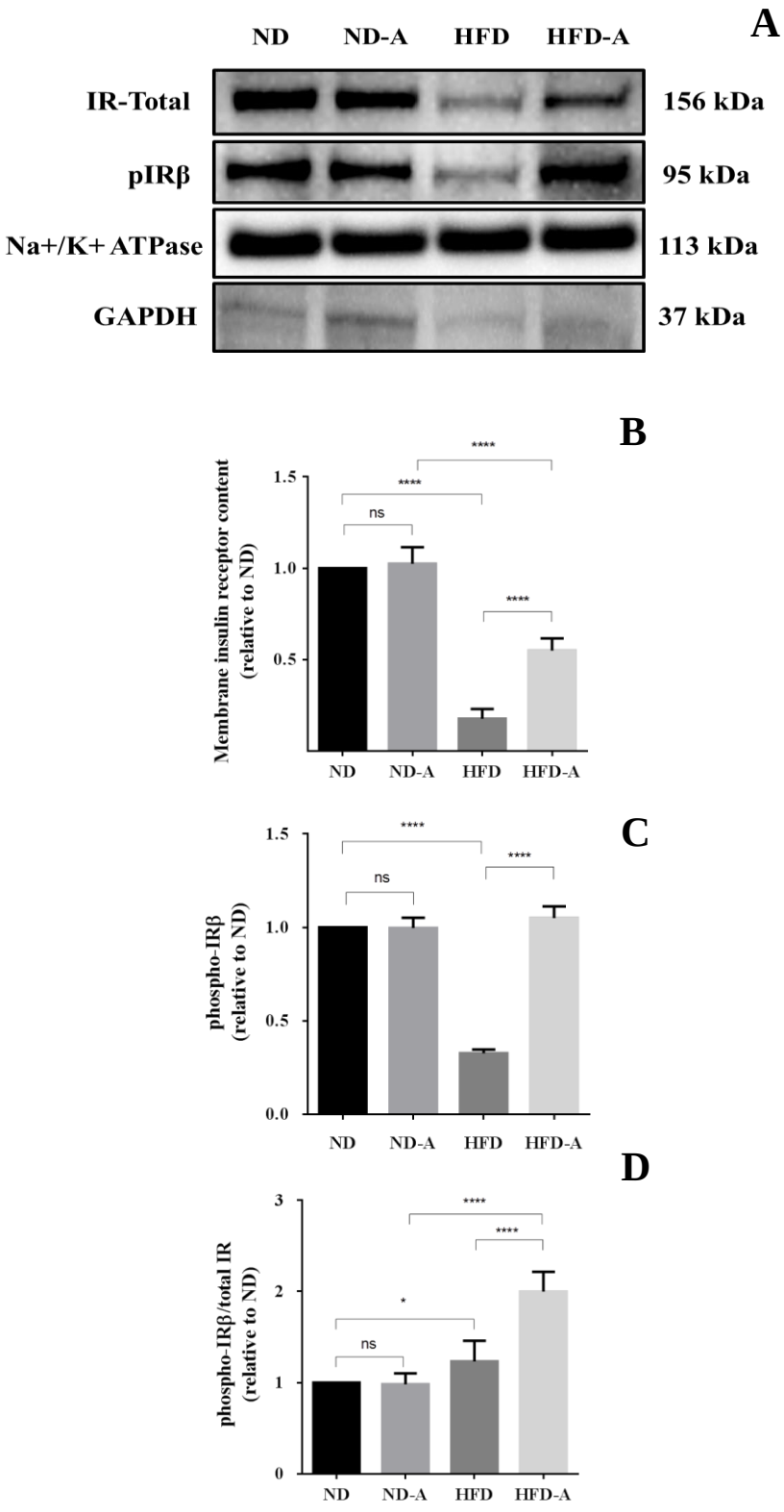
A
ND
ND-A
HFD
HFD-A
IR-Total
156 kDa
pIRβ
95 kDa
Na+/K+ ATPase
113 kDa
GAPDH
37 kDa
B
Membrane insulin receptor content (relative to ND)
1.5
1.0
0.5
****
****
ns
****
ND
ND-A
HFD
HFD-A
C
phospho-IRβ (relative to ND)
1.5
1.0
0.5
0.0
****
****
ns
ND
ND-A
HFD
HFD-A
D
phospho-IRβ/total IR (relative to ND)
3
2
1
0
****
****
*
ns
ND
ND-A
HFD
HFD-A

Figure 29. Effects of diet and statin treatment on Akt and glycogen synthase kinase 3β (GSK3β) phosphorylation. Cytosolic fractions were isolated from mice that were fed for 12 weeks either a normal diet (ND), a high fat diet (HFD), a normal diet whilst treated with atorvastatin (ND-A) or a high fat diet whilst treated with atorvastatin (HFD-A) as described in Methods, section 2.2.3.4. Total protein content in liver cytosolic fractions was estimated by BCA assay as described in section 2.2.3.5 and 25 µg of total cytosolic protein was separated using SDS-PAGE and Western blot analysis was conducted as described in section 2.2.3.7. One representative Western blot image out of seven experiments is shown in (A). Bands representing total (B) and phosphorylated (Thr 308) Akt (C), and total (E) phosphorylated (Ser 9) GSK3β (F) were quantitated by densitometry analysis and normalised to GAPDH expression. The ratios of phosphorylation of Akt and GSK3β to total Akt and GSK3β are shown in D and G. Data shown as mean ± SD is from seven separate experiments conducted for all the animals in each group (Tukey's multiple comparisons test: ns – not significant, * $P < 0.05$, ** $P < 0.01$, **** $P < 0.0001$, $n = 7$ animals per group).

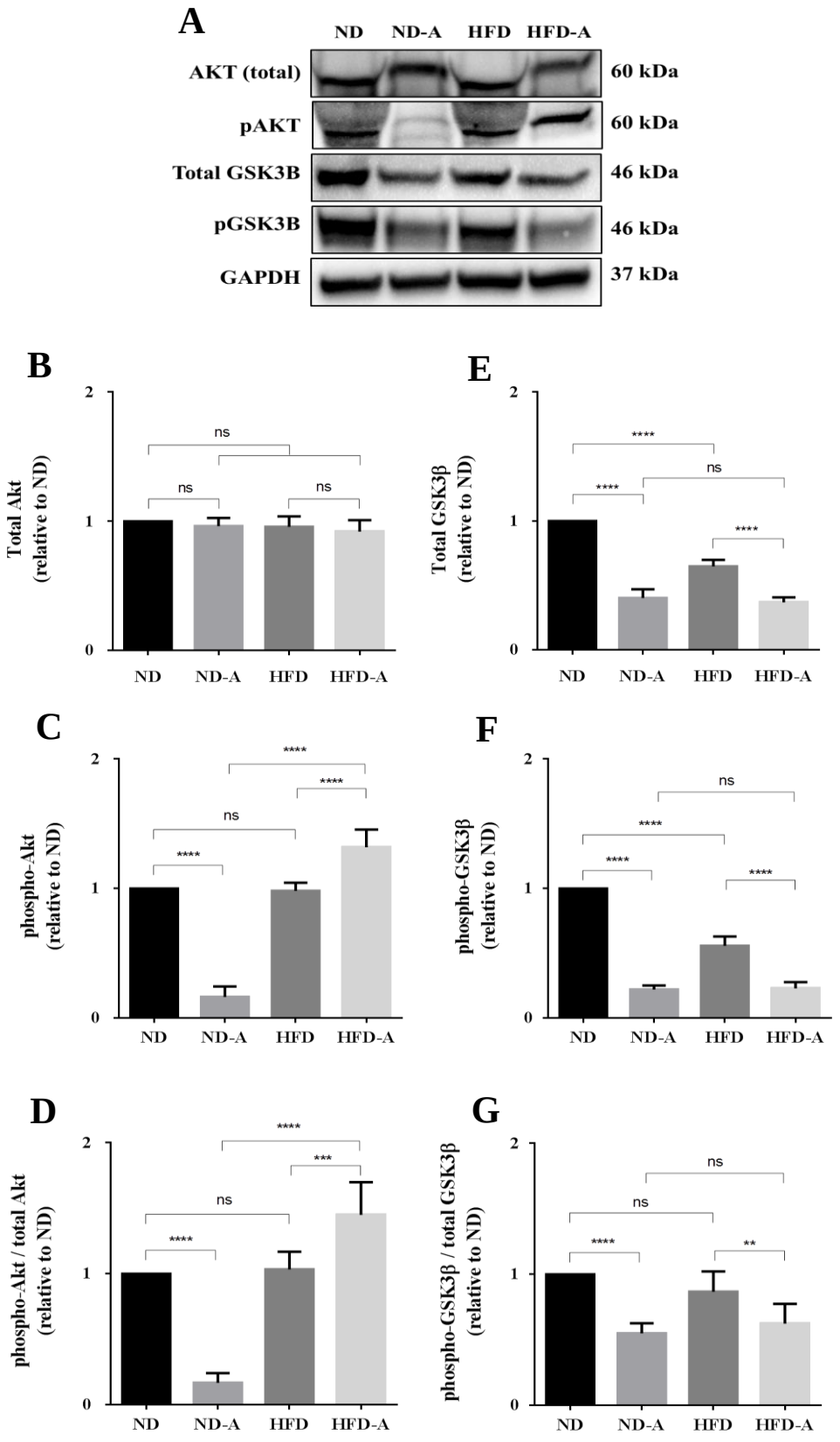
A
ND
ND-A
HFD
HFD-A
AKT (total)
60 kDa
pAKT
60 kDa
Total GSK3B
46 kDa
pGSK3B
46 kDa
GAPDH
37 kDa
B
Total Akt
(relative to ND)
C
phospho-Akt
(relative to ND)
D
phospho-Akt / total Akt
(relative to ND)
E
Total GSK3β
(relative to ND)
F
phospho-GSK3β
(relative to ND)
G
phospho-GSK3β / total GSK3β
(relative to ND)
ns
****
***
**
0
1
2

on Akt phosphorylation, a diet-dependent effect of atorvastatin was observed. A substantial decrease or increase in Akt phosphorylation was observed in mice treated with atorvastatin and fed the normal (ND-A) or high-fat diet (HFD-A), respectively (Fig. 29C). In contrast to Akt expression, total GSK3β expression decreased substantially as a result of high-fat diet and atorvastatin treatment (Fig. 29E). The decreases observed in total GSK3β as a result of diet and atorvastatin treatment almost mirrored the phosphorylation of GSK3β (Fig. 29F). The clear disconnect between the changes in phosphorylation of the insulin receptors and the effects on subsequent phosphorylation of Akt and GSK 3β is expanded in the Discussion sections 4.1 and 4.2 of this Thesis.

3.3. Development and characterization of virus-like particles as a novel membrane model to study the influence of membrane cholesterol on insulin binding

The cell and animal studies in this Thesis suggest a correlation between cell cholesterol content, insulin binding, and signalling. To complement these studies, the interaction of insulin with its receptor was studied in a novel membrane model, known as virus-like particles (VLPs). VLPs were generated from CHO K1 cells[3] [189], and CHO-T10 cells, which were derived from CHO K1 cells transfected with a mammalian transfection vector for insulin receptor-A overexpression as described in the Methods, Section 2.2.3.1. Since VLPs are generated from the cell membrane and are largely free of cellular components, they enable the interaction of insulin with its insulin receptor to be studied in a more "controlled" membrane environment. In particular, the influence of membrane cholesterol on the interaction of insulin with its receptor can be readily evaluated by treating the VLP membranes with either MBCD or cMBCD. Other advantages of using VLPs include their longer shelf-life and they eliminate the requirement of growing cells in culture under aseptic conditions.

The morphology of the VLPs extruded from the CHO-T10 cells was evaluated using both dynamic light scattering (DLS) and field emission scanning electron microscopy (FE-SEM) methods (Fig. 30A and 30B respectively). The dynamic light scattering (DLS) profile of VLPs derived from CHO T10 cells was consistent with

[3] CHO K1 cells were originally developed from a biopsy of an ovary of an adult Chinese hamster.

the presence of particles that were highly uniform in both size and shape (Fig 30A). The VLP particles were estimated to have an average diameter of ~159 nm. The narrow peak with polydispersity index (PDI) value of 0.332 observed in the DLS profile of VLPs indicates uniformity in size distribution of the particles and presence of minimal aggregates (Fig. 30A). The second peak towards the far right may indicate the presence of larger membrane fragments; however, larger particles scatter more light and therefore a small amount of them may be sufficient to result in the peak observed [190]. Field Emission - Scanning Electron Microscopy (FE-SEM) analysis of these VLPs confirmed the presence of uniform spherical particles with a diameter ranging from 140 – 150 nm (Fig. 30B).

Interestingly, the recovery of ^{125}I-insulin specific binding in the VLPs generated from CHO T10 cells was improved up to 3-fold (Fig. 31) by treating the cells with 100 nM insulin for approximately 18 h post-transfection of the cells with the lentiviral-Gag protein, as described in Methods section 2.2.3.1. This finding is not surprising as insulin receptors, when activated, accumulate to lipid-rafts [49, 191, 192]. Also, the multimerized-lentiviral-Gag protein in the cell egresses the cell by membrane fission (a process known as viral budding) in the lipid-raft region of the plasma membrane [193-195]. Thus, the co-occurrence of insulin receptor accumulation and VLP generation in the lipid-raft regions of the membrane may collectively lead to the increased recovery of insulin receptors in VLPs. This treatment of cells for 24 h with 100 nM insulin, post-transfection of cells with the lentiviral-Gag protein, was included for VLP generation in the current study. However, great care was taken to ensure that the VLPs were thoroughly washed to minimize the amount of free insulin that might carry over in the procedure as contaminating insulin would interfere with interpretation of the subsequent insulin binding study. The concentration of insulin in the VLP preparations at the dilution used for the competition binding study was estimated by ELISA to be about 5 pM. This residual concentration of insulin in the VLP preparations was accounted for during competitive binding analysis.

The comparison of insulin binding to CHO K1 and CHO T10 cells is shown in Fig. 32. As expected, the specific binding of ^{125}I-insulin to CHO T10 cells far exceeded that of the wild-type CHO K1 cells (Fig. 32). Based on a single-site fit to the data, CHO T10 cells expressed approximately 280-fold more receptors per cell than CHO

A

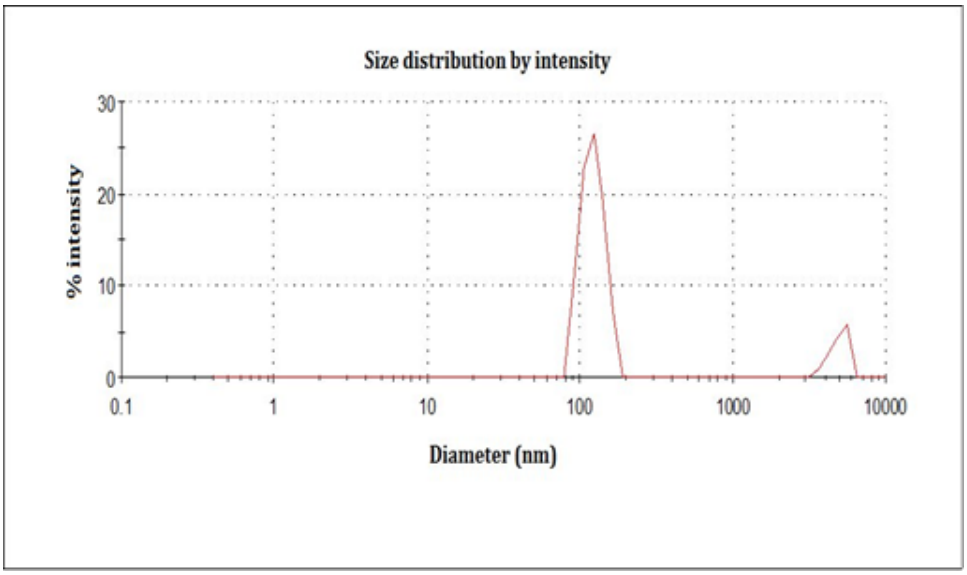

B

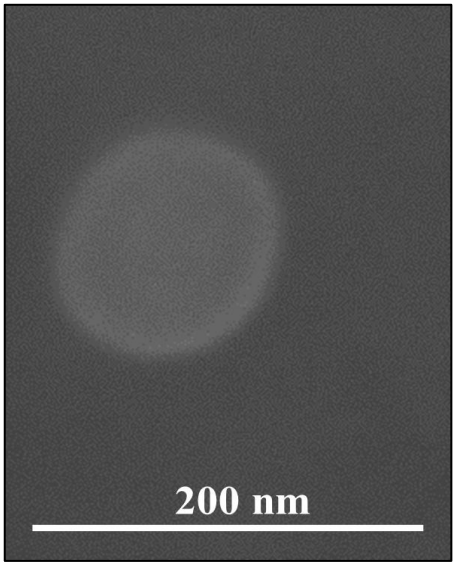

Figure 30. Morphological characterization of VLPs. A representative dynamic light scattering (DLS) profile of VLPs derived from CHO T10 cells is illustrated in caption **(A)** and depicts the intensity size distribution plot (average of three measurements) Z- Average diameter – 158.6 nm; Polydispersity Index (PDI) – 0.332. A field emission-scanning electron microscopy image of a formalin-fixed virus-like particle (VLP) derived from CHO T10 cells is shown **(B).** Scale bar: 200 nm.

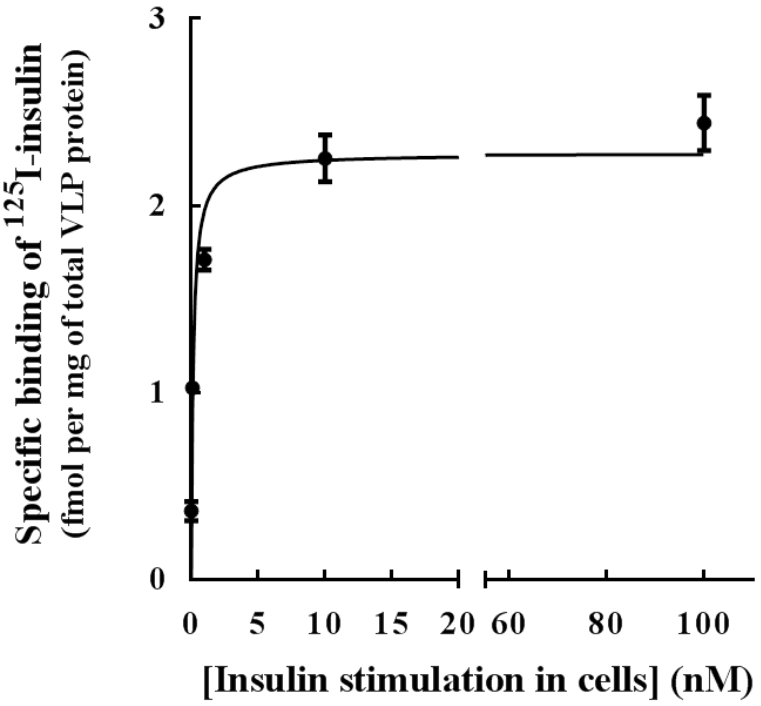

Figure 31. Influence of insulin pre-treatment of parental on insulin binding to generated VLPs. CHO T10 cells were transfected with the lenti-viral Gag protein as described in the Methods, section 2.2.3.1. After 24 h from transfection, the cells were cultured for 24 h with fresh RPMI media containing 0, 0.1, 1, 10 or 100 nM insulin. VLPs were harvested and insulin binding studies were conducted as described in the Methods, sections 2.2.3.1 and 2.2.3.4, respectively [4]. The experiment was conducted three times in triplicate but only one representative data set is illustrated as mean ± SD (n=3).

[4] The increases in ^{125}I insulin specific binding to VLPs in response to insulin stimulations in cells whilst generating VLPs were fitted to a one-site saturation binding curve. However, this fit to data is only used to demonstrate the significance of the increase in insulin binding as a function of the insulin concentration used to pre-treat the cells and not for binding saturation analysis.

K1 cells (Table 7). Interestingly, however, the affinity of insulin receptors in CHO K1 cells was estimated to be about 5-fold higher than in CHO T10 cells (Table 7).

This can also be visually observed by the clear rightward shift of the CHO T10 binding curve in Fig. 32. The binding of insulin to VLPs generated from CHO K1 and CHO-T10 cells is compared relative to their corresponding parental cell lines in Fig. 33. It is notable that the insulin binding curves for the parental cells and the corresponding VLPs generated from them are indistinguishable and this is reflected in the calculated affinity values for each parental cell and the derived VLPs (Fig. 33, Table 7). However, as was observed with the parental cell lines, there was about 5-fold higher affinity of insulin receptors in VLPs derived from CHO K1 cells relative to those derived from CHO-T10 cells (Table 7).

Quantitation of insulin receptor expression by Western blots of parental cell lysates (Fig. 34) and derived VLPs (Fig.35) generated from the cells generally supports the findings based on the competitive binding studies; more insulin receptors were detected in the CHO T10 cells than in the CHO K1 cells. However, the expression of insulin receptors in VLPs was surprisingly similar irrespective of whether the VLPs were generated from the CHO T10 or CHO K1 cell lines (Fig. 35). This is quite a remarkable observation given that the parental CHO K1 cell line expresses just a few percent of the insulin receptors that are expressed in the CHO T10 cell line (Table 7). It is evident from Fig. 35 that a large amount of insulin receptors still remain after VLP generation in the remaining CHO T10 cell matter, whereas insulin receptor content in the remainder CHO K1 cell matter appears to be essentially undetectable. As estimated by binding analysis, only about 2% of the insulin receptor population was captured in the VLPs generated from CHO T10 cells, whereas 105% (i.e. the entire insulin receptor population) was captured in the VLPs generated from the CHO K1 cells (Table 7). The possible reasons for the above somewhat surprising observations are detailed in the Discussion section 4.3 of this Thesis.

The effects of alterations in cholesterol content in CHO K1 and CHO T10 cells and VLPs generated from these cells on insulin binding were estimated. Similar to the observations in other cell culture studies, alterations in membrane cholesterol following treatment with either 10 mM MBCD (reduction) or cMBCD (enrichment) (Fig. 36) resulted in a significant decrease in insulin binding (Fig. 37). These results

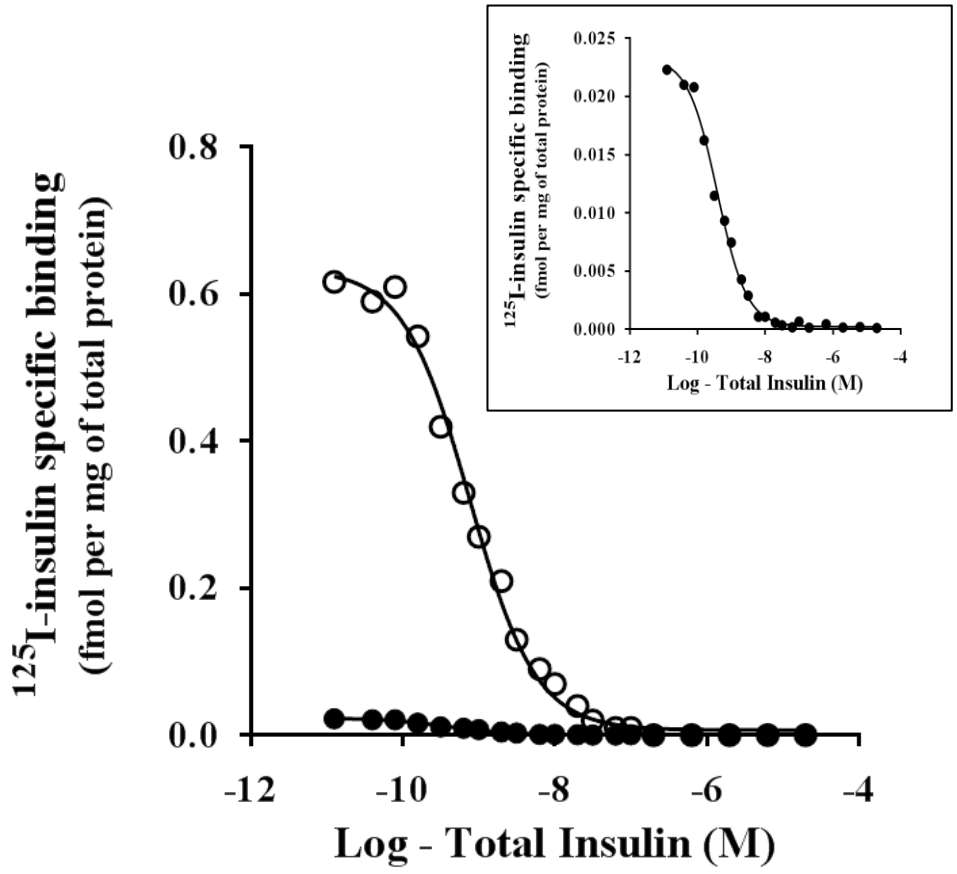

Figure 32. The competitive binding of ^{125}I-insulin to CHO K1 and CHO T10 cells. Competitive binding assays were conducted in wild-type CHO K1 (-●·) cells and CHO T10 (over-expressing the A-isoform of human insulin receptors) (-⊖) cells as described in Methods, Sections 2.2.1.7 and 2.2.3.4. Briefly, cells were incubated for 18 h at 4 °C with a single concentration of ^{125}I-insulin (~ 3 pM) and a wide range of competing unlabelled insulin (0 to 20.6 μM). The binding of ^{125}I-insulin to the VLPs was non-linearly fitted to a one-site model using GraphPad PRISM®. The binding curve for CHO K1 cells is expanded in the inset to the figure. The experiment was conducted three times in duplicate but only one representative data set is illustrated, with each data point shown as the mean of duplicate determinations.

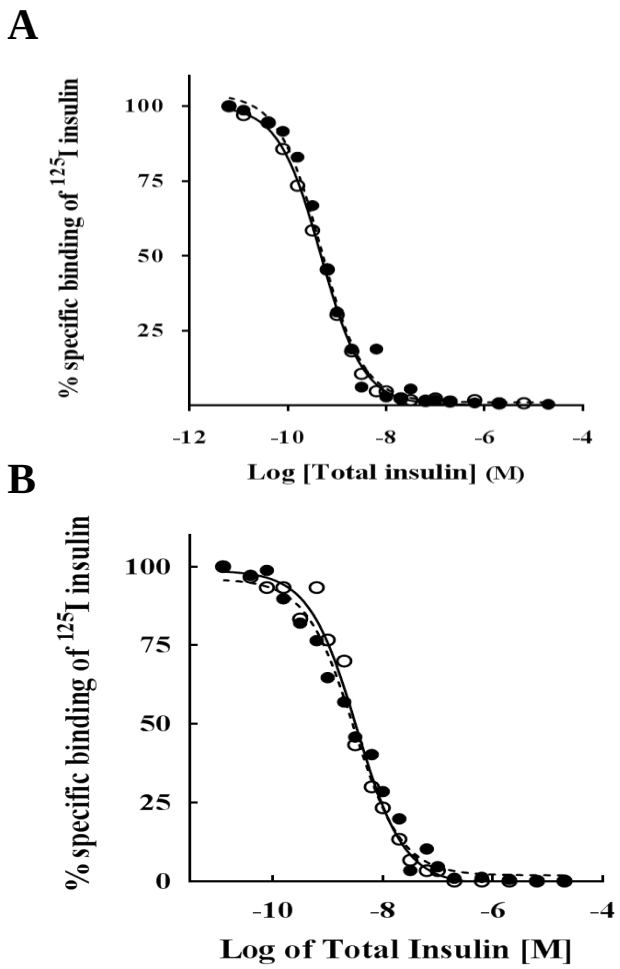

Figure 33. The competitive binding of ^{125}I-insulin to CHO K1 and CHO T10 cells and the VLPs generated from both parental cell lines. CHO K1 (**A)** and CHO T10 (**B)** cells (-⊖-) and derived VLPs (-●-) were incubated for 18 h at 4 °C with a single concentration of ^{125}I-insulin (~ 3 pM) and a wide range of competing unlabelled insulin (0 to 20.6 μM) as described in Methods, section 2.2.3.4. The binding of ^{125}I-insulin was non-linearly fitted to a one-site model using GraphPad PRISM®. The experiment was conducted three times in duplicate but only one representative data set is illustrated, with each data point shown as the mean of duplicate determinations. Statistical comparisons for affinity values were based on the data pooled from the three separate experiments (CHO K1 cells vs VLPs derived from CHO K1 cells, P = 0.1, CHO T10 cells vs VLPs derived CHO T10 cells, P = 0.2, see Table 7).

Table 7. Insulin receptor number and affinity estimates in parental cells and derived VLPs based on competitive binding analysis.

	CHO K1		CHO T10	
	Cells	**VLPs**	**Cells**	**VLPs**
Affinity K_D (nM)	0.5 (± 0.1)*	0.4 (± 0.1)	2.3 (± 0.4)*	2.1 (± 0.4)
Receptor per cell or Receptors in VLPs per cell	1926 (± 311)*	2021 (± 412)[#]	541625 (± 11032)*	10957 (± 1403)[#]
% Yield in VLPs[#]	-	105	-	2

The estimates of affinity and receptor number are based on a one-site fit of the data shown in Fig. 32. *For the parental cells, the reported affinity and receptor number are based on the basal state of expression, i.e., receptor expression prior to transfection of the parental cells for VLP generation. [#] The estimates on receptor recovery in the VLPs were calculated using receptor number per seeded parental cells, i.e., receptor number in parental cells prior to transfection for VLP generation.

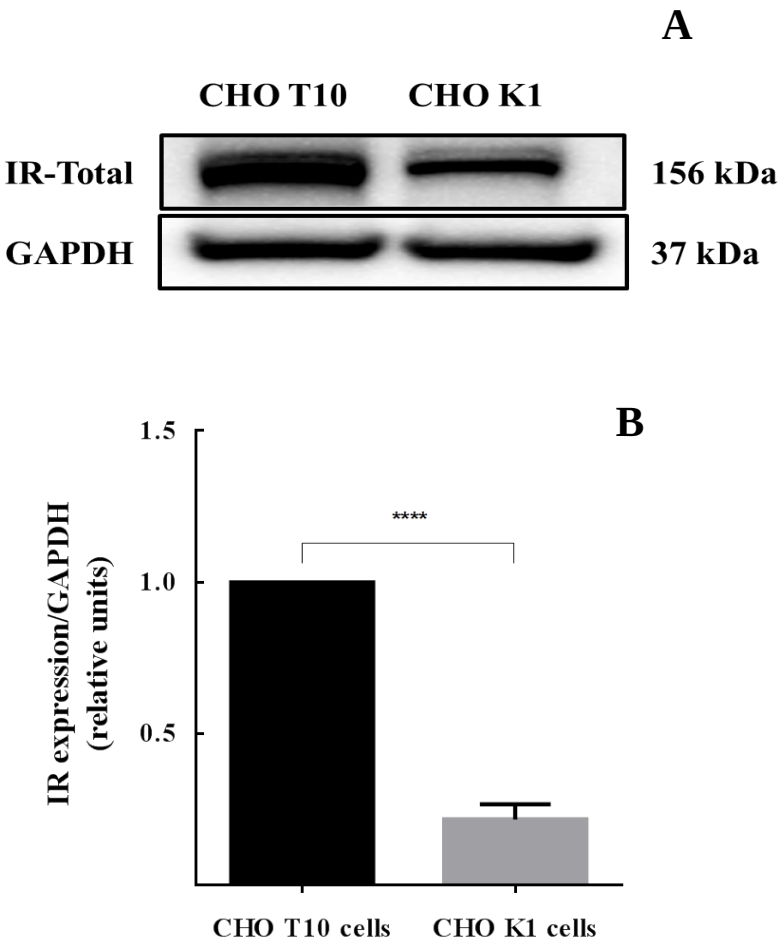

Figure 34. Insulin receptor expression in CHO K1 and CHO T10 cells prior to VLP generation. Cells were grown and whole cell lysates were collected for Western blot analyses as described in Methods, Section 2.2.3.7. A representative Western blot image highlighting the expression of total insulin receptor (IR-Total) and corresponding glyceraldehyde 3-phosphate dehydrogenase (GAPDH) is shown in (A). Bands representing the expression of insulin receptors were quantitated by densitometric analysis and normalised to GAPDH expression. The experiment was conducted three times and data from all three experiments is shown as mean ± SD (B) (Unpaired t-test: *** P = 0.0003, n = 3).

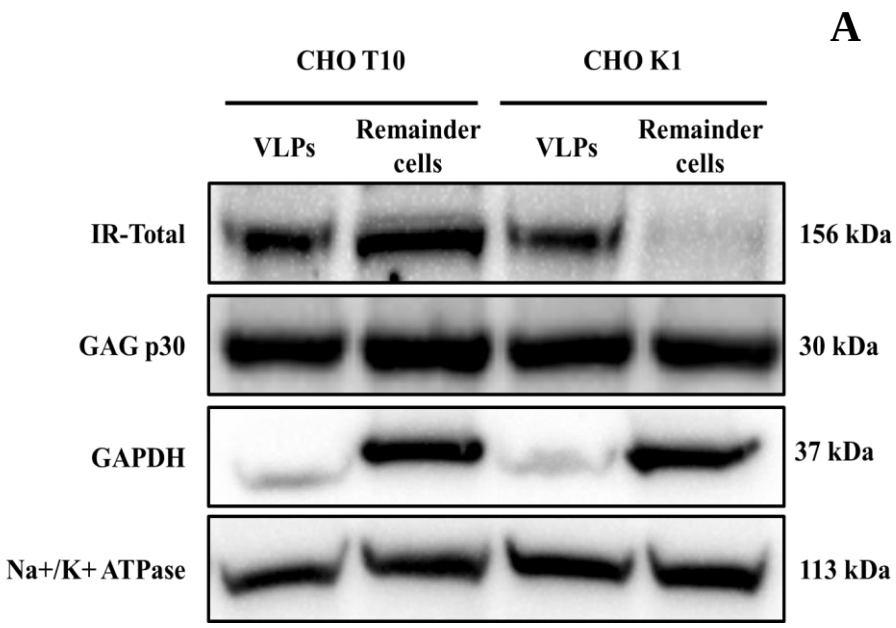

Figure 35. Insulin receptor expression in VLPs and remainder parental cells after VLP generation. VLPs and remainder cells[5], post-VLP generation, were lysed and samples were processed for Western blot analysis for the detection of total insulin receptors (IR-Total), retroviral core protein (Gag p30), glyceraldehyde 3-phosphate dehydrogenase (GAPDH-cytosolic marker) and sodium/potassium ATPase (Na+/K+ ATPase-plasma membrane marker), as described in the Methods, section 2.2.3.7. One representative Western blot image out of three separate experiments is shown.

[5] The 'remainder cells' includes cell matter of CHO T10 and CHO K1 cells that were left over after VLP generation.

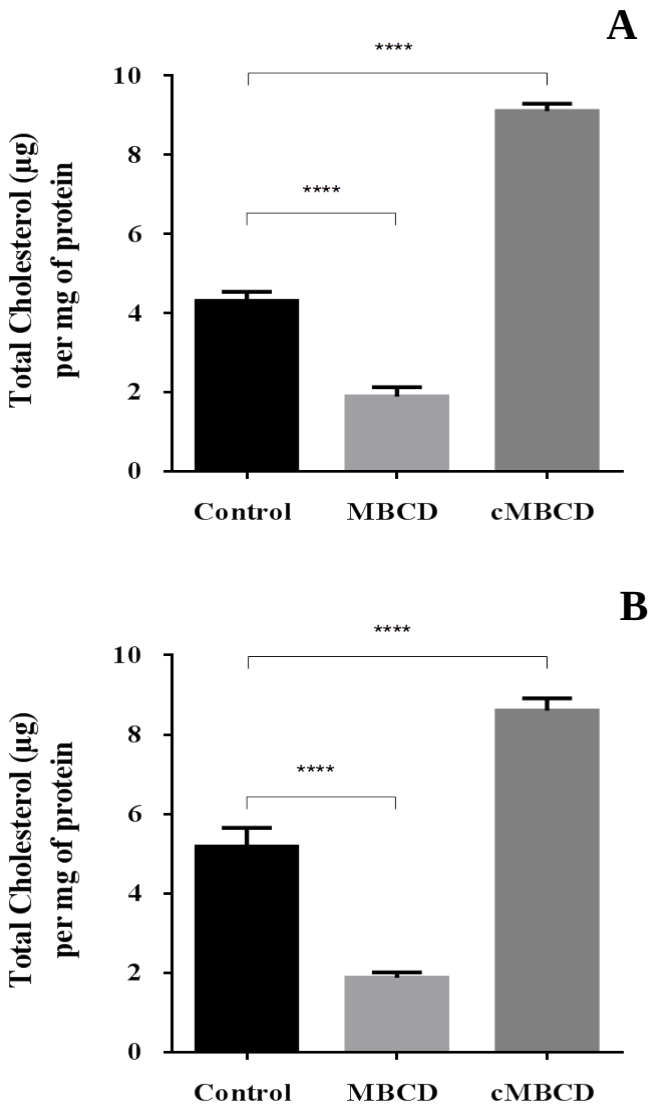

Figure 36. Effect of MBCD or cMBCD treatment on cholesterol content of CHO cells. CHO K1 (A) and CHO T10 cells (B) were treated for 30 min at room temperature with 10 mM MBCD or cMBCD. Total cholesterol and proteins were measured as described in Methods, Section 2.2.3.6. The experiment was conducted three times in triplicate but only one representative data-set is illustrated as mean ± SD (n = 3). Data from all three experiments was used for statistical analysis (Dunnett's multiple comparisons test: ** $P < 0.01$, *** $P < 0.001$, **** $P < 0.0001$, n = 9).

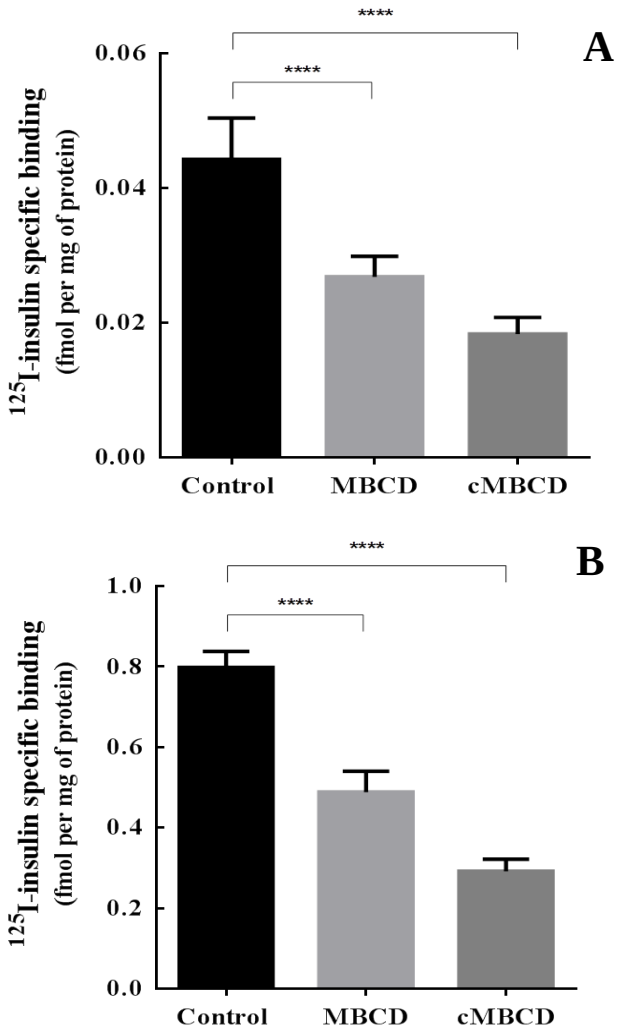

Figure 37. Effect of MBCD or cMBCD treatment on insulin binding to CHO cells. CHO K1 (A) and CHO T10 (B) cells were treated for 30 min at room temperature with MBCD or cMBCD and specific binding of ^{125}I-insulin was estimated. Following treatments, the cells were incubated for 18 h 4 °C with ^{125}I-insulin (approximately 3 pM) either in the absence (total) or presence of competing unlabelled insulin (20.6 μM) (non-specific binding). Specific binding of ^{125}I insulin was calculated from the difference between total and non-specific binding. The experiment was conducted three times in triplicate but only one representative data-set is illustrated as mean ± SD (n = 3). Data from all three experiments is considered for statistical analysis (Dunnett's multiple comparison test: **** $P < 0.0001$, n = 9).

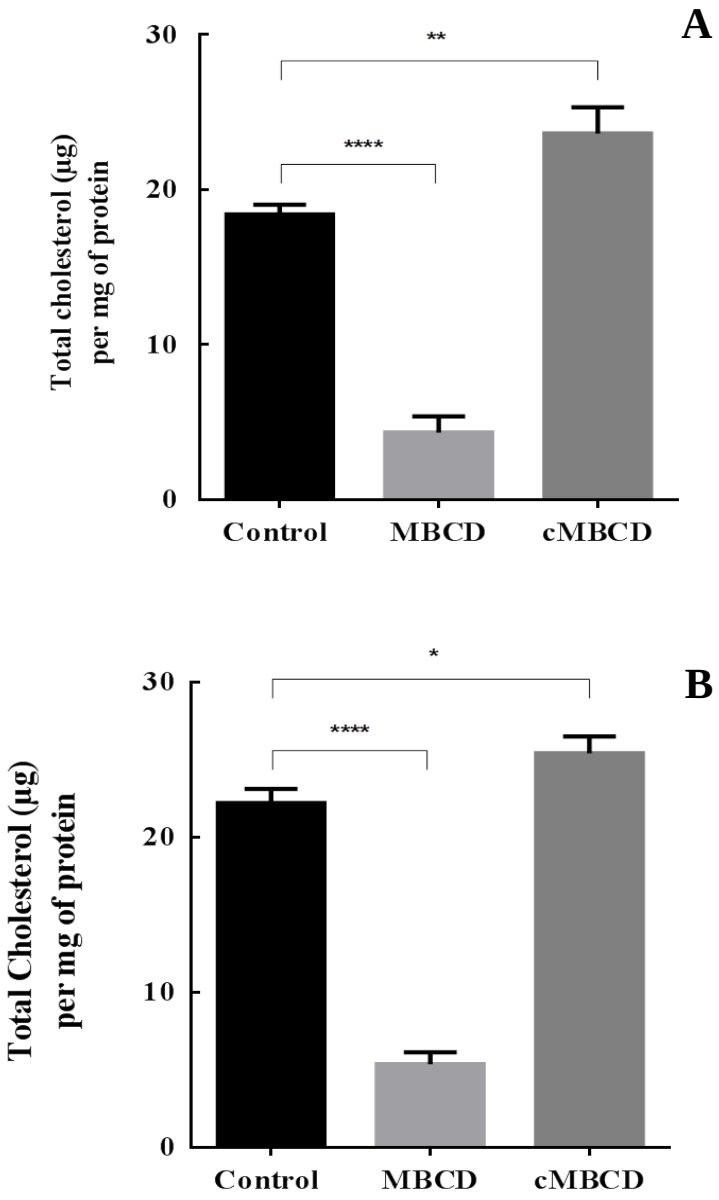

Figure 38. Effect of MBCD or cMBCD treatment on cholesterol content of VLPs. VLPs derived from CHO K1 (A) and CHO T10 cells (B) were treated for 30 min at room temperature with 10 mM MBCD or cMBCD. Following treatments, Total cholesterol and protein were measured as described in Methods, Section 2.2.3.6. The experiment was conducted three times in triplicate but only one representative data-set is illustrated as mean ± SD (n = 3). Data from all three experiments was considered for statistical analysis (Dunnett's multiple comparisons test: * $P < 0.05$, ** $P < 0.01$, **** $P < 0.0001$, n = 9).

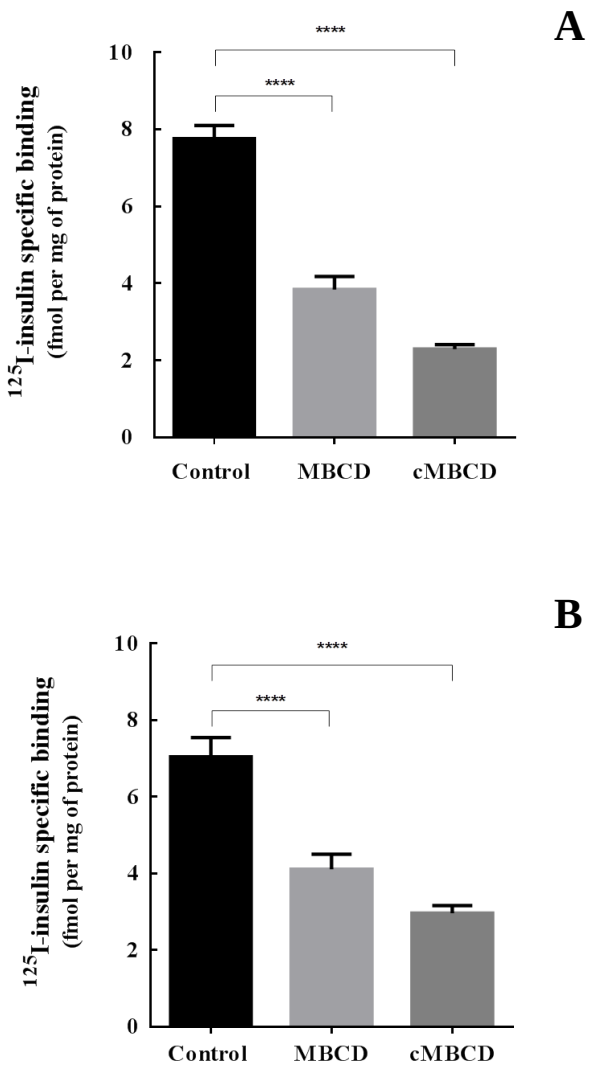

Figure 39. Effects of MBCD or cMBCD treatment on insulin binding in VLPs derived from CHO cells. VLPs derived from CHO K1 (A) and CHO T10 (B) cells were treated for 30 min at room temperature with MBCD or cMBCD. Following treatments, VLPs were incubated for 18 h 4 °C with ^{125}I insulin (approximately 3 pM) either in the absence (total) or presence of competing unlabelled insulin (20.6 μM) (non-specific binding). Specific binding of ^{125}I insulin was calculated from the difference between total and non-specific binding. The experiment was conducted three times in triplicates but only one representative data-set is illustrated as mean ± SD (n = 3). Data from all three experiments was considered for statistical analysis (Dunnett's multiple comparisons test: **** $P < 0.0001$, n = 9).

in CHO K1 and CHO T10 were closely mirrored in the VLPs generated from either the CHO T10 or CHO K1 cells (Fig. 38 and 39). This indicates that VLPs retain important properties of the plasma membrane of their parental cells and might serve as a valuable tool for receptor-ligand interaction studies in a native membrane environment.

4.0. DISCUSSION

4.1. Effects of cyclodextrins and statins on cholesterol content and insulin action in cultured cells

Effect of MBCD or cMBCD on insulin binding

Decreasing or increasing cholesterol content in CHO T10 cells, HepG2 cells and differentiated myotubes (HSMMs) using either MBCD (methyl-β-cyclodextrin) or cMBCD (cholesterol-loaded MBCD) significantly decreased insulin binding to the cells (Fig. 8A – C). In line with this observation, binding of epidermal growth factor (EGF) to its receptor (EGFR), is also influenced by cholesterol content; increasing following cholesterol reduction and decreasing following cholesterol enrichment using MBCD and cMBCD, respectively [196]. In other but less directly comparable studies, i.e., not examining ligand binding, the activation of several other growth factor receptors such as insulin-like growth factor receptor (IGF-1R) and vascular endothelial growth factor receptor (VEGF-R), and their subsequent signal propagation are also impaired by reduction in membrane cholesterol content [197, 198]. Thus, the present study adds to the evidence that plasma membrane cholesterol influences ligand binding to membrane receptor systems and suggests that, for the insulin receptor at least, there is an optimal cholesterol concentration in cells required for maximal insulin binding with either an increase or decrease of cholesterol in CHO T10, HepG2 or differentiated myotubes impairing binding.

Contrary to the findings in the current study, membrane cholesterol depletion by MBCD in primary rat adipocytes was reported to have no effect on insulin binding [199]. However, the binding data collected in that study were pooled from three experiments without differentiating data points between the different experiments. Due to significant experimental variation, it is difficult to support the authors' conclusion that cholesterol depletion in primary adipocytes does not affect insulin binding. It should also be noted that the binding experiments, in that study, were conducted at 37 °C, where ligand-induced receptor internalization and degradation of receptors can more readily occur [200], which further complicates the interpretation of their binding studies. By contrast, in the present study, the equilibrium of binding was measured at 4 °C to minimize the influence of receptor internalization and degradation on binding [201]. It is possible that the difference in observations

between the former and current studies may relate to cell specific differences. However, this is considered unlikely, given that in the present study insulin binding decreased with changes in cholesterol content by MBCD or cMBCD treatment in three different cell types. It will be interesting to further evaluate the effect of MBCD and cMBCD on insulin binding to primary adipocytes and other adipocyte cell culture models such as 3T3-L1 pre-adipocytes to investigate possible cell type-specific differences.

The decrease in insulin binding following treatment with either MBCD or cMBCD is most likely due to changes in plasma membrane cholesterol and not to changes in intracellular cholesterol levels. MBCD preferentially associates with the plasma membrane to alter its cholesterol content [139, 143, 202] and the majority of free cholesterol in most cells resides in the plasma membrane [118, 203]. MBCD primarily alters cholesterol content in plasma membranes, whilst minimally affecting the intracellular cholesterol content and other membrane lipids [142, 144, 204].

The decrease in insulin binding following treatment with either MBCD or cMBCD does not appear to be due to secondary effects of either treatment; that is, due to MBCD per se rather than its ability to extract or deliver cholesterol from or to the cell membrane, respectively. Indeed, when CHO T10 cells were sequentially cholesterol depleted using MBCD and then subsequently cholesterol replenished using cMBCD, both cholesterol content and insulin binding approached levels that were observed in the untreated cells (Fig. 14A and B). Thus, it is clear from this observation that the changes in insulin binding are directly linked with the changes in plasma membrane cholesterol content and not due to some secondary effects of MBCD or cMBCD treatment. Furthermore, insulin binding improved in CHO T10, HepG2 cells and differentiated myotubes (Fig. 13A - C) when they were allowed to "naturally" recover, by incubating for a 24 h period in media supplemented with 10% fetal bovine serum but free from MBCD or cMBCD. It is notable that the restoration in insulin binding was accompanied by restoration in cholesterol content in the recovery period following MBCD or cMBCD treatment (Fig. 12 and 13).

The decrease observed in insulin binding in CHO T10 and HepG2 cells following treatment with either MBCD or cMBCD (Fig. 8A and B) appears to be due to a decrease in the availability or accessibility of insulin receptors at the surface of the

cells as demonstrated by immunostaining and flow cytometry (Fig. 11). Detailed competitive binding analysis also confirmed the decrease in insulin binding and the consequent decrease in the estimates of apparent receptor number in CHO T10 and HepG2 cells following treatment with either 10 mM MBCD or 10 mM cMBCD (Fig. 10A, Table 2). There was no evidence that the affinity of insulin for its receptor changed following these treatments in CHO T10 and HepG2 cells. Thus, both detection of insulin receptors by flow cytometry and analysis by competitive binding plots confirmed that the decreased binding of insulin as cholesterol levels was altered in cells, was due to the decreased availability or accessibility of insulin receptors at the surface of the cells.

The apparent decrease in insulin receptor number detected at the surface of cells following treatment with either MBCD or cMBCD cannot be explained by the process of receptor internalization because the binding of insulin to plasma membrane purified from mouse liver also decreased following treatment with either MBCD or cMBCD (Fig. 27). Furthermore, virus-like particles (VLPs), which are unable to internalize receptors, as they lack the cell cytoplasmic component [54], also have their binding of insulin significantly reduced following treatment with either MBCD or cMBCD (Fig. 39), and in a manner that mirrored the observations in CHO K1 and CHO T10 cells (Fig. 37) from which the VLPs were generated.

One possible explanation for the observed decrease in insulin or antibody binding to the insulin receptors in the present study is that the changes in membrane cholesterol content by MBCD or cMBCD treatment could influence the disposition of insulin receptors in the membrane and subsequently limit their access to insulin. Indeed, such a scenario is observed with EGFR, which is localized in non-caveolar or caveolar raft regions, respectively, in the membrane following membrane cholesterol reduction or enrichment [196, 205]. Authors to the latter studies postulated that the increased probability of EGF-EGFR interactions results from the increased opportunity for EGFR dimerization favoured by the redistribution of the EGFR into non-caveolar regions of the plasma membrane following treatment with MBCD. However, it is difficult to explain the effect of MBCD or cMBCD on insulin binding and the availability of insulin receptors based on this postulate since insulin receptors are pre-formed, disulphide linked, dimers [206].

Another possible explanation for the effect of MBCD or cMBCD treatment on insulin binding and receptor "availability" is that the insulin receptors may associate with other membrane-associated protein(s) as it localizes in or out of the lipid-raft regions of the membrane. Indeed, the insulin receptor is known to interact with several other membrane-associated proteins [49, 207]. The localization of insulin receptors in caveloae is known to be crucial for its activation and signal propagation since disruption of caveolar invaginations by cyclodextrin treatment attenuates insulin receptor signalling [208], as also described in later discussion. Indeed, caveolin-1, a major structural protein of caveolae directly interacts with the insulin receptor, likely in the region containing amino acid residues 1175 – 1192 of the insulin receptor enhancing its tyrosine kinase activity [209]. As another example and by contrast, the interaction of the α-subunit of the insulin receptor with another transmembrane protein, plasma cell membrane glycoprotein (PC-1) decreases the insulin receptor's tyrosine kinase activity [207]. However, there is yet no direct evidence for the effect of these membrane proteins on insulin binding capacity of the insulin receptor. A study in our laboratory (David J Chandler, unpublished honours thesis, 2000) however, concluded that a "modulator" of insulin binding was removed from the insulin receptor during purification on insulin-agarose columns, but that this "modulator" was not PC-1.

Finally, the decrease in insulin binding or receptor availability following membrane cholesterol alterations could be related to the formation of insulin receptor clusters in various membrane micro-domains. The plasma membrane is organised into a number of sub-domains including the well-defined lipid rafts and membrane invaginations such as caveloae (consists of scaffolding protein, caveolin) and clathrin-coated pits [210]. For example, and in context of another tyrosine kinase receptor, disruption of these structures by membrane cholesterol depletion using MBCD results in the clustering of EGFR receptors to non-raft regions of the cell membrane and ligand-independent activation [211]. This is distinct from the concept previously described for EGFR concerning movement between caveolar and non-caveolar regions in the membrane. Given the evidence that insulin receptors, either in the presence or absence of insulin, tend to form clusters [212], which could decrease insulin binding [213], it would be interesting in future to likewise explore the organization of insulin receptors in both membrane raft and non-raft regions in membrane cholesterol

reduced or enriched conditions using super resolution imaging methods such as single molecule localization microscopy (SMLM) [212].

Effects of MBCD or cMBCD on insulin signalling

The decrease in insulin binding in HepG2 cells (Fig. 10B) and differentiated myotubes (Fig. 11C) following MBCD or cMBCD treatment coincided well with decreases in insulin stimulated phosphorylation of the insulin receptor, Akt and GSK3β (Fig. 17 and 18, respectively). As mentioned previously, changes in plasma membrane cholesterol content have also been shown to impair the activation of other growth factor/tyrosine kinase receptors such as the vascular endothelial growth factor receptor (VEGF-R) and nerve growth factor receptor (NGF-R) and their downstream signalling pathways [198, 214]. Ligand binding studies weren't conducted in the latter studies; therefore whether the effects observed were due to decreased binding or more distal events in receptor activation or signalling pathway hasn't been studied and thus remains unclear.

The link between decreased insulin binding and signalling events in HepG2 cells and differentiated myotubes following MBCD or cMBCD treatment was not observed in CHO T10 cells (Fig. 16). While a decrease in the autophosphorylation of the insulin receptors was observed in CHO T10 cells treated with both MBCD and cMBCD, Akt phosphorylation decreased following MBCD treatment but increased markedly following cMBCD treatment (Fig. 16D). Whilst it has been previously demonstrated that the disruption of lipid-rafts structures in the membrane by MBCD-mediated membrane cholesterol depletion impairs the full activation of Akt in response to other growth factor receptor signalling such as for IGF-1 [215, 216], the impact of cholesterol enrichment in the membrane on the integrity of lipid-raft structures, and subsequently, on Akt activity is unclear. Furthermore, no apparent change in GSK3β phosphorylation was observed following either MBCD or cMBCD treatment of CHO T10 cells, despite the apparent decrease in insulin receptor autophosphorylation (Fig. 16E). The observed disconnect between the autophosphorylation of the insulin receptors and Akt and GSK3β activities, which form a part of the 'metabolic pathway' of insulin signalling, might in part be explained by the predominant expression of the A-isoform of the insulin receptor in CHO T10 cells. The A-isoform

of the insulin receptors is of more importance to the regulation of the 'mitogenic pathway' of insulin signalling [28, 217, 218].

Another possibility for the apparent disconnect between insulin binding and signalling or action in CHO T10 cells, in particular, could be a lack of an adequate number of appropriate lipid-raft structures to accommodate the majority of overexpressed receptors on the surface of CHO T10 cells. The localization of the insulin receptor in these lipid-raft regions of the membrane is a key step in receptor activation and subsequent signal propagation [49, 191, 192]. That the majority of the insulin receptors are not located in these lipid-rafts in CHO T10 cells is supported by the observations in virus-like particles (VLPs) generated from CHO T10 and CHO K1 (wild-type) cells, detailed in section 3.3. Briefly, only 2% of the total insulin receptors expressed in CHO T10 cells were recovered in the VLPs (Table 7), the formation of which have an absolute requirement for lipid rafts [219, 220]. In future, it will be interesting to study the distribution of insulin receptors in various membrane micro-domains in CHO T10 cells and other insulin-sensitive cell types and how changes in membrane cholesterol content affect the distribution of insulin receptors.

It is possible that changes in membrane cholesterol content in CHO T10 cells could have a direct effect on the activation of Akt, since this event occurs in close proximity to the membrane and involves membrane-associated mediators [221]. Indeed, the rapid activation of Akt by phosphorylation, in response to growth factor signalling, involves the association of Akt with lipid-raft domains of the plasma membrane, and thus, the disruption of lipid-raft structures using MBCD may impair the full activation of Akt [215, 216]. However, a strong increase in Akt phosphorylation was observed in the present study following cMBCD treatment of CHO T10 cells (Fig. 18D). While the decrease in Akt phosphorylation, in response to cholesterol reduction by MBCD treatment, can be explained by a decrease in the production of phosphatidylinositol (3,4,5)-trisphosphate, a cell membrane bound second messenger [216], possible reasons for the observed increase in Akt phosphorylation following cMBCD-mediated cholesterol enrichment (Fig. 16D) is yet to be understood.

Effect of atorvastatin on insulin binding

Atorvastatin treatment of CHO T10 and HepG2 cells did not affect the binding of insulin to these cells (Fig. 15A and B), despite significant reductions in the total cholesterol content of these cells (Fig. 10). Whilst there is yet no evidence for the effects of statins on insulin binding, statins have been shown to impair insulin signalling and have been implicated in the development of insulin resistance and onset of diabetes [222, 223]. However, the results of the present study clearly demonstrate that there is no noticeable effect of atorvastatin either on insulin binding or on the affinity of insulin for its receptors in CHO T10 and HepG2 cells (Fig. 15, Table 3). These observations are in clear contrast to the insulin binding results from MBCD treatment of CHO T10 and HepG2 cells where even subtle decreases in cholesterol content decreased insulin binding to these cells (Fig. 9). One possible explanation for this observation could be that plasma membrane cholesterol content is much less affected by atorvastatin treatment.

In the present study, atorvastatin treatment in cells was carried out in a lipoprotein-deficient environment, which could be expected to limit the exogenous source of cholesterol for cells. Whilst statins lower cell cholesterol by limiting the *de novo* synthesis of cholesterol and promoting cellular uptake of cholesterol [224, 225], paradoxically, statin treatment also leads to an increase in the mRNA expression of *HMGCR* and other proteins involved in the upregulation of cholesterol synthesis in both *in vitro* and *in vivo* models [226]. This increase in cholesterol synthesis could potentially result in the transport of cholesterol from the endoplasmic reticulum to the plasma membrane, as this process is largely free of influences by other cellular stress conditions and regulatory mechanisms [227]. In the present study, it is notable that the high-fat diet-induced reduction in plasma membrane cholesterol content of mouse liver is restored by atorvastatin treatment (Fig. 24 and 25). Although this observation may not be directly comparable to the *in vitro* cell culture conditions of the present study, this regulatory effect of atorvastatin on cholesterol trafficking could be expected to also occur in cultured cells. Moreover, in the present study, cellular adaptations to the 48 h atorvastatin treatment may have occurred. In future, the effects of atorvastatin and other statins on cholesterol content should be investigated in purified plasma membrane preparations derived from cell culture models to explore these possibilities.

Effect of atorvastatin on insulin signalling

That atorvastatin did not influence insulin binding in CHO T10 and HepG2 cells correlated with the observation that it also had no considerable effect on insulin signalling in these cells, except for a marginal decrease in the phosphorylation of Akt (Fig. 21) in CHO T10 cells and a marginal increase in all the downstream insulin signalling events in HepG2 cells (Fig. 20). In contrast, atorvastatin treatment of differentiated myotubes significantly reduced the autophosphorylation of the insulin receptors and the phosphorylation of Akt and GSK3β (Fig. 21), despite having no appreciable effect on insulin binding. This is in keeping with previous observations that various statins cause insulin insensitivity in skeletal muscles [228-231]. Given that insulin receptor autophosphorylation was significantly impaired in differentiated myotubes with no alteration in insulin binding, it is likely that statins influence insulin receptor autophosphorylation independent of insulin binding. Indeed, simvastatin treatment impairs insulin signalling in L6 myotubes by elevating the activity of protein kinase C (PKC), which in turn leads to the inactivation of both IRS-1 and the insulin receptor itself [178].

While there are several intracellular modes of action (such as the increased PKC activity), proposed by which statins mediate insulin resistance [231, 232], it might also be possible that they influence more proximal events in the signalling pathway. Interestingly, the expression of caveolin-1, which promotes the tyrosine kinase activity of the insulin receptors following insulin binding, is decreased by statins in endothelial cells [233, 234]. Disruption of lipid-rafts/caveolae by inhibiting cholesterol bio-synthesis in 3T3-L1 pre-adipocytes also led to the redistribution of caveolin-1 out of caveolar invaginations to other regions in the membrane and subsequently impaired insulin signalling [67]. However, in contrast to signalling, there is no data on such effects insulin binding to its receptor. Other transmembrane proteins such as the plasma cell membrane glycoprotein (PC-1) have also been implicated to play a role in regulating the insulin receptor and its overexpression is observed in insulin resistant subjects [235, 236]. Thus, in future, studies may be focused on investigating the effects of atorvastatin, and other statins, on the interaction of the insulin receptor with these membrane-bound proteins by visualizing their co-localization using fluorescent probes or cross-linking mass

spectrometry to understand statin-mediated regulation of insulin sensitivity and action on target cells.

4.2. Effects of a high fat diet and atorvastatin treatment on cholesterol content and insulin action in mouse liver

Effect of high-fat diet on cholesterol content and insulin binding in mouse liver plasma membrane

The effect of plasma membrane cholesterol on insulin binding observed in this study in cultured cells was further assessed in liver tissue obtained from mice that were fed either a normal or high-fat diet with or without atorvastatin treatment over a 12-week period as detailed in Methods, section 2.2.2.1. The cholesterol content in purified liver plasma membranes decreased markedly (about 10-fold) in mice fed the high-fat diet, relative to those fed the normal diet (Fig. 24 and 25). It is notable this decrease in plasma membrane cholesterol content appeared to be mirrored in the cytosolic fraction of the livers obtained from the high-fat diet fed mice. Interestingly, this decrease was accompanied by a substantial increase in cholesterol in the microsomal fraction (Fig. 24 and 25). Indeed, the decrease in total plasma membrane and cytosolic cholesterol in liver tissue was almost entirely accounted for by a redistribution of cholesterol to the microsomal compartment in the high-fat diet group (Fig. 24 and 25). The mode(s) by which a high-fat diet results in this redistribution of cholesterol from the plasma membrane to the microsomal compartment is unclear, but given this is a novel and quite remarkable finding, this needs further investigation. While it is understood that the trafficking between the plasma membrane and endoplasmic reticulum helps maintain cholesterol homeostasis, the specific biochemical processes and points of control need to be detailed before the effect of high-fat diet on these process can be resolved. Given that the pathways for the transport of cholesterol from the endoplasmic reticulum to the plasma membrane appears to be distinct from the transport of cholesterol from the plasma membrane to the endoplasmic reticulum [227], detailing this process of cholesterol homeostasis, including the influence of variables such as diet, might prove to be quite challenging.

Insulin binding to the plasma membranes purified from the livers of mice that were fed the high-fat diet was markedly decreased relative to those from mice that were

fed the normal diet (Fig. 26). This observation is consistent with several other studies which have highlighted the negative regulatory effect of a high-fat diet to insulin binding in insulin sensitive tissues [237-239]. Notably, the latter studies did not examine the effects of high-fat diet on the changes in cell membrane cholesterol content. Analysis of the competitive binding data in this Thesis suggests that the decreased binding of insulin to the liver plasma membranes in response to the high-fat diet was related to a 2-fold decrease in the apparent number of insulin receptors relative to that of plasma membranes from mice fed a normal diet (Table 6) and was also in keeping with the findings by Western blot for insulin receptors in the plasma membrane (Fig. 28). As was also observed in the VLPs (section 3.3) and cells in culture (section 3.1), there was a correlation between the decreased cholesterol in the liver plasma membrane and the decreased insulin binding in the mice.

It is also notable that when plasma membranes, purified from the livers of mice fed a normal diet, were treated with either MBCD or cMBCD, insulin binding decreased (Fig.27) in a manner similar to that observed in the cultured cell models (Fig. 9) and VLPs (Fig. 39). The decreased binding of insulin in a membrane environment, as cholesterol content changes, cannot be due to receptor down-regulation, as the liver plasma membranes and VLPs that bud from plasma membrane are free of other cellular organisation that are essential for receptor internalisation or recycling. This may indicate that changes in membrane cholesterol content could potentially lead to the redistribution or other alterations in the organization of the insulin receptors in the membrane. Some possible explanations for this correlation between cholesterol composition in the plasma membrane and the apparent number of insulin receptors detected are articulated in section 4.1 and 4.3, respectively.

Effect of high-fat diet on insulin signalling in mouse liver

The decrease in available insulin receptors in the plasma membrane of the high-fat diet group was associated with a significant decrease in insulin receptor autophosphorylation (Fig. 28). However, the decrease in insulin receptor activation did not seem to have any appreciable effect on the phosphorylation of Akt (Fig. 29). Although this disconnect may appear counterintuitive, it is not totally unexpected, especially in *in vivo* models, since the activation of Akt is central to numerous pathways involved in cell regulation other than insulin signalling [240] and

influences by other growth factors and mediators may be at play. In addition, hepatic Akt, in response to insulin action, is only required to inhibit FOXO1, which is a transcription factor for several gluconeogenic enzymes and when FOXO1 is removed, the normal metabolic activities occurred in the absence of hepatic Akt [241]. Therefore, it is also likely that insulin may regulate the metabolic activities in liver through a pathway(s) that is independent from the participation of Akt.

No significant change in GSK3β phosphorylation was observed high-fat diet group relative to normal diet group (Fig. 29), which correlates with the absence of an influence on Akt phosphorylation by high-fat diet. The activity of GSK3β is regulated by a spectrum of modalities including phosphorylation, subcellular compartmentalization, substrate priming etc., during various physiological states [242-244] and, therefore, the findings in the present study, may not directly represent the effects of insulin action alone [245]. Given that the activation of Akt and GSK3β are associated with various cellular functions other than insulin action per se [246, 247], future studies should include screening for additional targets in both proximal insulin signalling events such as the activation of insulin receptor substrate family (IRS-1/2/3/4) and phosphatidylinositol 3-kinase (PI 3-K) [248], and downstream signalling events such as the regulation by mechanistic target of rapamycin complex 1 (mTORC1) [249].

Effect of atorvastatin on cholesterol content and insulin binding in mouse liver plasma membrane

In context of a normal diet, 12 weeks of atorvastatin treatment has no influence on the cholesterol content in plasma membrane and microsomes (Fig. 24 and 25). Similarly, insulin binding to the liver plasma membranes purified from the livers of these mice that were fed the normal diet was also unaffected by the atorvastatin treatment (Fig. 26). It is notable that total cholesterol content in cell culture models decreased following atorvastatin treatment in a lipoprotein deficient environment (section 3.1, Fig. 8). By contrast, atorvastatin treatment, in the presence of fetal bovine serum i.e., in presence of lipoproteins, did not change the total cholesterol content in these cultured cell models (figure not shown), which may indicate the ability of cells to uptake cholesterol from exogenous sources when the *de novo* synthesis of cholesterol is inhibited by statins [250, 251] and more closely reflects

the *in vivo* context. Hence, atorvastatin, in an *in vivo* context may not influence overall hepatic cholesterol possibly due to exogenous sources of cholesterol (eg: lipoproteins) compensating the deficiency. Interestingly, insulin binding to cultured cells, either in the presence of fetal bovine serum (figure not shown) or lipoprotein deficient serum, were unaffected by atorvastatin treatment (section 3.1, Fig. 15). Given the significance of cholesterol in the integrity of the plasma membrane and in the topology and functions of membrane bound receptors [252], it may be possible that cholesterol content in the plasma membrane of cell culture models is minimally affected by atorvastatin treatment. However, future studies are needed to clarify whether atorvastatin treatment specifically alters cholesterol content in the actual plasma membranes as opposed to total cholesterol content of cells in culture.

By stark contrast to mice fed the normal diet, atorvastatin treatment dramatically influenced cholesterol and insulin binding in mice fed the high-fat diet; cholesterol levels in both the plasma membrane and microsomes approached the 'normal' levels observed in mice that were only fed the normal diet, and there was concomitant increase in insulin binding to plasma membranes towards those observed in mice fed the normal diet. This is consistent with the observation that atorvastatin treatment in high-fat diet fed guinea pigs results in a ~ 30% reduction in its hepatic microsomal cholesterol content [253]. However, the mode by which atorvastatin treatment leads to the redistribution of cholesterol between the microsomal and plasma membrane compartment is unclear and thus, requires further investigation.

The 'normalizing' effect of atorvastatin treatment on plasma membrane cholesterol and insulin binding in high-fat diet mice coincided with an increase in detectable total insulin receptor in the plasma membrane towards that observed in mice fed a normal diet (Fig. 28). Moreover, atorvastatin normalized the autophosphorylation of the insulin receptors in liver plasma membranes in mice that were fed the high-fat diet to levels indistinguishable from mice fed the normal diet. That the ratio of activated to total receptors increased significantly in mice fed the high-fat diet and treated with atorvastatin indicates that atorvastatin not only 'normalized' the availability of insulin receptors towards levels observed in mice fed the normal diet but acted to also promote the autophosphorylation of the insulin receptors by a mechanism independent of the expression of the receptor itself.

Effect of atorvastatin on insulin signalling in mouse liver

The diet-dependent effect of atorvastatin was apparent in the phosphorylation status of Akt, decreasing in response to normal diet and increasing on a high-fat diet, respectively (Fig. 29C and 29D). These changes were independent of insulin receptor autophosphorylation or the expression of total Akt itself. The decrease in Akt phosphorylation on a normal diet is interesting given the potential link between statin therapy and insulin resistance and should be further investigated. Numerous other studies have demonstrated decreased activation of Akt and subsequently mTOR by statins [254, 255] and their cytotoxic effects in skeletal muscle cells [256-258]. Deleterious influences by atorvastatin on Akt activation have also been described in pancreatic cancer cells but is thought to have implications in cancer treatment by sensitizing cancer cells for chemotherapy drugs [259]. However, there is no direct explanation for the slight but significant increase in Akt activity following atorvastatin treatment in mice fed the high-fat diet (Fig. 29C). In contrast, the total expression and activity of GSK3β decreased following atorvastatin treatment but this effect was independent of the diet. (Fig. 29F and 29G). Further studies that detail the activity of additional downstream targets pertinent to the insulin signalling pathway should be conducted to improve the understandings of the effects of atorvastatin on insulin signalling in response to a high-fat diet.

In conclusion, the high-fat diet had a remarkable impact on plasma membrane cholesterol content and insulin receptor availability in mice. This was reflected in a decrease in insulin binding and in the autophosphorylation of the insulin receptors. While the link between a high-fat diet and insulin resistance is well established, the impact of a high-fat diet on cholesterol distribution in cells needs further investigation. Atorvastatin treatment restores cholesterol and insulin receptor availability for insulin and entirely restores insulin receptor autophosphorylation in the plasma membrane of mice fed the high-fat diet. Thus, atorvastatin treatment appears to benefit insulin sensitivity in mice fed a high-fat diet but may have other consequences in mice fed a normal diet.

4.3. Development and characterization of virus-like particles as a novel membrane model to study the influence of membrane cholesterol on insulin binding

Virus-like particles (VLPs), in the present study, were generated from either CHO K1 (wild-type) or CHO T10 (insulin receptor overexpressing) cells based on the self-assembly of a Gag-protein, which predominantly occurs in the lipid-raft regions in the plasma membrane [193, 260, 261]. In keeping with Gag-based VLPs generated by others [54], VLPs in the present study were spherical and relatively uniform with an average diameter of 159 nm (Fig. 30), which equates to a circumference of about 500 nm. A lipid-raft from which a VLP buds is estimated to be about 40-100 nm in width [262]. Thus, it might be expected that a lipid raft micro-domain would likely not make up the entire membrane component of a VLP, but that other regions of the membrane would also co-exist. Based on this expectation, VLPs might mimic at least some other general properties of the plasma membrane and not exclusively that of lipid-rafts alone. Since there are no reports yet on the lipid membrane environment of VLPs, future studies should include lipidomic and proteomic analysis of VLPs. These studies might provide valuable insights to gain better understanding of the role of lipid-rafts and other non-raft regions, and structural proteins pertinent to various membrane domains on receptor functioning in VLPs.

Whilst the precise organization of membrane lipids and proteins integral to VLPs is not yet well understood, it is generally recognized that VLPs contain plasma membrane proteins that remain in their native conformation [54, 263]. Indeed, the VLPs generated for the present study, bound insulin in a manner indistinguishable from their corresponding parental cell lines. The affinity of insulin for its receptor in the VLPs and their corresponding parental cells was not significantly different (Table 7). Moreover, the decrease in insulin binding to its receptor in VLPs, in response to either cholesterol reduction (MBCD) or cholesterol enrichment (cMBCD) (Fig. 39), also mimicked the observations in their parental cell lines (Fig. 37) and also to the observation in context of membrane cholesterol reduction or enrichment in HepG2 cells and differentiated myotubes (Fig. 7). This decrease in insulin binding in VLPs cannot be due to receptor internalization, since the VLPs lack the cytoplasmic

component of a cell. As discussed in section 4.1, changes related to the activity of transmembrane proteins such as PC-1 and caveolin-1 may influence insulin binding to its receptor. However, this postulate requires that such modulatory factors influence insulin access to the insulin receptor to explain the observation that the decreased binding is due to receptor availability to insulin or certain insulin receptor (α-subunit) antibodies. Understanding the changes in insulin receptor localization in various membrane micro-domains and its interaction with modulatory factor(s) in the membrane, will present a significant challenge for future research.

It is interesting to note that the insulin receptor content of VLPs derived from CHO T10 (overexpressing) cells and CHO K1 cells were similar (Fig. 35), despite the marked difference in insulin receptor content observed between the parental cells (Fig. 34). Based on competitive binding analysis, almost all the insulin receptors expressed in the wild-type CHO K1 cells were incorporated into the VLPs generated from these cells (Table 7). However, by contrast, only 2% of the insulin receptors expressed in CHO T10 cells was recovered in the VLPs generated from these cells. Thus, the 98% of the insulin receptors expressed in CHO T10 cells were not recovered in VLPs, which preferentially egress from the lipid-raft regions in the membrane. This majority of insulin receptors in CHO T10 cells thereby reside outside the lipid-raft regions of the plasma membrane. As a consequence, the majority of the overexpressed insulin receptors may not function in a manner that fully mimics the insulin receptor in the wild-type cell line. Indeed, as discussed in section 4.1, there appears to be a clear disconnect between insulin binding and insulin signalling in the CHO T10 cells. This is an important observation that potentially impacts many cell models overexpressing growth factor receptors and other proteins that signal via specific membrane micro-domains such as the lipid-rafts. Therefore, caution must be exercised when using cell models that overexpress proteins that are associated with lipid-rafts as cells may have a limited capacity to localize these proteins where they are needed to function normally. Also, future studies using more direct approaches such as flow cytometric analysis should be conducted to quantify insulin receptor content and other associated proteins that may influence insulin receptor function in VLPs. This approach was attempted in the present study but without success, with the smaller size of the VLPs being a limitation to the analysis by flow cytometry. Immunostaining the VLPs with

antibodies for the target protein and coupling them with aldehyde/sulfate latex beads may overcome this limitation [264].

It is notable that insulin bound to the insulin receptors in CHO T10 cells or the VLPs generated from these cells, with approximately 5-fold lower affinity than to insulin receptors in CHO K1 cells or the VLPs generated from these wild-type CHO-K1 cells. This decrease in the calculated affinity of insulin for its receptor in CHO T10 cells or VLPs generated from these cells can be visibly verified by the rightward shift of the competitive binding plots (Fig. 33). This difference in affinity cannot be explained on the basis of the difference in insulin receptor isoforms expressed in the wild-type CHO K1 cells and CHO T10 cells, since the A-isoform overexpressed in CHO T10 cells, is expected to have up to a 2-fold higher affinity for insulin than the B-isoform [36, 42, 265]; the latter is likely the predominant isoform in the CHO K1 cells since they are epithelial cell lines derived from the ovary of the Chinese hamster [189]. Finally, the difference observed in affinity between CHO T10 and CHO K1 cells, and in the VLPs derived from these cells is unlikely to be due to any experimental artefact arising from inappropriate assumptions or errors in the competitive binding assays. Insulin binding to VLPs derived from both CHO K1 and CHO T10 cells were measured at the same time. All assumptions inherent in competitive ligand binding assays were also carefully observed. Care was taken to ensure data was collected over the entire competitive binding curves and that the receptor concentrations in the assays were at least one tenth the value of the equilibrium dissociation constant calculated from the data. Furthermore, given that the recovery of insulin receptors in VLPs derived from either CHO K1 cells or CHO T10 cells was essentially indistinguishable, the concentrations of insulin receptors in the assays must have been very similar. Furthermore, the observations were highly reproducible in three independent experiments.

The difference in apparent affinity observed between insulin binding to the CHO K1 and CHO T10 cells appears genuine but is quite perplexing. Future research investigating the kinetics of binding might be informative, to either confirm or refute the interpretation of the equilibrium binding studies detailed in the present study, as inconsistencies between the equilibrium and kinetic evaluation of insulin binding between isoforms has been noted previously [266]. Application of real-time

technologies such as surface plasmon resonance and VLPs immobilized to sensor chips may provide powerful tools for such future research [53]. Indeed, VLPs were successfully immobilized to L1 sensor chips by the author and preliminary studies were conducted. However, choosing an appropriate reference or control VLPs that lack insulin receptors has been problematic as VLPs generated from CHO K1 cells also contain as many insulin receptors as VLPs derived from CHO T10 cells. It may be necessary in future to block insulin binding to the reference VLPs with an appropriate monoclonal antibody. It would not be possible to develop a CHO K1 insulin receptor knockout as insulin is the only growth hormone for these cells, which remains in the G1 phase in its absence [267].

Much is still to be discovered before the utility of VLPs can be fully realised. A better understanding of the composition of VLPs describing the inherent lipid-rafts and other membrane micro-domains, and the proteins associated with these domains is needed. However, description of the proteome or array of integral membrane proteins in lipid-rafts is now emerging. Several thousand proteins, identified using iTRAQ/mass spectrometry in lipid-rafts isolated from different cells, form the basis of RaftProt database [268]. Likewise, the protein content of Gag-based VLPs and other virus-like particles are currently being studied with the help of mass spectrometry-based, label-free quantitative proteomics [264, 269]. These insights into the proteome of VLPs in their lipid-raft (and non-raft regions) will improve our understanding of protein localization and assembly within VLPs and membranes in general.

Finally, VLPs present as an intriguing platform to study membrane protein functions, especially those that localize in and out of lipid-rafts, in response to changes in membrane cholesterol composition. The insulin receptor as detailed in this Thesis is one such example. It will be interesting to evaluate the VLP topology of the insulin receptors and its association with other membrane proteins within the VLP using electron microscopy. The influence of cholesterol depletion and enrichment on the localization of the insulin receptors within the lipid micro-domains constitutive to the VLPs will be intriguing. VLPs offer many advantages over whole cells; in the absence of the cell cytosol, VLPs could be largely free of proteases that can denature inherent proteins. In addition, processes involving receptor

downregulation/internalization, which can complicate ligand binding analyses, are also absent in the VLPs. VLPs can also be conveniently immobilized on sensor chips to enable ligand binding analysis using surface plasmon resonance (SPR). This approach will provide a powerful platform in the future to study the interaction of insulin with the insulin receptors, within its native membrane environment, in real-time and without the need for the use of radioactive or fluorescent labels [53, 270]. Thus, in future, VLPs in conjunction with technologies such as SPR or micro-scale thermophoresis will enable the analysis of the insulin-insulin receptor interaction in greater detail compared to the conventional approaches currently used for binding analyses.

5.0. CONCLUSIONS AND FUTURE DIRECTIONS

The binding of insulin to the insulin receptor was markedly influenced by the cholesterol content of the plasma membrane. Indeed, there appears to be an optimal level of cholesterol that supports maximal insulin binding. Cholesterol within the plasma membrane influenced insulin binding by altering the apparent number of available or accessible insulin receptors in the plasma membrane for insulin or antibody binding. Altering cholesterol levels in the plasma membrane of cells likely impacts the location of integral membrane proteins such as the insulin receptors within various plasma membrane micro-domains. But how these postulated changes in the location of other membrane proteins could influence the accessibility of the insulin receptor to its ligand is unclear. It may affect the access of the insulin receptors to modulatory factors that impact ligand binding. This however does not explain the reduced accessibility of anti-insulin receptor monoclonal antibody (83-7) to the insulin receptors, which was also affected by changes in cholesterol content. One possible explanation for the decreased binding of insulin following membrane cholesterol alteration could be that insulin receptors may aggregate to form clusters in various membrane micro-domains that in turn, may affect their ability to bind insulin, or indeed the antibody used; this however needs further investigation.

Cholesterol within the plasma membranes supports the formation of lipid-raft micro-domains that harbour various tyrosine kinase based receptors, including the insulin receptor and the location of receptors within or outside these regions is believed to affect the functionality of these receptors. It is notable in this study that the full

complement of insulin receptors within the plasma membrane of wild-type CHO K1 cells in culture appeared to be located in lipid-rafts since they were all recovered in the VLPs that egress from these raft regions of the plasma membrane. It is also notable that in the CHO T10 cells, which overexpress insulin receptors (~ 280-fold vs CHO K1 cells), only 2% of the total insulin receptors were recovered in the VLPs generated from this cell type. Thus, it appears that insulin receptor localization to lipid-rafts in CHO T10 cell membranes is substantially impaired. Also, there was an apparent disconnect between insulin binding and the availability or accessibility of the insulin receptor from downstream signalling events of the metabolic aspects of insulin action in CHO T10 cells. While this disconnect in CHO T10 cells could be more readily explained by the selective overexpression of the A-isoform of insulin receptors, which mediates the mitogenic aspect of insulin action; it could also be possible that there is not adequate and appropriate raft structures in the membrane of CHO T10 cells to accommodate the enormous number of overexpressed insulin receptors in the membrane. Therefore, a cell's capacity to localize receptor proteins to appropriate membrane micro-domains could be an important consideration whilst employing any overexpressing cell model for the study of receptor interactions or indeed, other membrane proteins.

The effect of the high-fat diet in decreasing the cholesterol content of mouse liver plasma membrane and in decreasing insulin binding, and of atorvastatin treatment in ameliorating these changes are among the novel findings of this Thesis. The decrease or increase in plasma membrane cholesterol by the high-fat diet or atorvastatin treatment, respectively, was almost entirely accounted for by the changes in the cholesterol content of the microsomal fraction. Thus, future studies should explore the mechanisms underlying the relative distribution of cholesterol in the plasma membrane and the endoplasmic reticulum and in other organellar membranes, and its impact on other vital functions of liver such as the synthesis and release of bile acids.

While the development and use of VLPs has previously been described in the context of the IGF receptor (IGFR) and IGF-IGFR interactions, the studies in this Thesis represents the first demonstration of the development and use insulin receptor bearing VLPs, as is the demonstration of their insulin binding characteristics, which were very similar to the distinct characteristics (e.g binding affinities) of their cells of origin (CHOK1 and CHOT10 cells). The studies on VLPs also added to the evidence

supporting the influence of plasma membrane cholesterol on insulin receptor binding observed in the cell culture and mouse studies. That the VLPs generated either from an over-expressing cell model (CHO T10) or a wild-type cell model (CHO K1), carried a similar number of insulin receptors is an unexpected and another novel finding of this Thesis. The lack of available membrane raft structures to accommodate the over-expressed insulin receptors in CHO T10 cells was considered to be a possible reason for this finding. In context of the physical properties of the VLPs, the stability of VLPs over a wide range of temperature and their longer shelf-life period increases their ease of handling and suggests VLPs are a viable alternative model for study of insulin-insulin receptor interactions. Being highly uniform spherical particles, as estimated by dynamic light scattering analysis in this study, VLPs could be conveniently immobilized on sensor chips for interaction analysis by advanced analytic techniques such as surface plasmon resonance (SPR). The use of insulin receptor bearing VLPs in SPR would enable real-time analysis of the kinetics and equilibrium constants of the interaction of insulin with its receptor.

In conclusion, the findings of this Thesis highlight the influence of plasma membrane cholesterol content on the binding of insulin to its receptor. This Thesis provides a basis for further investigation concerning the distribution of cholesterol and its role in various membrane domains and how this might be affected by dietary changes or by cholesterol-lowering medication such as the statins, and within the broader context of insulin resistance.

6.0. REFERENCES

[1] S.S. Abdulazeez, Diabetes treatment: A rapid review of the current and future scope of stem cell research, Saudi Pharmaceutical Journal, 23 (2015) 333-340.
[2] A.B. Olokoba, O.A. Obateru, L.B. Olokoba, Type 2 diabetes mellitus: a review of current trends, Oman medical journal, 27 (2012) 269.
[3] M.A. Atkinson, G.S. Eisenbarth, Type 1 diabetes: new perspectives on disease pathogenesis and treatment, The Lancet, 358 (2001) 221-229.
[4] D.B. Dunger, M.A. Sperling, C.L. Acerini, D.J. Bohn, D. Daneman, T.P. Danne, N.S. Glaser, R. Hanas, R.L. Hintz, L.L. Levitsky, European Society for Paediatric Endocrinology/Lawson Wilkins Pediatric Endocrine Society consensus statement on diabetic ketoacidosis in children and adolescents, Pediatrics, 113 (2004) e133-e140.
[5] S.E. Kahn, M.E. Cooper, S. Del Prato, Pathophysiology and treatment of type 2 diabetes: perspectives on the past, present, and future, The Lancet, 383 (2014) 1068-1083.
[6] E. Wilmot, I. Idris, Early onset type 2 diabetes: risk factors, clinical impact and management, Therapeutic advances in chronic disease, 5 (2014) 234-244.
[7] J.G. Menting, J. Whittaker, M.B. Margetts, L.J. Whittaker, G.K.-W. Kong, B.J. Smith, C.J. Watson, L. Žáková, E. Kletvíková, J. Jiráček, How insulin engages its primary binding site on the insulin receptor, Nature, 493 (2013) 241.
[8] J.P. Mayer, F. Zhang, R.D. DiMarchi, Insulin structure and function, Peptide Science, 88 (2007) 687-713.
[9] E. Standl, Insulin analogues–State of the art, Hormone Research in Paediatrics, 57 (2002) 40-45.
[10] T. Blundell, J. Cutfield, S. Cutfield, E. Dodson, G. Dodson, D. Hodgkin, D. Mercola, Three-dimensional atomic structure of insulin and its relationship to activity, Diabetes, 21 (1972) 492-505.
[11] M. Weiss, D.F. Steiner, L.H. Philipson, Insulin biosynthesis, secretion, structure, and structure-activity relationships, (2014).
[12] Z. Fu, E. R Gilbert, D. Liu, Regulation of insulin synthesis and secretion and pancreatic Beta-cell dysfunction in diabetes, Current diabetes reviews, 9 (2013) 25-53.
[13] P. De Meyts, Insulin and its receptor: structure, function and evolution, Bioessays, 26 (2004) 1351-1362.
[14] P. De Meyts, J. Whittaker, Structural biology of insulin and IGF1 receptors: implications for drug design, Nature reviews. Drug discovery, 1 (2002) 769.
[15] J. Lee, P.F. Pilch, The insulin receptor: structure, function, and signaling, American Journal of Physiology-Cell Physiology, 266 (1994) C319-C334.
[16] Y. Ebina, L. Ellis, K. Jarnagin, M. Edery, L. Graf, E. Clauser, J.-h. Ou, F. Masiarz, Y. Kan, I. Goldfine, The human insulin receptor cDNA: the structural basis for hormone-activated transmembrane signalling, Cell, 40 (1985) 747-758.
[17] S. Jacobs, P. Cuatrecasas, Phosphorylation of receptors for insulin and insulin-like growth factor I. Effects of hormones and phorbol esters, Journal of Biological Chemistry, 261 (1986) 934-939.
[18] B. Cheatham, S.E. Shoelson, K. Yamada, E. Goncalves, C.R. Kahn, Substitution of the erbB-2 oncoprotein transmembrane domain activates the insulin receptor and modulates the action of insulin and insulin-receptor substrate 1, Proceedings of the National Academy of Sciences, 90 (1993) 7336-7340.
[19] L.G. Sparrow, N.M. McKern, J.J. Gorman, P.M. Strike, C.P. Robinson, J.D. Bentley, C.W. Ward, The disulfide bonds in the C-terminal domains of the human insulin receptor ectodomain, Journal of Biological Chemistry, 272 (1997) 29460-29467.
[20] C.R. Kahn, M. White, The insulin receptor and the molecular mechanism of insulin action, Journal of Clinical Investigation, 82 (1988) 1151.

[21] V. Duronio, S. Jacobs, P. Romero, A. Herscovics, Effects of inhibitors of N-linked oligosaccharide processing on the biosynthesis and function of insulin and insulin-like growth factor-I receptors, Journal of Biological Chemistry, 263 (1988) 5436-5445.
[22] S. Seino, M. Seino, S. Nishi, G.I. Bell, Structure of the human insulin receptor gene and characterization of its promoter, Proceedings of the National Academy of Sciences, 86 (1989) 114-118.
[23] S. Seino, G.I. Bell, Alternative splicing of human insulin receptor messenger RNA, Biochemical and biophysical research communications, 159 (1989) 312-316.
[24] J.A. Hedo, C.R. Kahn, M. Hayashi, K. Yamada, M. Kasuga, Biosynthesis and glycosylation of the insulin receptor. Evidence for a single polypeptide precursor of the two major subunits, Journal of Biological Chemistry, 258 (1983) 10020-10026.
[25] J. Bass, C. Turck, M. Rouard, D.F. Steiner, Furin-mediated processing in the early secretory pathway: sequential cleavage and degradation of misfolded insulin receptors, Proceedings of the National Academy of Sciences, 97 (2000) 11905-11909.
[26] B.J. Robertson, J. Moehring, T. Moehring, Defective processing of the insulin receptor in an endoprotease-deficient Chinese hamster cell strain is corrected by expression of mouse furin, Journal of Biological Chemistry, 268 (1993) 24274-24277.
[27] H. Benecke, J.S. Flier, D.E. Moller, Alternatively spliced variants of the insulin receptor protein. Expression in normal and diabetic human tissues, Journal of Clinical Investigation, 89 (1992) 2066.
[28] A. Belfiore, F. Frasca, G. Pandini, L. Sciacca, R. Vigneri, Insulin receptor isoforms and insulin receptor/insulin-like growth factor receptor hybrids in physiology and disease, Endocrine reviews, 30 (2009) 586-623.
[29] A. Ullrich, J. Bell, E.Y. Chen, R. Herrera, L. Petruzzelli, T.J. Dull, A. Gray, L. Coussens, Y.-C. Liao, M. Tsubokawa, Human insulin receptor and its relationship to the tyrosine kinase family of oncogenes, Nature, 313 (1985) 756-761.
[30] Y. Ebina, M. Edery, L. Ellis, D. Standring, J. Beaudoin, R.A. Roth, W.J. Rutter, Expression of a functional human insulin receptor from a cloned cDNA in Chinese hamster ovary cells, Proceedings of the National Academy of Sciences, 82 (1985) 8014-8018.
[31] D.A. Bravo, J.B. Gleason, R.I. Sanchez, R.A. Roth, R.S. Fuller, Accurate and efficient cleavage of the human insulin proreceptor by the human proprotein-processing protease furin. Characterization and kinetic parameters using the purified, secreted soluble protease expressed by a recombinant baculovirus, Journal of Biological Chemistry, 269 (1994) 25830-25837.
[32] S. Tian, A 20 residues motif delineates the furin cleavage site and its physical properties may influence viral fusion, Biochemistry Insights, 2 (2009) BCI. S2049.
[33] I. Kara, M. Poggi, B. Bonardo, R. Govers, J.-F. Landrier, S. Tian, I. Leibiger, R. Day, J.W. Creemers, F. Peiretti, The Paired Basic Amino Acid-cleaving Enzyme 4 (PACE4) Is Involved in the Maturation of Insulin Receptor Isoform B AN OPPORTUNITY TO REDUCE THE SPECIFIC INSULIN RECEPTOR-DEPENDENT EFFECTS OF INSULIN-LIKE GROWTH FACTOR 2 (IGF2), Journal of Biological Chemistry, 290 (2015) 2812-2821.
[34] D.E. Moller, A. Yokota, J.F. Caro, J.S. Flier, Tissue-specific expression of two alternatively spliced insulin receptor mRNAs in man, Molecular Endocrinology, 3 (1989) 1263-1269.
[35] Z. Huang, N.L. Bodkin, H.K. Ortmeyer, B.C. Hansen, A.R. Shuldiner, Hyperinsulinemia is associated with altered insulin receptor mRNA splicing in muscle of the spontaneously obese diabetic rhesus monkey, Journal of Clinical Investigation, 94 (1994) 1289.
[36] Y. Yamaguchi, J.S. Flier, A. Yokota, H. Benecke, J.M. Backer, D.E. Moller, Functional properties of two naturally occurring isoforms of the human insulin receptor in Chinese hamster ovary cells, Endocrinology, 129 (1991) 2058-2066.

[37] B. Vogt, J.M. Carrascosa, B. Ermel, A. Ullrich, H.-U. Häring, The two isotypes of the human insulin receptor (HIR-A and HIR-B) follow different internalization kinetics, Biochemical and biophysical research communications, 177 (1991) 1013-1018.
[38] D.A. McClain, Different ligand affinities of the two human insulin receptor splice variants are reflected in parallel changes in sensitivity for insulin action, Molecular Endocrinology, 5 (1991) 734-739.
[39] M. Kellerer, G. Sesti, E. Seffer, B. Obermaier-Kusser, D. Pongratz, L. Mosthaf, H. Häring, Altered pattern of insulin receptor isotypes in skeletal muscle membranes of type 2 (non-insulin-dependent) diabetic subjects, Diabetologia, 36 (1993) 628-632.
[40] L. Mosthaf, B. Vogt, H. Häring, A. Ullrich, Altered expression of insulin receptor types A and B in the skeletal muscle of non-insulin-dependent diabetes mellitus patients, Proceedings of the National Academy of Sciences, 88 (1991) 4728-4730.
[41] D. Dardevet, K. Komori, C. Grunfeld, S.A. Rosenzweig, M.G. Buse, Increased hepatic insulin proreceptor-to-receptor ratio in diabetes: a possible processing defect, American Journal of Physiology-Endocrinology and Metabolism, 261 (1991) E562-E571.
[42] P. Malakar, L. Chartarifsky, A. Hija, G. Leibowitz, B. Glaser, Y. Dor, R. Karni, Insulin receptor alternative splicing is regulated by insulin signaling and modulates beta cell survival, Scientific reports, 6 (2016).
[43] P. De Meyts, J. Roth, D.M. Neville, J.R. Gavin, M.A. Lesniak, Insulin interactions with its receptors: experimental evidence for negative cooperativity, Biochemical and biophysical research communications, 55 (1973) 154-161.
[44] M.C. Lawrence, N.M. McKern, C.W. Ward, Insulin receptor structure and its implications for the IGF-1 receptor, Current opinion in structural biology, 17 (2007) 699-705.
[45] M.E. Rentería, N.S. Gandhi, P. Vinuesa, E. Helmerhorst, R.L. Mancera, A comparative structural bioinformatics analysis of the insulin receptor family ectodomain based on phylogenetic information, PloS one, 3 (2008) e3667.
[46] P. De Meyts, The structural basis of insulin and insulin-like growth factor-I receptor binding and negative co-operativity, and its relevance to mitogenic versus metabolic signalling, Diabetologia, 37 (1994) S135-S148.
[47] R.Z.-T. Luo, D.R. Beniac, A. Fernandes, C.C. Yip, F. Ottensmeyer, Quaternary structure of the insulin-insulin receptor complex, Science, 285 (1999) 1077-1080.
[48] C.W. Ward, M.C. Lawrence, Landmarks in insulin research, Frontiers in endocrinology, 2 (2011).
[49] S. Vainio, S. Heino, J.E. Månsson, P. Fredman, E. Kuismanen, O. Vaarala, E. Ikonen, Dynamic association of human insulin receptor with lipid rafts in cells lacking caveolae, EMBO reports, 3 (2002) 95-100.
[50] R. Kohanski, M.D. Lane, Binding of insulin to solubilized insulin receptor from human placenta. Evidence for a single class of noninteracting binding sites, Journal of Biological Chemistry, 258 (1983) 7460-7468.
[51] S. Wanant, M.J. Quon, Insulin receptor binding kinetics: modeling and simulation studies, Journal of theoretical Biology, 205 (2000) 355-364.
[52] B.H. Ginsberg, T.J. Brown, I. Simon, A.A. Spector, Effect of the membrane lipid environment on the properties of insulin receptors, Diabetes, 30 (1981) 773-780.
[53] R.G. Heym, W.B. Hornberger, V. Lakics, G.C. Terstappen, Label-free detection of small-molecule binding to a GPCR in the membrane environment, Biochimica et Biophysica Acta (BBA)-Proteins and Proteomics, 1854 (2015) 979-986.
[54] S. Willis, C. Davidoff, J. Schilling, A. Wanless, B.J. Doranz, J. Rucker, Virus-like particles as quantitative probes of membrane protein interactions, Biochemistry, 47 (2008) 6988-6990.

[55] M.J. Endres, S. Jaffer, B. Haggarty, J.D. Turner, B.J. Doranz, P.J. O'brien, D.L. Kolson, J.A. Hoxie, Targeting of HIV-and SIV-infected cells by CD4-chemokine receptor pseudotypes, Science, 278 (1997) 1462-1464.
[56] D.H. Nguyen, D. Taub, Cholesterol is essential for macrophage inflammatory protein 1β binding and conformational integrity of CC chemokine receptor 5, Blood, 99 (2002) 4298-4306.
[57] S. Campbell, K. Gaus, R. Bittman, W. Jessup, S. Crowe, J. Mak, The raft-promoting property of virion-associated cholesterol, but not the presence of virion-associated Brij 98 rafts, is a determinant of human immunodeficiency virus type 1 infectivity, Journal of virology, 78 (2004) 10556-10565.
[58] Z. Liao, L.M. Cimakasky, R. Hampton, D.H. Nguyen, J.E. Hildreth, Lipid rafts and HIV pathogenesis: host membrane cholesterol is required for infection by HIV type 1, AIDS research and human retroviruses, 17 (2001) 1009-1019.
[59] C. Gilbert, M. Bergeron, S. Méthot, J.-F. Giguère, M.J. Tremblay, Statins could be used to control replication of some viruses, including HIV-1, Viral immunology, 18 (2005) 474-489.
[60] A.R. Saltiel, C.R. Kahn, Insulin signalling and the regulation of glucose and lipid metabolism, Nature, 414 (2001) 799-806.
[61] R.T. Watson, M. Kanzaki, J.E. Pessin, Regulated membrane trafficking of the insulin-responsive glucose transporter 4 in adipocytes, Endocrine reviews, 25 (2004) 177-204.
[62] A.R. Saltiel, J.E. Pessin, Insulin signaling in microdomains of the plasma membrane, Traffic, 4 (2003) 711-716.
[63] A. Mora, D. Komander, D.M. van Aalten, D.R. Alessi, PDK1, the master regulator of AGC kinase signal transduction, Seminars in cell & developmental biology, Elsevier, 2004, pp. 161-170.
[64] S. Martin, C.A. Millar, C.T. Lyttle, T. Meerloo, B.J. Marsh, G.W. Gould, D.E. James, Effects of insulin on intracellular GLUT4 vesicles in adipocytes: evidence for a secretory mode of regulation, Journal of Cell Science, 113 (2000) 3427-3438.
[65] K. Siddle, Signalling by insulin and IGF receptors: supporting acts and new players, Journal of molecular endocrinology, 47 (2011) R1-R10.
[66] J.S. Freeman, The increasing epidemiology of diabetes and review of current treatment algorithms, Journal of the American Osteopathic Association, 110 (2010) eS2.
[67] J. Sánchez-Wandelmer, A. Dávalos, E. Herrera, M. Giera, S. Cano, G. de la Peña, M.A. Lasunción, R. Busto, Inhibition of cholesterol biosynthesis disrupts lipid raft/caveolae and affects insulin receptor activation in 3T3-L1 preadipocytes, Biochimica et Biophysica Acta (BBA)-Biomembranes, 1788 (2009) 1731-1739.
[68] P. Singleton, Bacteria in biology, biotechnology and medicine, John Wiley & Sons2004.
[69] S.J. Singer, G.L. Nicolson, The fluid mosaic model of the structure of cell membranes, Science, 175 (1972) 720-731.
[70] C. Tanford, The Hydrophobic Effect: Formation of Micelles and Biological Membranes 2d Ed, J. Wiley.1980.
[71] B. Alberts, A. Johnson, J. Lewis, P. Walter, M. Raff, K. Roberts, Molecular Biology of the Cell 4th Edition: International Student Edition, Routledge, 2002.
[72] G. van Meer, A.I. de Kroon, Lipid map of the mammalian cell, J Cell Sci, 124 (2011) 5-8.
[73] G. Van Meer, D.R. Voelker, G.W. Feigenson, Membrane lipids: where they are and how they behave, Nature reviews. Molecular cell biology, 9 (2008) 112.
[74] J.E. Vance, D.E. Vance, Biochemistry of lipids, lipoproteins and membranes, Elsevier2008.
[75] E.J. Smart, Y.-s. Ying, W.C. Donzell, R.G. Anderson, A role for caveolin in transport of cholesterol from endoplasmic reticulum to plasma membrane, Journal of Biological Chemistry, 271 (1996) 29427-29435.

[76] M.S. Brown, J.L. Goldstein, Receptor-mediated control of cholesterol metabolism, Science, 191 (1976) 150-154.
[77] P. Goluszko, B. Nowicki, Membrane cholesterol: a crucial molecule affecting interactions of microbial pathogens with mammalian cells, Infection and immunity, 73 (2005) 7791-7796.
[78] N.M. Cerqueira, E.F. Oliveira, D.S. Gesto, D. Santos-Martins, C. Moreira, H.N. Moorthy, M.J. Ramos, P. Fernandes, Cholesterol Biosynthesis: A Mechanistic Overview, Biochemistry, 55 (2016) 5483-5506.
[79] H.-S. Shieh, L. Hoard, C. Nordman, The structure of cholesterol, Acta Crystallographica Section B: Structural Crystallography and Crystal Chemistry, 37 (1981) 1538-1543.
[80] J. Fantini, F.J. Barrantes, How cholesterol interacts with membrane proteins: an exploration of cholesterol-binding sites including CRAC, CARC, and tilted domains, Frontiers in physiology, 4 (2013).
[81] J. Dai, M. Alwarawrah, J. Huang, Instability of cholesterol clusters in lipid bilayers and the cholesterol's umbrella effect, The Journal of Physical Chemistry B, 114 (2009) 840-848.
[82] M.R. Ali, K.H. Cheng, J. Huang, Assess the nature of cholesterol–lipid interactions through the chemical potential of cholesterol in phosphatidylcholine bilayers, Proceedings of the National Academy of Sciences, 104 (2007) 5372-5377.
[83] A. Parker, K. Miles, K.H. Cheng, J. Huang, Lateral distribution of cholesterol in dioleoylphosphatidylcholine lipid bilayers: cholesterol-phospholipid interactions at high cholesterol limit, Biophysical journal, 86 (2004) 1532-1544.
[84] I.A. Rose, K.R. Hanson, K.D. Wilkinson, M.J. Wimmer, A suggestion for naming faces of ring compounds, Proceedings of the National Academy of Sciences, 77 (1980) 2439-2441.
[85] T.P. Trouard, A.A. Nevzorov, T.M. Alam, C. Job, J. Zajicek, M.F. Brown, Influence of cholesterol on dynamics of dimyristoylphosphatidylcholine bilayers as studied by deuterium NMR relaxation, The Journal of chemical physics, 110 (1999) 8802-8818.
[86] T. Róg, M. Pasenkiewicz-Gierula, I. Vattulainen, M. Karttunen, What happens if cholesterol is made smoother: importance of methyl substituents in cholesterol ring structure on phosphatidylcholine–sterol interaction, Biophysical journal, 92 (2007) 3346-3357.
[87] M. Bloom, E. Evans, O.G. Mouritsen, Physical properties of the fluid lipid-bilayer component of cell membranes: a perspective, Quarterly reviews of biophysics, 24 (1991) 293-397.
[88] K. Kawakami, Y. Nishihara, K. Hirano, Rigidity of lipid membranes detected by capillary electrophoresis, Langmuir, 15 (1999) 1893-1895.
[89] A.R. Waldeck, M.H. Nouri-Sorkhabi, D.R. Sullivan, P.W. Kuchel, Effects of cholesterol on transmembrane water diffusion in human erythrocytes measured using pulsed field gradient NMR, Biophysical chemistry, 55 (1995) 197-208.
[90] J. Kwik, S. Boyle, D. Fooksman, L. Margolis, M.P. Sheetz, M. Edidin, Membrane cholesterol, lateral mobility, and the phosphatidylinositol 4, 5-bisphosphate-dependent organization of cell actin, Proceedings of the National Academy of Sciences, 100 (2003) 13964-13969.
[91] O.G. Mouritsen, K. Jørgensen, Dynamical order and disorder in lipid bilayers, Chemistry and physics of lipids, 73 (1994) 3-25.
[92] J.A. Urbina, S. Pekerar, H.-b. Le, J. Patterson, B. Montez, E. Oldfield, Molecular order and dynamics of phosphatidylcholine bilayer membranes in the presence of cholesterol, ergosterol and lanosterol: a comparative study using 2H-, 13C-and 31P-NMR spectroscopy, Biochimica et Biophysica Acta (BBA)-Biomembranes, 1238 (1995) 163-176.
[93] C. Ege, M.K. Ratajczak, J. Majewski, K. Kjaer, K.Y.C. Lee, Evidence for lipid/cholesterol ordering in model lipid membranes, Biophysical journal, 91 (2006) L01-L03.

[94] T. Róg, M. Pasenkiewicz-Gierula, I. Vattulainen, M. Karttunen, Ordering effects of cholesterol and its analogues, Biochimica et Biophysica Acta (BBA)-Biomembranes, 1788 (2009) 97-121.
[95] B. Ramstedt, J.P. Slotte, Interaction of cholesterol with sphingomyelins and acyl-chain-matched phosphatidylcholines: a comparative study of the effect of the chain length, Biophysical journal, 76 (1999) 908-915.
[96] P. Dynarowicz-Łątka, K. Hąc-Wydro, Interactions between phosphatidylcholines and cholesterol in monolayers at the air/water interface, Colloids and Surfaces B: Biointerfaces, 37 (2004) 21-25.
[97] H. Martinez-Seara, T. Róg, M. Pasenkiewicz-Gierula, I. Vattulainen, M. Karttunen, R. Reigada, Interplay of unsaturated phospholipids and cholesterol in membranes: effect of the double-bond position, Biophysical journal, 95 (2008) 3295-3305.
[98] H. Ohvo-Rekilä, B. Ramstedt, P. Leppimäki, J.P. Slotte, Cholesterol interactions with phospholipids in membranes, Progress in lipid research, 41 (2002) 66-97.
[99] K. Simons, E. Ikonen, Functional rafts in cell membranes, Nature, 387 (1997) 569.
[100] J. Fantini, N. Garmy, R. Mahfoud, N. Yahi, Lipid rafts: structure, function and role in HIV, Alzheimer's and prion diseases, Expert reviews in molecular medicine, 4 (2002) 1-22.
[101] M. Alwarawrah, J. Dai, J. Huang, A molecular view of the cholesterol condensing effect in DOPC lipid bilayers, The journal of physical chemistry B, 114 (2010) 7516-7523.
[102] J.M. Smaby, M.M. Momsen, H.L. Brockman, R.E. Brown, Phosphatidylcholine acyl unsaturation modulates the decrease in interfacial elasticity induced by cholesterol, Biophysical journal, 73 (1997) 1492-1505.
[103] M.R. Ali, K.H. Cheng, J. Huang, Ceramide drives cholesterol out of the ordered lipid bilayer phase into the crystal phase in 1-palmitoyl-2-oleoyl-sn-glycero-3-phosphocholine/cholesterol/ceramide ternary mixtures, Biochemistry, 45 (2006) 12629-12638.
[104] A. Lee, Lipid–protein interactions in biological membranes: a structural perspective, Biochimica et Biophysica Acta (BBA)-Biomembranes, 1612 (2003) 1-40.
[105] J. Fantini, D. Carlus, N. Yahi, The fusogenic tilted peptide (67–78) of α-synuclein is a cholesterol binding domain, Biochimica et Biophysica Acta (BBA)-Biomembranes, 1808 (2011) 2343-2351.
[106] A. Radhakrishnan, T.G. Anderson, H.M. McConnell, Condensed complexes, rafts, and the chemical activity of cholesterol in membranes, Proceedings of the National Academy of Sciences, 97 (2000) 12422-12427.
[107] H. Cao, N. Tokutake, S.L. Regen, Unraveling the mystery surrounding cholesterol's condensing effect, Journal of the American Chemical Society, 125 (2003) 16182-16183.
[108] N. Garmy, N. Taïeb, N. Yahi, J. Fantini, Interaction of cholesterol with sphingosine physicochemical characterization and impact on intestinal absorption, Journal of lipid research, 46 (2005) 36-45.
[109] J. Fantini, F.J. Barrantes, Sphingolipid/cholesterol regulation of neurotransmitter receptor conformation and function, Biochimica et Biophysica Acta (BBA)-Biomembranes, 1788 (2009) 2345-2361.
[110] M.A. Hanson, V. Cherezov, M.T. Griffith, C.B. Roth, V.-P. Jaakola, E.Y. Chien, J. Velasquez, P. Kuhn, R.C. Stevens, A specific cholesterol binding site is established by the 2.8 Å structure of the human β 2-adrenergic receptor, Structure, 16 (2008) 897-905.
[111] S. Mukherjee, A. Chattopadhyay, Membrane organization at low cholesterol concentrations: a study using 7-nitrobenz-2-oxa-1, 3-diazol-4-yl-labeled cholesterol, Biochemistry, 35 (1996) 1311-1322.
[112] C.J. Baier, J. Fantini, F.J. Barrantes, Disclosure of cholesterol recognition motifs in transmembrane domains of the human nicotinic acetylcholine receptor, Scientific reports, 1 (2011) 69.

[113] M.M. Hussain, D.K. Strickland, A. Bakillah, The mammalian low-density lipoprotein receptor family, Annual review of nutrition, 19 (1999) 141-172.
[114] H. Rudney, R.C. Sexton, Regulation of cholesterol biosynthesis, Annual review of nutrition, 6 (1986) 245-272.
[115] J. Thomas, T. Shentu, D.K. Singh, Cholesterol: biosynthesis, functional diversity, homeostasis and regulation by natural products, Biochemistry, InTech2012.
[116] J.M. Risley, Cholesterol biosynthesis: Lanosterol to cholesterol, J. Chem. Educ, 79 (2002) 377.
[117] R. Coxey, P. Pentchev, G. Campbell, E. Blanchette-Mackie, Differential accumulation of cholesterol in Golgi compartments of normal and Niemann-Pick type C fibroblasts incubated with LDL: a cytochemical freeze-fracture study, Journal of lipid research, 34 (1993) 1165-1176.
[118] Y. Lange, Disposition of intracellular cholesterol in human fibroblasts, Journal of lipid research, 32 (1991) 329-339.
[119] R.E. Soccio, J.L. Breslow, Intracellular cholesterol transport, Arteriosclerosis, thrombosis, and vascular biology, 24 (2004) 1150-1160.
[120] P. Dupree, R. Parton, G. Raposo, T. Kurzchalia, K. Simons, Caveolae and sorting in the trans-Golgi network of epithelial cells, The EMBO journal, 12 (1993) 1597.
[121] W. Möbius, E. Van Donselaar, Y. Ohno‐Iwashita, Y. Shimada, H. Heijnen, J. Slot, H. Geuze, Recycling compartments and the internal vesicles of multivesicular bodies harbor most of the cholesterol found in the endocytic pathway, Traffic, 4 (2003) 222-231.
[122] E. Ikonen, Cellular cholesterol trafficking and compartmentalization, Nature reviews Molecular cell biology, 9 (2008) 125-138.
[123] S. Colles, J. Woodford, D. Moncecchi, S. Myers-Payne, L. McLean, J. Billheimer, F. Schroeder, Cholesterol interaction with recombinant human sterol carrier protein-2, Lipids, 30 (1995) 795-803.
[124] M. Hao, S.X. Lin, O.J. Karylowski, D. Wüstner, T.E. McGraw, F.R. Maxfield, Vesicular and non-vesicular sterol transport in living cells The endocytic recycling compartment is a major sterol storage organelle, Journal of Biological Chemistry, 277 (2002) 609-617.
[125] C.T. Beh, C.R. McMaster, K.G. Kozminski, A.K. Menon, A detour for yeast oxysterol binding proteins, Journal of Biological Chemistry, 287 (2012) 11481-11488.
[126] R.E. Soccio, J.L. Breslow, StAR-related lipid transfer (START) proteins: mediators of intracellular lipid metabolism, Journal of Biological Chemistry, 278 (2003) 22183-22186.
[127] S. Lusa, S. Heino, E. Ikonen, Differential mobilization of newly synthesized cholesterol and biosynthetic sterol precursors from cells, Journal of Biological Chemistry, 278 (2003) 19844-19851.
[128] B. Mesmin, N.H. Pipalia, F.W. Lund, T.F. Ramlall, A. Sokolov, D. Eliezer, F.R. Maxfield, STARD4 abundance regulates sterol transport and sensing, Molecular biology of the cell, 22 (2011) 4004-4015.
[129] A. Radhakrishnan, J.L. Goldstein, J.G. McDonald, M.S. Brown, Switch-like control of SREBP-2 transport triggered by small changes in ER cholesterol: a delicate balance, Cell metabolism, 8 (2008) 512-521.
[130] Y. Lange, J. Ye, M. Rigney, T.L. Steck, Regulation of endoplasmic reticulum cholesterol by plasma membrane cholesterol, Journal of lipid research, 40 (1999) 2264-2270.
[131] Y. Lange, J. Ye, T.L. Steck, How cholesterol homeostasis is regulated by plasma membrane cholesterol in excess of phospholipids, Proceedings of the National Academy of Sciences of the United States of America, 101 (2004) 11664-11667.
[132] A. Radhakrishnan, H.M. McConnell, Chemical activity of cholesterol in membranes, Biochemistry, 39 (2000) 8119-8124.
[133] M.J. Ronis, S. Korourian, M. Zipperman, R. Hakkak, T.M. Badger, Dietary saturated fat reduces alcoholic hepatotoxicity in rats by altering fatty acid metabolism and membrane composition, The Journal of nutrition, 134 (2004) 904-912.

[134] R. Dirkx Jr, M. Solimena, Cholesterol‐enriched membrane rafts and insulin secretion, Journal of diabetes investigation, 3 (2012) 339-346.
[135] S. Shrivastava, T.J. Pucadyil, Y.D. Paila, S. Ganguly, A. Chattopadhyay, Chronic cholesterol depletion using statin impairs the function and dynamics of human serotonin1A receptors, Biochemistry, 49 (2010) 5426-5435.
[136] L. Zhuang, J. Kim, R.M. Adam, K.R. Solomon, M.R. Freeman, Cholesterol targeting alters lipid raft composition and cell survival in prostate cancer cells and xenografts, Journal of Clinical Investigation, 115 (2005) 959.
[137] S. Fedida-Metula, S. Elhyany, S. Tsory, S. Segal, M. Hershfinkel, I. Sekler, D. Fishman, Targeting lipid rafts inhibits protein kinase B by disrupting calcium homeostasis and attenuates malignant properties of melanoma cells, Carcinogenesis, 29 (2008) 1546-1554.
[138] P. Grosse, F. Bressolle, F. Pinguet, Antiproliferative effect of methyl-β-cyclodextrin in vitro and in human tumour xenografted athymic nude mice, British journal of cancer, 78 (1998) 1165-1169.
[139] R. Zidovetzki, I. Levitan, Use of cyclodextrins to manipulate plasma membrane cholesterol content: evidence, misconceptions and control strategies, Biochimica et Biophysica Acta (BBA)-Biomembranes, 1768 (2007) 1311-1324.
[140] M.E. Davis, M.E. Brewster, Cyclodextrin-based pharmaceutics: past, present and future, Nature Reviews Drug Discovery, 3 (2004) 1023-1035.
[141] K. Uekama, Design and evaluation of cyclodextrin-based drug formulation, Chemical and Pharmaceutical Bulletin, 52 (2004) 900-915.
[142] Y. OHTANI, T. IRIE, K. UEKAMA, K. FUKUNAGA, J. PITHA, Differential effects of α‐, β‐and γ‐cyclodextrins on human erythrocytes, The FEBS Journal, 186 (1989) 17-22.
[143] H. Ohvo, J.P. Slotte, Cyclodextrin-mediated removal of sterols from monolayers: effects of sterol structure and phospholipids on desorption rate, Biochemistry, 35 (1996) 8018-8024.
[144] E.P. Kilsdonk, P.G. Yancey, G.W. Stoudt, F.W. Bangerter, W.J. Johnson, M.C. Phillips, G.H. Rothblat, Cellular cholesterol efflux mediated by cyclodextrins, Journal of Biological Chemistry, 270 (1995) 17250-17256.
[145] V.M. Atger, M. de la Llera Moya, G.W. Stoudt, W.V. Rodrigueza, M.C. Phillips, G.H. Rothblat, Cyclodextrins as catalysts for the removal of cholesterol from macrophage foam cells, Journal of Clinical Investigation, 99 (1997) 773.
[146] I. Levitan, A.E. Christian, T.N. Tulenko, G.H. Rothblat, Membrane cholesterol content modulates activation of volume-regulated anion current in bovine endothelial cells, The Journal of general physiology, 115 (2000) 405-416.
[147] S.-L. Niu, D.C. Mitchell, B.J. Litman, Manipulation of cholesterol levels in rod disk membranes by methyl-β-cyclodextrin effects on receptor activation, Journal of Biological Chemistry, 277 (2002) 20139-20145.
[148] U. Klein, G. Gimpl, F. Fahrenholz, Alteration of the myometrial plasma membrane cholesterol content with beta-cyclodextrin modulates the binding affinity of the oxytocin receptor, Biochemistry, 34 (1995) 13784-13793.
[149] E.D. Sheets, D. Holowka, B. Baird, Critical role for cholesterol in Lyn-mediated tyrosine phosphorylation of FcεRI and their association with detergent-resistant membranes, The Journal of cell biology, 145 (1999) 877-887.
[150] S. Grimmer, B. van Deurs, K. Sandvig, Membrane ruffling and macropinocytosis in A431 cells require cholesterol, Journal of cell science, 115 (2002) 2953-2962.
[151] D. Steinberg, Thematic review series: the pathogenesis of atherosclerosis. An interpretive history of the cholesterol controversy, part V: the discovery of the statins and the end of the controversy, Journal of lipid research, 47 (2006) 1339-1351.

[152] J. Avigan, D. Steinberg, M.J. Thompson, E. Mosettig, Mechanism of action of MER-29, an inhibitor of cholesterol biosynthesis, Biochemical and biophysical research communications, 2 (1960) 63-65.
[153] E. Raviña, The evolution of drug discovery: from traditional medicines to modern drugs, John Wiley & Sons2011.
[154] T.R. Blohm, R.D. MacKenzie, Specific inhibition of cholesterol biosynthesis by a synthetic compound (MER-29), Archives of biochemistry and biophysics, 85 (1959) 245-249.
[155] J. Avigan, D. Steinberg, Deposition of desmosterol in the lesions of experimental atherosclerosis, The Lancet, 279 (1962) 572.
[156] R. Altschul, A. Hoffer, J. Stephen, Influence of nicotinic acid on serum cholesterol in man, Archives of biochemistry and biophysics, 54 (1955) 558-559.
[157] S.S. Bergen Jr, T.B. Van Itallie, D.M. Tennent, W. Sebrell, Effect of an Anion Exchange Resin on Serum Cholesterol in Man.∗, Proceedings of the Society for Experimental Biology and Medicine, 102 (1959) 676-679.
[158] D.M. Tennent, H. Siegel, M.E. Zanetti, G.W. Kuron, W.H. Ott, F.J. Wolf, Plasma cholesterol lowering action of bile acid binding polymers in experimental animals, Journal of lipid research, 1 (1960) 469-473.
[159] A. Endo, Y. Tsujita, M. Kuroda, K. TANZAWA, Inhibition of Cholesterol Synthesis in vitro and in vivo by ML‐236A and ML‐236B, Competitive Inhibitors of 3‐Hydroxy‐3‐methylglutaryl‐Coenzyme A Reductase, The FEBS Journal, 77 (1977) 31-36.
[160] T. Kazuhiko, K. Masao, E. Akira, Time-dependent, irreversible inhibition of 3-hydroxy-3-methylglutaryl-coenzyme A reductase by the antibiotic citrinin, Biochimica et Biophysica Acta (BBA)-Lipids and Lipid Metabolism, 488 (1977) 97-101.
[161] M.S. Brown, J.R. Faust, J.L. Goldstein, I. Kaneko, A. Endo, Induction of 3-hydroxy-3-methylglutaryl coenzyme A reductase activity in human fibroblasts incubated with compactin (ML-236B), a competitive inhibitor of the reductase, Journal of Biological Chemistry, 253 (1978) 1121-1128.
[162] P.R. Vagelos, Are prescription drug prices high?, JSTOR, 1991.
[163] A. Endo, A gift from nature: the birth of the statins, Nature medicine, 14 (2008) 1050-1052.
[164] S. Ramkumar, A. Raghunath, S. Raghunath, Statin therapy: review of safety and potential side effects, Acta Cardiologica Sinica, 32 (2016) 631.
[165] C. Baigent, L. Blackwell, J. Emberson, L. Holland, C. Reith, N. Bhala, R. Peto, E. Barnes, A. Keech, J. Simes, Efficacy and safety of more intensive lowering of LDL cholesterol: a meta-analysis of data from 170,000 participants in 26 randomised trials, Elsevier, 2010.
[166] N.J. Stone, J.G. Robinson, A.H. Lichtenstein, C.N.B. Merz, C.B. Blum, R.H. Eckel, A.C. Goldberg, D. Gordon, D. Levy, D.M. Lloyd-Jones, 2013 ACC/AHA guideline on the treatment of blood cholesterol to reduce atherosclerotic cardiovascular risk in adults: a report of the American College of Cardiology/American Heart Association Task Force on Practice Guidelines, Journal of the American College of Cardiology, 63 (2014) 2889-2934.
[167] Ž. Reiner, A.L. Catapano, G. De Backer, I. Graham, M.-R. Taskinen, O. Wiklund, S. Agewall, E. Alegria, M.J. Chapman, P. Durrington, ESC/EAS Guidelines for the management of dyslipidaemias: the Task Force for the management of dyslipidaemias of the European Society of Cardiology (ESC) and the European Atherosclerosis Society (EAS), European heart journal, 32 (2011) 1769-1818.
[168] P. Lochhead, A.T. Chan, Statins and colorectal cancer, Clinical Gastroenterology and Hepatology, 11 (2013) 109-118.
[169] D. Pradelli, D. Soranna, L. Scotti, A. Zambon, A. Catapano, G. Mancia, C. La Vecchia, G. Corrao, Statins and primary liver cancer: a meta-analysis of observational studies, European Journal of Cancer Prevention, 22 (2013) 229-234.

[170] H.-F. Chiu, S.-C. Ho, C.-C. Chang, T.-N. Wu, C.-Y. Yang, Statins are associated with a reduced risk of gastric cancer: a population-based case–control study, The American journal of gastroenterology, 106 (2011) 2098-2103.
[171] S.-W. Lai, K.-F. Liao, H.-C. Lai, C.-H. Muo, F.-C. Sung, Atorvastatin correlates with decreased risk of esophageal cancer: a population-based case–control study from Taiwan, Libyan Journal of Medicine, 7 (2012) 18830.
[172] J. Pedro-Botet, J.M. Núñez-Cortés, J. Flores, J. Rius, Muscle symptoms related with statin therapy in general practice, Atherosclerosis, 241 (2015) e197.
[173] M.W. Russo, M. Scobey, H.L. Bonkovsky, Drug-induced liver injury associated with statins, Seminars in liver disease, © Thieme Medical Publishers, 2009, pp. 412-422.
[174] V.G. Athyros, K. Tziomalos, T.D. Gossios, T. Griva, P. Anagnostis, K. Kargiotis, E.D. Pagourelias, E. Theocharidou, A. Karagiannis, D.P. Mikhailidis, Safety and efficacy of long-term statin treatment for cardiovascular events in patients with coronary heart disease and abnormal liver tests in the Greek Atorvastatin and Coronary Heart Disease Evaluation (GREACE) Study: a post-hoc analysis, The Lancet, 376 (2010) 1916-1922.
[175] M. Ekstedt, L.E. Franzén, U.L. Mathiesen, M. Holmqvist, G. Bodemar, S. Kechagias, Statins in non-alcoholic fatty liver disease and chronically elevated liver enzymes: a histopathological follow-up study, Journal of hepatology, 47 (2007) 135-141.
[176] H. Cederberg, A. Stančáková, N. Yaluri, S. Modi, J. Kuusisto, M. Laakso, Increased risk of diabetes with statin treatment is associated with impaired insulin sensitivity and insulin secretion: a 6 year follow-up study of the METSIM cohort, Diabetologia, 58 (2015) 1109-1117.
[177] M. Nakata, S. Nagasaka, I. Kusaka, H. Matsuoka, S. Ishibashi, T. Yada, Effects of statins on the adipocyte maturation and expression of glucose transporter 4 (SLC2A4): implications in glycaemic control, Diabetologia, 49 (2006) 1881-1892.
[178] V. Kain, B. Kapadia, P. Misra, U. Saxena, Simvastatin may induce insulin resistance through a novel fatty acid mediated cholesterol independent mechanism, Scientific reports, 5 (2015).
[179] K. Yokote, H. Shimano, M. Urashima, T. Teramoto, Efficacy and safety of pitavastatin in Japanese patients with hypercholesterolemia: LIVES study and subanalysis, Expert review of cardiovascular therapy, 9 (2011) 555-562.
[180] E.P. Navarese, A. Buffon, F. Andreotti, M. Kozinski, N. Welton, T. Fabiszak, S. Caputo, G. Grzesk, A. Kubica, I. Swiatkiewicz, Meta-analysis of impact of different types and doses of statins on new-onset diabetes mellitus, The American journal of cardiology, 111 (2013) 1123-1130.
[181] M.R. Castro, G. Simon, S.S. Cha, B.P. Yawn, L.J. Melton, P.J. Caraballo, Statin use, diabetes incidence and overall mortality in normoglycemic and impaired fasting glucose patients, Journal of general internal medicine, 31 (2016) 502-508.
[182] J. Clendening, L. Penn, Targeting tumor cell metabolism with statins, Oncogene, 31 (2012) 4967-4978.
[183] A. Day, S. Bellavia, O. Jones, D. Stansbie, Effect of simvastatin therapy on cell membrane cholesterol content and membrane function as assessed by polymorphonuclear cell NADPH oxidase activity, Annals of clinical biochemistry, 34 (1997) 269-275.
[184] C. Kirsch, G.P. Eckert, W.E. Mueller, Statin effects on cholesterol micro-domains in brain plasma membranes, Biochemical pharmacology, 65 (2003) 843-856.
[185] B. Rituper, A. Flašker, A. Guček, H.H. Chowdhury, R. Zorec, Cholesterol and regulated exocytosis: a requirement for unitary exocytotic events, Cell calcium, 52 (2012) 250-258.
[186] P. Robinet, Z. Wang, S.L. Hazen, J.D. Smith, A simple and sensitive enzymatic method for cholesterol quantification in macrophages and foam cells, Journal of lipid research, 51 (2010) 3364-3369.

[187] J.M. Suski, M. Lebiedzinska, A. Wojtala, J. Duszynski, C. Giorgi, P. Pinton, M.R. Wieckowski, Isolation of plasma membrane–associated membranes from rat liver, Nature protocols, 9 (2014) 312.
[188] A. DeBlasi, K. O'Reilly, H.J. Motulsky, Calculating receptor number from binding experiments using same compound as radioligand and competitor, Trends in pharmacological sciences, 10 (1989) 227-229.
[189] T.T. Puck, S.J. Cieciura, A. Robinson, Genetics of somatic mammalian cells: III. Long-term cultivation of euploid cells from human and animal subjects, Journal of Experimental Medicine, 108 (1958) 945-956.
[190] J. Stetefeld, S.A. McKenna, T.R. Patel, Dynamic light scattering: a practical guide and applications in biomedical sciences, Biophysical reviews, 8 (2016) 409-427.
[191] S. Morino‐Koga, S. Yano, T. Kondo, Y. Shimauchi, S. Matsuyama, Y. Okamoto, M.A. Suico, T. Koga, T. Sato, T. Shuto, Insulin receptor activation through its accumulation in lipid rafts by mild electrical stress, Journal of cellular physiology, 228 (2013) 439-446.
[192] S. Vainio, I. Bykov, M. Hermansson, E. Jokitalo, P. Somerharju, E. Ikonen, Defective insulin receptor activation and altered lipid rafts in Niemann–Pick type C disease hepatocytes, Biochemical Journal, 391 (2005) 465-472.
[193] A. Ono, A.A. Waheed, A. Joshi, E.O. Freed, Association of human immunodeficiency virus type 1 gag with membrane does not require highly basic sequences in the nucleocapsid: use of a novel Gag multimerization assay, Journal of virology, 79 (2005) 14131-14140.
[194] O.W. Lindwasser, M.D. Resh, Multimerization of human immunodeficiency virus type 1 Gag promotes its localization to barges, raft-like membrane microdomains, Journal of virology, 75 (2001) 7913-7924.
[195] L. Ding, A. Derdowski, J.-J. Wang, P. Spearman, Independent segregation of human immunodeficiency virus type 1 Gag protein complexes and lipid rafts, Journal of virology, 77 (2003) 1916-1926.
[196] K. Roepstorff, P. Thomsen, K. Sandvig, B. van Deurs, Sequestration of epidermal growth factor receptors in non-caveolar lipid rafts inhibits ligand binding, Journal of Biological Chemistry, 277 (2002) 18954-18960.
[197] H. Huo, X. Guo, S. Hong, M. Jiang, X. Liu, K. Liao, Lipid rafts/caveolae are essential for insulin-like growth factor-1 receptor signaling during 3T3-L1 preadipocyte differentiation induction, Journal of Biological Chemistry, 278 (2003) 11561-11569.
[198] L. Labrecque, I. Royal, D.S. Surprenant, C. Patterson, D. Gingras, R. Béliveau, Regulation of vascular endothelial growth factor receptor-2 activity by caveolin-1 and plasma membrane cholesterol, Molecular biology of the cell, 14 (2003) 334-347.
[199] S. Parpal, M. Karlsson, H. Thorn, P. Strålfors, Cholesterol depletion disrupts caveolae and insulin receptor signaling for metabolic control via insulin receptor substrate-1, but not for mitogen-activated protein kinase control, Journal of Biological Chemistry, 276 (2001) 9670-9678.
[200] A. Green, J.M. Olefsky, Evidence for insulin-induced internalization and degradation of insulin receptors in rat adipocytes, Proceedings of the National Academy of Sciences, 79 (1982) 427-431.
[201] A. Kolychev, E. Ternovskaya, A. Arsenieva, E. Shapkina, Differences in time course of internalization of receptors of insulin and insulin-like growth factor (IGF-1) in isolated rat hepatocytes, Journal of Evolutionary Biochemistry and Physiology, 49 (2013) 597-607.
[202] C.A. López, A.H. de Vries, S.J. Marrink, Molecular mechanism of cyclodextrin mediated cholesterol extraction, PLoS computational biology, 7 (2011) e1002020.
[203] J. Kim, K. Maxwell, D. Hajjar, J. Berliner, Beta-VLDL increases endothelial cell plasma membrane cholesterol, Journal of lipid research, 32 (1991) 1125-1131.

[204] E.B. Neufeld, A.M. Cooney, J. Pitha, E.A. Dawidowicz, N.K. Dwyer, P.G. Pentchev, E.J. Blanchette-Mackie, Intracellular trafficking of cholesterol monitored with a cyclodextrin, Journal of Biological Chemistry, 271 (1996) 21604-21613.
[205] L.J. Pike, L. Casey, Cholesterol levels modulate EGF receptor-mediated signaling by altering receptor function and trafficking, Biochemistry, 41 (2002) 10315-10322.
[206] S.R. Hubbard, The insulin receptor: both a prototypical and atypical receptor tyrosine kinase, Cold Spring Harbor perspectives in biology, 5 (2013) a008946.
[207] B.A. Maddux, I. D GOLDFINE, PC-1 Inhibition of Insulin Receptor Function Occurs via Direct Interaction with the Receptor Alpha Subunit: Reversal with Monoclonal Antibodies, Diabetes, 48 (1999) SA219-SA219.
[208] J. Gustavsson, S. Parpal, M. Karlsson, C. Ramsing, H. Thorn, M. Borg, M. Lindroth, K.H. Peterson, K.-E. Magnusson, P. Strålfors, Localization of the insulin receptor in caveolae of adipocyte plasma membrane, The FASEB Journal, 13 (1999) 1961-1971.
[209] M. Yamamoto, Y. Toya, C. Schwencke, M.P. Lisanti, M.G. Myers, Y. Ishikawa, Caveolin is an activator of insulin receptor signaling, Journal of Biological Chemistry, 273 (1998) 26962-26968.
[210] P. Lajoie, J.G. Goetz, J.W. Dennis, I.R. Nabi, Lattices, rafts, and scaffolds: domain regulation of receptor signaling at the plasma membrane, The Journal of cell biology, 185 (2009) 381-385.
[211] S. Lambert, D. Vind-Kezunovic, S. Karvinen, R. Gniadecki, Ligand-independent activation of the EGFR by lipid raft disruption, Journal of Investigative Dermatology, 126 (2006) 954-962.
[212] P. Křížek, P.W. Winter, Z. Švindrych, J. Borkovec, M. Ovesný, D.A. Roess, B.G. Barisas, G.M. Hagen, Imaging of insulin receptors in the plasma membrane of cells using super-resolution single molecule localization microscopy, Formatex, 2014, pp. 259-266.
[213] P.W. Winter, A.K. Van Orden, D.A. Roess, B.G. Barisas, Actin-dependent clustering of insulin receptors in membrane microdomains, Biochimica et Biophysica Acta (BBA)-Biomembranes, 1818 (2012) 467-473.
[214] A. Spencer, L. Yu, V. Guili, F. Reynaud, Y. Ding, J. Ma, J. Jullien, D. Koubi, E. Gauthier, D. Cluet, Nerve Growth Factor Signaling from Membrane Microdomains to the Nucleus: Differential Regulation by Caveolins, International journal of molecular sciences, 18 (2017) 693.
[215] X. Gao, J. Zhang, Spatiotemporal analysis of differential Akt regulation in plasma membrane microdomains, Molecular biology of the cell, 19 (2008) 4366-4373.
[216] X. Gao, J. Zhang, Akt signaling dynamics in plasma membrane microdomains visualized by FRET-based reporters, Communicative & integrative biology, 2 (2009) 32-34.
[217] R. Vigneri, I. Goldfine, L. Frittitta, Insulin, insulin receptors, and cancer, Journal of endocrinological investigation, 39 (2016) 1365-1376.
[218] F. Frasca, G. Pandini, P. Scalia, L. Sciacca, R. Mineo, A. Costantino, I. Goldfine, A. Belfiore, R. Vigneri, Insulin receptor isoform A, a newly recognized, high-affinity insulin-like growth factor II receptor in fetal and cancer cells, Molecular and cellular biology, 19 (1999) 3278-3288.
[219] A. Ono, E.O. Freed, Role of lipid rafts in virus replication, Advances in virus research, 64 (2005) 311-358.
[220] N. Chazal, D. Gerlier, Virus entry, assembly, budding, and membrane rafts, Microbiology and Molecular Biology Reviews, 67 (2003) 226-237.
[221] B.D. Manning, L.C. Cantley, AKT/PKB signaling: navigating downstream, Cell, 129 (2007) 1261-1274.
[222] B. Chogtu, R. Magazine, K. Bairy, Statin use and risk of diabetes mellitus, World journal of diabetes, 6 (2015) 352.
[223] O.P. Ganda, Statin-induced diabetes: incidence, mechanisms, and implications, F1000Research, 5 (2016).

[224] H. Scharnagl, R. Schinker, H. Gierens, M. Nauck, H. Wieland, W. März, Effect of atorvastatin, simvastatin, and lovastatin on the metabolism of cholesterol and triacylglycerides in HepG2 cells, Biochemical pharmacology, 62 (2001) 1545-1555.
[225] T. Funatsu, K. Suzuki, M. Goto, Y. Arai, H. Kakuta, H. Tanaka, S. Yasuda, M. Ida, S. Nishijima, K. Miyata, Prolonged inhibition of cholesterol synthesis by atorvastatin inhibits apo B-100 and triglyceride secretion from HepG2 cells, Atherosclerosis, 157 (2001) 107-115.
[226] M. Schonewille, J.F. de Boer, L. Mele, H. Wolters, V.W. Bloks, J.C. Wolters, J.A. Kuivenhoven, U.J. Tietge, G. Brufau, A.K. Groen, Statins increase hepatic cholesterol synthesis and stimulate fecal cholesterol elimination in mice, Journal of lipid research, 57 (2016) 1455-1464.
[227] F.J. Field, E. Born, S. Murthy, S.N. Mathur, Transport of cholesterol from the endoplasmic reticulum to the plasma membrane is constitutive in CaCo-2 cells and differs from the transport of plasma membrane cholesterol to the endoplasmic reticulum, Journal of lipid research, 39 (1998) 333-343.
[228] L. Duvnjak, K. Blaslov, Statin treatment is associated with insulin sensitivity decrease in type 1 diabetes mellitus: A prospective, observational 56-month follow-up study, Journal of clinical lipidology, 10 (2016) 1004-1010.
[229] S. Larsen, N. Stride, M. Hey-Mogensen, C.N. Hansen, L.E. Bang, H. Bundgaard, L.B. Nielsen, J.W. Helge, F. Dela, Simvastatin effects on skeletal muscle: relation to decreased mitochondrial function and glucose intolerance, Journal of the American College of Cardiology, 61 (2013) 44-53.
[230] G. Muscogiuri, G. Sarno, A. Gastaldelli, S. Savastano, A. Ascione, A. Colao, F. Orio, The good and bad effects of statins on insulin sensitivity and secretion, Endocrine research, 39 (2014) 137-143.
[231] Z.H. Park, A. Juska, D. Dyakov, R.V. Patel, Statin-associated incident diabetes: a literature review, The Consultant Pharmacist®, 29 (2014) 317-334.
[232] B.D. Henriksbo, T.C. Lau, J.F. Cavallari, E. Denou, W. Chi, J.S. Lally, J.D. Crane, B.M. Duggan, K.P. Foley, M.D. Fullerton, Fluvastatin causes NLRP3 inflammasome-mediated adipose insulin resistance, Diabetes, 63 (2014) 3742-3747.
[233] P. Bonetti, L.O. Lerman, C. Napoli, A. Lerman, Statin effects beyond lipid lowering—are they clinically relevant?, European heart journal, 24 (2003) 225-248.
[234] G.A. Plenz, O. Hofnagel, H. Robenek, Differential modulation of caveolin-1 expression in cells of the vasculature by statins, Circulation, 109 (2004) e7-e8.
[235] L. Frittitta, J. Youngren, R. Vigneri, B. Maddux, V. Trischitta, I. Goldfine, PC-1 content in skeletal muscle of non-obese, non-diabetic subjects: relationship to insulin receptor tyrosine kinase and whole body insulin sensitivity, Diabetologia, 39 (1996) 1190-1195.
[236] L. Frittitta, D. Spampinato, A. Solini, R. Nosadini, I.D. Goldfine, R. Vigneri, V. Trischitta, Elevated PC-1 content in cultured skin fibroblasts correlates with decreased in vivo and in vitro insulin action in nondiabetic subjects: evidence that PC-1 may be an intrinsic factor in impaired insulin receptor signaling, Diabetes, 47 (1998) 1095-1100.
[237] M.L. Grundleger, S.W. Thenen, Decreased insulin binding, glucose transport, and glucose metabolism in soleus muscle of rats fed a high fat diet, Diabetes, 31 (1982) 232-237.
[238] P.A. Hansen, D.H. Han, B.A. Marshall, L.A. Nolte, M.M. Chen, M. Mueckler, J.O. Holloszy, A high fat diet impairs stimulation of glucose transport in muscle functional evaluation of potential mechanisms, Journal of Biological Chemistry, 273 (1998) 26157-26163.
[239] J.V. Sun, H.M. Tepperman, J. Tepperman, A comparison of insulin binding by liver plasma membranes of rats fed a high glucose diet or a high fat diet, Journal of lipid research, 18 (1977) 533-539.
[240] B.D. Manning, A. Toker, AKT/PKB signaling: navigating the network, Cell, 169 (2017) 381-405.

[241] M. Lu, M. Wan, K.F. Leavens, Q. Chu, B.R. Monks, S. Fernandez, R.S. Ahima, K. Ueki, C.R. Kahn, M.J. Birnbaum, Insulin regulates liver metabolism in vivo in the absence of hepatic Akt and Foxo1, Nature medicine, 18 (2012) 388.
[242] R.S. Jope, G.V. Johnson, The glamour and gloom of glycogen synthase kinase-3, Trends in biochemical sciences, 29 (2004) 95-102.
[243] M.J. Hart, R. de los Santos, I.N. Albert, B. Rubinfeld, P. Polakis, Downregulation of β-catenin by human Axin and its association with the APC tumor suppressor, β-catenin and GSK3β, Current Biology, 8 (1998) 573-581.
[244] C. Sutherland, I.A. Leighton, P. Cohen, Inactivation of glycogen synthase kinase-3β by phosphorylation: new kinase connections in insulin and growth-factor signalling, Biochemical Journal, 296 (1993) 15-19.
[245] B. Hibbert, J.R. Lavoie, X. Ma, T. Seibert, J.E. Raizman, T. Simard, Y.-X. Chen, D. Stewart, E.R. O'Brien, Glycogen synthase kinase-3β inhibition augments diabetic endothelial progenitor cell abundance and functionality via cathepsin B: a novel therapeutic opportunity for arterial repair, Diabetes, 63 (2014) 1410-1421.
[246] Z. Cheng, M.F. White, The AKTion in non-canonical insulin signaling, Nature medicine, 18 (2012) 351.
[247] B.-Y. Zhang, C.-M. Liu, R.-Y. Wang, Q. Zhu, Z. Jiao, F.-Q. Zhou, Akt-independent GSK3 inactivation downstream of PI3K signaling regulates mammalian axon regeneration, Biochemical and biophysical research communications, 443 (2014) 743-748.
[248] J.E. Pessin, A.R. Saltiel, Signaling pathways in insulin action: molecular targets of insulin resistance, The Journal of clinical investigation, 106 (2000) 165-169.
[249] S. Menon, C.C. Dibble, G. Talbott, G. Hoxhaj, A.J. Valvezan, H. Takahashi, L.C. Cantley, B.D. Manning, Spatial control of the TSC complex integrates insulin and nutrient regulation of mTORC1 at the lysosome, Cell, 156 (2014) 771-785.
[250] C.B. Blum, Comparison of properties of four inhibitors of 3-hydroxy-3-methylglutaryl-coenzyme A reductase, American Journal of Cardiology, 73 (1994) D3-D11.
[251] C. Stancu, A. Sima, Statins: mechanism of action and effects, Journal of cellular and molecular medicine, 5 (2001) 378-387.
[252] M.R. Krause, S.L. Regen, The structural role of cholesterol in cell membranes: from condensed bilayers to lipid rafts, Accounts of chemical research, 47 (2014) 3512-3521.
[253] K. Conde, M. Vergara-Jimenez, B. Krause, R. Newton, M. Fernandez, Hypocholesterolemic actions of atorvastatin are associated with alterations on hepatic cholesterol metabolism and lipoprotein composition in the guinea pig, Journal of lipid research, 37 (1996) 2372-2382.
[254] A. Bonifacio, G.M. Sanvee, J. Bouitbir, S. Krähenbühl, The AKT/mTOR signaling pathway plays a key role in statin-induced myotoxicity, Biochimica et Biophysica Acta (BBA)-Molecular Cell Research, 1853 (2015) 1841-1849.
[255] P.J. Mullen, A. Zahno, P. Lindinger, S. Maseneni, A. Felser, S. Krähenbühl, K. Brecht, Susceptibility to simvastatin-induced toxicity is partly determined by mitochondrial respiration and phosphorylation state of Akt, Biochimica et Biophysica Acta (BBA)-Molecular Cell Research, 1813 (2011) 2079-2087.
[256] T.R. Joy, R.A. Hegele, Narrative review: statin-related myopathy, Annals of internal medicine, 150 (2009) 858-868.
[257] S.K. Baker, Molecular clues into the pathogenesis of statin‐mediated muscle toxicity, Muscle & nerve, 31 (2005) 572-580.
[258] R. Laaksonen, On the mechanisms of statin‐induced myopathy, Clinical Pharmacology & Therapeutics, 79 (2006) 529-531.
[259] O. Mistafa, U. Stenius, Statins inhibit Akt/PKB signaling via P2X7 receptor in pancreatic cancer cells, Biochemical pharmacology, 78 (2009) 1115-1126.

[260] R.C. Aloia, F.C. Jensen, C.C. Curtain, P.W. Mobley, L.M. Gordon, Lipid composition and fluidity of the human immunodeficiency virus, Proceedings of the National Academy of Sciences, 85 (1988) 900-904.
[261] R.C. Aloia, H. Tian, F.C. Jensen, Lipid composition and fluidity of the human immunodeficiency virus envelope and host cell plasma membranes, Proceedings of the National Academy of Sciences, 90 (1993) 5181-5185.
[262] C. Yuan, J. Furlong, P. Burgos, L.J. Johnston, The size of lipid rafts: an atomic force microscopy study of ganglioside GM1 domains in sphingomyelin/DOPC/cholesterol membranes, Biophysical journal, 82 (2002) 2526-2535.
[263] J.W. Balliet, P. Bates, Efficient infection mediated by viral receptors incorporated into retroviral particles, Journal of virology, 72 (1998) 671-676.
[264] R. Kurg, O. Reinsalu, S. Jagur, K. Õunap, L. Võsa, S. Kasvandik, K. Padari, K. Gildemann, M. Ustav, Biochemical and proteomic characterization of retrovirus Gag based microparticles carrying melanoma antigens, Scientific reports, 6 (2016) 29425.
[265] A. Kosaki, T.S. Pillay, L. Xu, N.J. Webster, The B isoform of the insulin receptor signals more efficiently than the A isoform in HepG2 cells, Journal of Biological Chemistry, 270 (1995) 20816-20823.
[266] L. Whittaker, C. Hao, W. Fu, J. Whittaker, High-affinity insulin binding: insulin interacts with two receptor ligand binding sites, Biochemistry, 47 (2008) 12900-12909.
[267] M. Mamounas, D. Gervin, E. Englesberg, The insulin receptor as a transmitter of a mitogenic signal in Chinese hamster ovary CHO-K1 cells, Proceedings of the National Academy of Sciences, 86 (1989) 9294-9298.
[268] Z. Wang, K.L. Schey, Proteomic analysis of lipid raft-like detergent-resistant membranes of lens fiber cells, Investigative ophthalmology & visual science, 56 (2015) 8349-8360.
[269] J.-M. Song, C.-W. Choi, S.-O. Kwon, R.W. Compans, S.-M. Kang, S.I. Kim, Proteomic characterization of influenza H5N1 virus-like particles and their protective immunogenicity, Journal of proteome research, 10 (2011) 3450-3459.
[270] R. Chu, D. Reczek, W. Brondyk, Capture-stabilize approach for membrane protein SPR assays, Scientific reports, 4 (2014) 7360.